

Association EURATOM – MESCS
ANNUAL REPORT 2013



Slovenska Fuzijska Asociacija
Slovenian Fusion Association

Association EURATOM – MESCS **ANNUAL REPORT 2013**

The Annual Report 2013
of the Association EURATOM-MESCS
covers the period 1 January to 31 December 2013

Compiled by Milan Čerček, Aljaž Ivekovič
and Bojan Žefran

This work, supported by the European Communities
under the contract of Association between EURATOM
and MESCS, was carried out within the framework
of the European Fusion Development Agreement (EFDA).
The views and opinions expressed herein do not
necessarily reflect those of the European Commission.

Association EURATOM-MESCS

Jožef Stefan Institute
Jamova cesta 39
SI-1000 Ljubljana
Tel. +386 1 5885 450
<http://www.sfa-fuzija.si>

Ljubljana, September 2014

Figure on the front cover:

Large Eddy Simulation (LES) of impinging jets representing the coolant flow in DEMO divertor cooling finger - top view of vorticity field.

Authors: Martin Draksler, Boštjan Končar

Association EURATOM-MESCS
ANNUAL REPORT 2013

Slovenska fuzijska asociacija
Slovenian fusion association EURATOM-MESCS

ISSN 1855-2072

Ljubljana, 2014

CONTENTS

1. Introduction	
1.1 Foreword	1
1.2 Executive Summary	3
2. Fusion Physics Programme	
2.1 Improvement of diagnostics in edge plasma of fusion devices	15
2.2 Processes with neutral hydrogen atoms and molecules	21
2.3 Removal of deposits by neutral oxygen and nitrogen atoms	31
2.4 Application of Ion Beam Analytical methods to the studies of plasma-wall interaction in tokamaks (IBAF)	41
2.5 Permeation measurements of mixed Be/W layers on eurofer plasma deposition of H:C-metal coatings	51
2.6 Visualization support with Kepler actors and VisIt UAL plugin within ITM Advanced visualisation tools	59
3. JET Programme	
3.1 Upgrade of the 360° model of JET – calculations, to support neutron yield calibration	71
3.2 Neutron studies for neutron calibration - calculations to support JET neutron yield calibration	79
3.3 Shutdown dose rate at JET with the new ilw and prediction of the expected dose level after future tritium experiment	87
3.4 Escaping alpha particle measurements by activation foils in JET - MCNP simulation of the neutron flux at the KA2 location	89
3.5 Activation analysis of JET in-vessel components following DT irradiation – neutron flux calculations	93
4. Emerging Technology Programme	
4.1 Fabrication and characterisation of W-SiC composites	97
4.2 Optimization of SiC-based composites	103
4.3 Thermal-hydraulic analyses of square helium-cooled multi-jet finger using T111 as thimble material	107
4.4 Divertor high flux helium cooling: large eddy simulation (LES) of multiple jet impingement case	115
4.5 Tritium breeding ratio study of the WCLL and the DCLL	121
5. Public Information	
5.1 Public Information Activities	131
5.2 Fusion Expo Support Action	133

6. Publications	139
Annex 1. General Information	145
Annex 2. Slovenian Representatives in EU Committees	146
Annex 3. Statistics	147

FOREWORD

Europe is determined to explore the feasibility of utilizing the energy of fusion to fulfil the needs of the society. Industrial orders for the components of ITER are placed and the construction of ITER is steadily progressing, in spite of some delays, which should be viewed from the perspective that magnetic confinement fusion is one of the largest scientific and technological projects of our time. We are proud to be a part of this joint undertaking through the EURATOM-MESCS (Slovenian Fusion Association) contributions to the European fusion programme in the year of 2013.

The challenges of ITER construction within a constrained budget necessitated a complete reorganisation of the way in which research activities are coordinated and funded. The basis for the changes was the “Roadmap”, which laid down the strategy and identified the priorities for research and development, focused specifically on the ITER construction as the first priority, with due consideration for follow-up activities in the DEMO design to meet the goal of energy from fusion by the year 2050. The reorganisation gave the task leaders more flexibility to steer the allocation of available resources according to the needs and priorities. Consequently the National Associations with a formal contract with the European Commission are no longer necessary; within the new scheme active research groups join forces through a consortium, within which the tasks are distributed as appropriate. Special care is being given to the educational aspect, since the new technology will require many more researchers and engineers with sound background knowledge in the field. The new scheme essentially came into force at the beginning of the new year.

The research groups that constituted the Slovenian Fusion Association adapted well to the new system by successfully completing the tasks assigned to them for the year 2013 and expressing interest to participate in the activities under the new scheme on JET, ITER Physics and Power Plant Physics and Technology.

The extensive reorganisation at the European level also required a reorganisation locally. As the leader of the Slovenian Fusion Association I felt that it was time to let the younger generation with new ideas to take over. We were fortunate to find our colleague dr. Boštjan Končar able and willing to accept the leadership responsibilities with full dedication and competence.

At this point I would like to thank all members and collaborators of the Slovenian Fusion Association and partners from the EU for their hard work and support and I wish them success in their endeavours under the new leadership in the future.

Dr. Andrej Trkov

Head of the Research Unit



EXECUTIVE SUMMARY

1 ITER Physics Basics

1.1 Improvement of diagnostics in edge plasma of fusion devices

In 2013 we were involved in one BS task and one PS task, both dealing with probe measurements in tokamak scrape-off-layer.

In the first task we were actively involved in the development of an emissive probe for use in tokamaks together with ÖAW group from Innsbruck. The final design has been completed, but unfortunately the construction has not been finished. We have however continued our work on the theoretical models for emissive probes. Additionally, we have performed kinetic simulations of an electron emitting surface in realistic SOL plasma which provided interesting results. Namely, if the surface, e.g. divertor plates, is heated sufficiently to reach the point of critical emission, the sheath drop is decreased in the way that the total heat flux to the wall increases for a factor of 1.4.

In the second task we were more involved in the kinetic modelling of the SOL, making a connection with the probe measurements performed with INRNE.BG in COMPASS tokamak. We provided theoretical modelling and PIC simulations in support of the electron energy distribution function probe measurements with the advanced First derivative probe method. The measurements show a strong presence of high energy electrons at the divertor strike points, which we tried to reproduce with PIC simulation of the parallel transport in a single flux tube. The simulation results showed that the mechanisms in parallel transport were not sufficient to explain the occurrence of the high energy tail of the distribution. In the subsequent evaluation of the radial profile measurements we could conclude, that radial transport is crucial.

In 2014 we will continue our work in the improvement of the probe measurements in tokamaks and we are also involved in the development of a 2d3v fully-kinetic code through an Enabling research project under EUROFUSION.

1.2 Processes with neutral hydrogen atoms and molecules

The goal of this project was to contribute to understanding and to provide quantitative data for processes with neutral hydrogen atoms and molecules relevant to the fusion development program in particular to the field of plasma surface interaction. Processes at the surface and bulk of materials relevant for plasma facing components as well as volume processes in edge plasma were studied.

In 2013 we continued the study of H and D interaction, with tungsten irradiated by high energy W ions (neutron-like-damaged tungsten) and with undamaged tungsten as a reference. Samples were exposed to a well characterised beam of thermal deuterium atoms (~ 0.2 eV). We have performed first study of D retention in undamaged and damaged W exposed to D atoms at sample temperatures from 500 to 700 K by *in situ* NRA, where depth profile was measured during the exposure. *In situ* measurements

provide direct information about the dynamics of D migration in damaged and undamaged W. The isotope exchange in damaged W was also studied for the first time by *in situ* NRA. Complete isotope exchange was achieved for 590 K sample temperature. Initial measurements with dual beam irradiation (He ion + D atom) were also performed confirming the concept for the measurement procedure of forthcoming experimental studies. Above work is conducted in collaboration with Max-Planck Institute für Plasmaphysik (IPP), Garching, Germany and was the subject of a PS task within EFDA IPH WP2013.

Study about the efficiency and technological applicability of methods for fuel removal on tungsten was continued in 2013. We have focused on the determination of deuterium release and re-absorption in W surfaces treated by RF discharges. This work proceeds through the collaboration with CEA, Cadarache, France and the PIIM laboratory, University of Provence (Aix-Marseille), Marseille, France, and was also a subject of a PS task within EFDA IPH WP2013. A detailed study of thermal desorption of D from W subjected to different ion fluences was performed and results compared to available data from other experiments. A detailed study of the influence of the storage time in vacuum on decrease of the amount of retained deuterium was performed, showing that the dynamic retention is very large. The NRA study on samples exposed to 5 keV and 500 eV D_2^+ ions was performed; showing that the deuterium was retained mainly at the surface for the long storage time, whereas increased concentration up to 1 μm below the surface was observed for short storage time.

Spectrometer for vibrational diagnostics of hydrogen molecules based on the properties of low energy dissociative electron attachment was further upgraded by new electron gun with trochoidal electron monochromator in order to improve the energy resolution. The simple numerical model for determining particle concentration in partially dissociated low pressure neutral hydrogen gas in a metal reaction cell where flowing gas is partially dissociated by a hot tungsten filament was completed and made operational in 2013.

1.3 Removal of deposits by neutral oxygen and nitrogen atoms

In 2013, we managed to demonstrate that active neutral species coming from NH_3 plasmas can be effective in a-C:H removal. In previous years, we have developed a method of a-C:H removal based on the chemical activity of neutral oxygen atoms. As concerns were raised about the potential damage they could cause to plasma facing components, alternative methods of chemical fuel removal were researched. In collaboration with CIEMAT, Madrid, we investigated the a-C:H removal efficiency of NH_3 plasmas. In the experiments performed in 2013, we managed to demonstrate that it is possible to achieve removal of a-C:H deposits even without ionic species. The method relies only on the interaction of neutral species with the surface, and can thus replace oxidation by atomic oxygen in fuel removal application. Fuel removal methods were also tested on a graphite limiter tile from the COMPASS tokamak, and a remote atom source was developed for use on COMPASS.

Carbon based PFCs, however, are being phased out of fusion devices, in favour of a full-metal first wall. As carbon is being phased out, new problems linked to a full-metal wall arise. In order to replace the carbon as intrinsic radiating species, and to reduce the heat loads to divertor surfaces, nitrogen is being seeded into the plasma to

promote radiation. While nitrogen was found to successfully replace carbon as a radiating impurity, it can also cause the formation of ammonia, which could pose as a serious issue to ITER operation. The formation of ammonia was another focal point in 2013, both in laboratory plasmas of $H_2 - N_2$ mixtures, as well as during N_2 seeded discharges at JET.

Working in collaboration with CNRS LAPLACE, Toulouse, we continued our dusty plasma research. Departing from the original research topic, we studied the frequency spectrum of the floating potential of the C_2H_2 ECR plasma at different values of the discharge parameters. While more data analysis and additional research is needed to fully explain our findings, the initial results indicate that observing the frequency spectrum of the floating potential could be a basis to develop a new, inexpensive and robust method of dust detection in magnetised plasmas.

1.4 Application of Ion Beam Analytical methods to the studies of plasma-wall interaction in tokamaks (IBAF)

During 2013 we have performed an initial study of deuterium release and uptake by mixed material layers of composition relevant for ITER. Various mixed layers containing Be, W, C and Al were produced by Thermionic Vacuum Arc method at MEdC. Some samples were produced in presence of D_2 gas so that deuterium was initially already incorporated in the layer. Few others were produced in the presence of nitrogen gas during deposition in order to enable study of this seeding impurity on deuterium retention. The samples initially not containing deuterium were exposed to the D-atom beam so that deuterium uptake could be observed. Deuterium release was measured from the samples during thermal desorption (TD) induced by sample temperature ramping by simultaneous monitoring deuterium content in the sample by 3He NRA and in the background gas by mass analyser. Layer structure was also continuously recorded by RBS during experiment. This is the first time that such experiments were performed *in situ* without sample transport through air. It was observed that in all cases of C containing mixed layers some deuterium still remained in the layer. Moreover, the desorption temperatures for C:W mixed layer were quite high, having desorption maximum at around 1000 K. This temperature is higher than typical desorption temperatures for polycrystalline W, normally detected at the temperatures from 400 K to 800 K, as well as for the amorphous deuterated carbon films, which amount 870 K for hard and 740 K for soft layers. Such high desorption temperatures were observed for deposited W layers, meaning that tungsten substantially influences the release of deuterium. However, the maximum of deuterium desorption for multilayered sample C on W is close to the amorphous deuterated carbon films. The C:W:Al mixed layer has also high desorption temperature, close to the C:W mixed layer. Two samples with 500 nm thick Be layer with co-deposited D have been studied by *in situ* TD. One of the layers was on graphite and another on Si substrate. For both layers a low temperature desorption was observed and D was completely removed at around 580 °C. Both of these samples were strongly modified after TD was completed even the temperature ramping was performed only up to 730 °C. Two Al containing layers suffered transformation during TD at the temperatures between 560 and 620 °C for W:Al and between 700 and 820 °C for W:Al (N_2) as clearly indicated by RBS spectra but also clearly visible by eye. This is an important issue as mixed layers in

tokamaks are created by numerous heating cycles so that caution is needed in using laboratory produced mixed layers as proxy to realistic mixed material deposits. Much higher deuterium uptake was observed in W:Al (N₂) sample than in W:Al one indicating influence of nitrogen presence during layer formation. This finding calls for further effort in order to quantify and confirm observed influence of seeding impurity nitrogen to hydrogen retention. W:Be (N₂) sample was meant to be measured in order to indicate variation of retention capacity of Be versus Al but due to much smaller thickness this is not possible. However, even though layer is ten times thinner than the two Al-containing ones the total accumulated amount of D is comparable to the W - Al (N₂) sample. This result also calls for further systematic work in order to fully quantify Be vs. Al retention capacity. For this sample no variation of layer structure could be observed.

In 2013 was also performed a study of deuterium retention in tungsten micro-particle which was subjected to the deuterium plasma in Casimir reactor, CEA. High-energy focused beam of ³He ions was used for this measurement. 2D map of the particle was readily obtained by 3HIXE, whereas the deuterium concentration determined by simultaneously acquired NRA signal.

1.5 Deuterium interaction kinetics with Be, W and mixtures relevant to ITER and DEMO

In 2013 we took part in two tasks related to permeation through Be/W films with various Be/W ratio and the role of nanostructure on permeation in Be/W films. The aim of the tasks was to provide quantitative data on the influence of thickness and structure of Be/W layers on D-retention and release.

The main points, set in the program, were generally achieved even if many details are still overlapped by the influence of film microstructure and extremely high reactivity of beryllium.

Hydrogen permeation through pure W films and Be/W films all deposited by thermionic vacuum arc (TVA) technique on Eurofer substrates was performed. Each sample was outgassed in vacuum before the hydrogen was applied as this data could enable reconstruction of trapped hydrogen. Retention of tritium could be the issue in similar Be/W deposits inside ITER. Pure Be films, deposited also by the TVA method, have been investigated previously. The correlation between permeation flux and W film morphology was searched first. W surface was characterized by various surface sensitive techniques while the XRD was applied for determination of average grain size. The results were then applied in further studies for Be/W films, deposited by the TVA technique. Complementary SEM, XPS, XRD, AFM methods were applied for characterization. Four pure W films and 8 samples with Be/W films were investigated. As the complex and mutual dependence of film nanostructure and additionally beryllium high chemical activity on overall observed permeation properties, all samples were deposited with the same thickness of 8 μm and in atomic ratio Be:W = 3:1.

1.6 Plasma deposition of H:C-metal coatings

We have worked on three types of fusion-relevant deposits. The first one is based on amorphous carbon, originating in carbon fibre reinforced composites – a common type of structural materials in tokamaks. The amorphous carbon samples produced in our group served as substitutes for carbon deposits encountered in tokamak walls, with the primary advantage of being available in large quantities at a low price. The sister group of this project used these samples to study the plasma cleaning phenomena and was able to perform enough experiments to quantify them.

Amorphous carbon comes in many forms. It can be hydrogenated (a-C:H) or not (a-C), predominantly sp²-bound, also known as "soft" (a-C), or predominantly sp³-bound i.e. "hard" (ta-C). It can be alloyed with additional non-metallic elements (a-C:N) or metals (a-C:W). They were successfully deposited by three diverse deposition techniques: lab-scale triode sputtering, lab-scale anode layer source, and industrial-scale magnetron sputtering. In all these three techniques we encountered the problem of poor adhesion (connected primarily to large internal stress) which was successfully overcome by introducing interlayers or manipulating the structure/composition through various deposition parameters

In a minor extent, we have also worked on two other types of deposits. The first type contains tungsten, another fusion-relevant structural material. The other is beryllium, however, due to its high toxicity we cannot perform sputtering experiments. We have neither the equipment nor the certification. Nevertheless, chemical similarity between beryllium and magnesium can be used to apply magnesium-containing deposits (which are not toxic) to study beryllium deposits indirectly. Some experiments were thus performed using magnesium.

1.7 Visualization support with Kepler actors and VisIt UAL plugin within ITM Advanced visualisation tools

The European Integrated Tokamak Modelling Task Force (ITM-TF) requires specialized visualization plugins and Kepler actors that are used within integrated fusion simulations. In an effort to provide diversity and at the same time universality of visualizations for different backends, ITMVis library provides a common description of the specialized plots contributed by users. Besides specialized plots many "standard" plots are used and are described within ITM-TF database. Within this database we describe standard plots for several computer languages and visualization tools. For complex 3D visualizations plugin for VisIt visualization tool is developed that allows all possible plots from the database. It was soon realized, given that the same plots are needed by other tools within different languages, that standard visualizations are needed to be described generally. To lower the burden of translation for different tools we introduced an intermediate plot description with XML, that is easily interpreted. With such unified approach standard and custom plots are available for different backends such as VisIt and matplotlib. Additionally, VisIt Kepler Actor was upgraded for use with DDF workflows with multiple CPOs as input for visualizations.

2 JET Programme

2.1 JET MCNP model

The aim of the project was the further upgrade of the MCNP model for JET and its adjustment in order to be used for calculations of the correction/calibration factors during the 2013 calibration of JET neutron diagnostics systems. Another goal was the support of the experimental programs at JET with transport calculations of the relevant neutron and gamma fluxes. The calculations are focused also on the diagnostics needs. In 2013 a calibration of neutron detectors was made with a strong Cf-source and the upgraded MCNP model was used for calculations in support of the calibration. The main goal of the project was to determine detector responses and correction factors for individual detector positions for many effects, e.g. corrections which originate from the undesired shielding of the source by the mascot robot arm holding the source. Prior to the calculations the MCNP model was upgraded, one of the major items was the insertion of the remote handling boom, which holds the neutron source during the calibration, in place. Since calculations for more than 200 calibration points were performed, the model was adjusted for an automatic procedure for insertion of the different boom configurations. Finally for all calibration points correction factors were calculated, which resulted in a huge amount of computer time, equalling 14 CPU years on a larger cluster.

2.2 Calculations to support JET neutron yield calibration

JET neutron yield measurements are the basis for the determination of the absolute fusion reaction rate and the operational monitoring with respect to the neutron budget during any campaign.

After the Carbon wall to ITER-Like Wall (Beryllium/Tungsten/Carbon) transition in 2010, confirmation of the neutron yield calibration will be ensured by direct measurements using a calibrated ^{252}Cf neutron source deployed inside the JET vacuum vessel. This calibration will allow direct confirmation of the KN1 calibration (which was the standard on JET originally) and provide the first direct calibration of the JET activation system KN2. Diagnostics system KN1 consist of a sets of fission chambers (FC) mounted on three JET transformer limbs, which provide the time-dependent neutron yield used to assess a JET pulse. The KN2 system pneumatically delivers capsules to positions just at the edge of the vacuum-vessel inside JET, where they are irradiated during the pulse, pneumatically retrieved, and the induced activity is counted to provide a time-independent absolute fusion yield measurement. All these measurements will be relevant to the D-D plasma calibrations.

In order to understand the important contributing factors of the calibration and to significantly improve the accuracy, a whole suite of calculations is required to support the JET neutron calibration project. Many are based on Monte Carlo modelling using advanced Monte Carlo transport codes, such as MCNP.

The purpose of the work is to:

- estimate the validity of calibration (Rates, statistics, dependencies),

- estimate calibration corrections and dose estimates to define limits to manual operations of neutron source
- perform calculations to analyse and evaluate the JET neutron yield calibration after the experimental campaign (e.g. evaluation of differences between calibration conditions and later JET operational conditions)
- develop and maintain computational models for neutron and gamma transport calculations
- study the response of all JET neutron monitors
- perform calculations to verify and understand the JET neutron yield measurements
- use experimental results in order to verify and validate the computational tools and models

2.3 Upgrade of octant 1 JET model

The main objective of the task was the measurement and corresponding calculation of the shutdown dose rate at short cooling times. Additional information on the main contributors to the doses is also obtained through gamma spectrometry. The goals are the validation of the shutdown dose rate calculation with the new ILW through dose measurements during 2012 off-operational period and estimation of shutdown dose rate following hypothetical DT irradiations in preparation of the future tritium experiment. The task of the MESCS-SFA was the preparation/upgrade of the MCNP model for the calculations. The last version of MCNP model of Octant 1, used to estimate the preliminary effect of ILW in the frame of a previous task has been modified in order to include the description of relevant components (geometry and material). In 2013 the focus was on the improvement of the model, especially on the elimination of geometry errors, resulting in particles being lost during calculations. In long runs a few spots were identified in the model, where small geometrical errors were present and particles got lost. The spots were corrected and in this way the number of lost particles largely reduced.

2.4 Support for charge particle measurement

The aim of the project was the test and development of escaping alpha particle measurements using the foil activation technique for real D-T fusion conditions and to provide for an absolute measurement of the fluence and the energy spectrum of escaping alpha particles at several poloidal positions and the collection of data for assessment of the activation induced at the reactor walls by MeV escaping ions. In addition to measurement, simulations and calculational study of the response of the activation foils are required, what is done by the described work. The aim of the sub-task was the improvement of the 2012 preliminary simulation results by taking a more realistic neutron spectrum into account. These neutron spectra were calculated with MCNP at the proposed location for the foils, i.e. the KA2-diagnostic, with the new model of the JET ITER like wall configuration and materials. The data were

subsequently used for calculation of the reaction rates of charged particle detector material to neutrons.

2.5 Activation analysis of JET in-vessel components following DT irradiation

The forthcoming DT campaign at JET will induce a significant activation of the system components. It is desirable to calculate the temporal evolution of the radioactive species in the main in-vessel components after the end of the future DT campaign. The topic of the sub-task was the calculation of the neutron spectra in the selected components what was done by the MCNP code using the emission source of a typical DT plasma discharge using a three-dimensional model of the JET machine, upgraded with ITER-like wall. The Monte Carlo approach allows a detailed treatment of the geometrical configuration. The flux has been calculated in four locations. In order to determine the change of the spectra with the depth in material the spectrum has been determined in the poloidal limiter in the depth of 0-2 cm and 2-4 cm. The possible influence on results due to the usage of a specific data library for fusion applications rather than the ENDF library was also investigated. The FENDL 2.1 library was used and the difference in the total neutron fluxes did not exceed 3% for any of the components. This has been assumed to be the uncertainty due to the influence of the data library on results. The resulting neutron spectra are intended to be used as input for the FISPACT code that computes the evolution of the radioactive species generated by the neutron activation process. For each irradiation scenario, the time behaviour of the contact dose rate is then determined.

3 Emerging Technology Programme

3.1 Development of SiC-based composite for structural parts in fusion reactor

The main objective of the work aimed at development of a SiC-based composite for use at extremely severe environment in structural part of future fusion reactors is full impregnation of 3D woven SiC-fiber preform with a low activation SiC matrix. The work has followed rather tough requirements for the material: The composite must possess high mechanical strength and reliability at temperatures up to 1100 °C, gas impermeability and high through-thickness thermal conductivity. Low neutron-activation is expected in order to minimise production of radioactive wastes. Presently available techniques are unable to satisfy all the demands for a successful implementation of SiC-based composites as a structural material in future fusion power plants. In our work we are trying to apply an alternative process termed SITE, based on electrophoretic (infiltration) deposition and polymer infiltration and pyrolysis, to the fabrication of low activation SiC-based structural components for fusion environments. The SITE-SiC_f/SiC composite is predominantly composed of crystalline β -SiC and was characterised with high thermal conductivity and homogeneous microstructure with a more favourable pore size and porosity distribution in comparison to other state-of-art

materials. Further development of SITE process is aimed at improvement of the fibre-matrix interphase layer to ensure good mechanical behaviour, further improvement of high temperature through thickness thermal conductivity and application of a coating layer to ensure materials hermeticity.

Large effort is also placed onto development of novel W-SiC composite materials with possible applications as a matrix, coating or joining material in SiC-based composites or as stand-alone fusion structural material.

3.2 Thermal-hydraulic analyses of square helium-cooled multi-jet finger using Ta-alloy as thimble material

The main objective of the task was to carry out thermal-hydraulic analyses of square shape cooling finger with thimble made of Ta-alloy (T111), which was fabricated in Karlsruhe Institute of Technology (KIT) - Institute for Applied Materials-Materials Processing Technology. Based on our previous investigations, the prerequisite for the new finger design was the square shape of the tile with the same plasma facing area as in the case of the reference hexagonal tile. For fabrication purposes, the commercially available Ta-alloy T-222 was used for thimble material in order to enable low temperature cooling below 450 °C. The cartridge design was also slightly changed; the upper part of the cartridge was much shorter than for the reference finger. The CAD model of the square-shaped finger assembly prepared at KIT was used to construct a fully hexagonal numerical mesh. Thermal-hydraulic performance of the fabricated finger and heat loading on the structure materials was evaluated using the code ANSYS-CFX. The operating conditions at two different heat fluxes (10 MW/m² and 8.7 MW/m²), two mass flow rates (6.8 and 9 g/s) and two helium inlet temperatures (350 and 450 °C) were assessed. The results were compared with previous simulations of 16.5 mm square finger (task WP12-DAS-02-T06). The tile temperature was higher for the new finger as a consequence of larger tile edge (17.1 mm). On the contrary, the maximum thimble temperature was slightly lower for the new design, originating from different shape of the cartridge upper part.

3.3 Divertor high flux helium cooling: large eddy simulation (LES) of multiple jet impingement case

Large eddy simulation (LES) was carried out in order to study the flow characteristics and heat transfer of multiple circular impinging jets at configurations and Reynolds numbers comparable to those in the cooling finger of helium-cooled divertor. In the simulated test case the nozzles were arranged in hexagonal configuration around the central nozzle, in the same way as in the case of conceptual DEMO cooling finger. The jet exit Reynolds number of around 20000 is similar as for real divertor nozzles. LES modelling and simulation work started in the second half of the 2012 with simulations of the instantaneous flow fields and setting up the necessary statistical methods for analysis of transient results. In 2013 the LES simulations are being continued with the focus on validation against the experimental data, interpretation of results and carrying out the LES simulations of the heat transfer. The results show that

the LES simulation accurately predicts the key flow phenomena of multiple highly turbulent impinging jets. Flow field and secondary turbulent stresses show very good agreement with experimental data. Accurate LES results could serve either as a benchmark case for validation of RANS turbulence models or could contribute to in depth interpretation of the local flow and heat transfer phenomena in multiple impinging jets. Ultimately, these results can serve as a validation benchmark for CFD models used in pre-conceptual and optimisation studies of divertor cooling finger. The work was performed in cooperation with the Paul Scherrer Institute (PSI), Laboratory for Thermal-Hydraulics, Switzerland.

3.4 Tritium breeding ratio study of the WCLL and the DCLL

A comparative study on the neutron shielding and tritium breeding ratio (TBR) of the WCLL and the DCLL blanket concepts was performed. A model of DEMO, prepared originally for activation calculations was used for the MCNP transport calculations; it included empty blanket boxes which were filled with appropriate materials. Simplified models using homogenous breeding blanket mixtures were then used. The results show the highest intensity of tritium breeding in the modules around the mid-plane.

Additionally the neutron multiplication was studied. It was found, that the dominant reaction is the $(n,2n)$ in lead of the breeding blankets, accounting roughly to two thirds of all multiplication in the torus. The rest of reactions take place outside the breeding blankets. The $(n,3n)$ reaction was found to negligibly contribute to neutron multiplication.

The corresponding values of the TBR were also calculated for both concepts, they are however, due to the simplification of using homogeneous BB material mixtures, of limited practical significance.

4 Public Information

4.1 Public Information in the Association

Public information activities in 2013 consist of the permanent exposition run by the Nuclear Training Centre and on other regular activities.

Permanent fusion exhibition at the Nuclear training centre of the Jožef Stefan Institute (<http://www.icjt.org/an/index.htm>) was visited in 2013 by 162 organized groups of 7100 visitors altogether, mainly youngsters from primary, secondary and high schools. We were often visited also by graduate and postgraduate students and organized groups of adults.

We gave 20 lectures on Fusion technology and ITER project and 23 on Radioactivity and radioactive waste. We also gave 117 lectures on electricity from nuclear energy, where we talk also about fusion as safe, sustainable and environmentally responsible source of energy in the future. We performed experiments on radioactivity and ionizing radiation and provided guided tours of the permanent exhibition on fusion.

There were also other activities in 2013: a lecture on fusion within the annual Jožef Stefan week, a lecture on fusion within the action “Science on the street, knowledge and ideas on the go” - lectures for general public, interviews for Slovenian national television and different newspapers (Delo, Dnevnik).

4.2 Fusion Expo Support Action

Slovenian Fusion Association (SFA) EURATOM – MESCS has taken over responsibility to run the Fusion Expo from 6th October 2008. The first Fusion Expo Support Action (WP08-PIN-FUSEX) has finished on 31st July 2010. The new support action WP10-PIN-FUSEX started on 1st August 2010 and was extended until the end of June 2014. The main goal and intention of this project remain the same since beginning of our task agreement: to run the Fusion Expo in the most efficient way possible and to follow our tasks, which needs to be fulfilled: scheduling the exhibition, supervising the local organization, graphical work and printing Fusion Expo panels, moving the exhibits, assembling/disassembling Fusion Expo, maintenance, continuous report to EFDA, organization of a supporting participation in international events for young generations and providing the Fusion Expo with Fusion Show for larger events.

Fusion Expo is an itinerant exhibition presenting various aspects of fusion research such as: fusion as a natural phenomenon and energy source science, fusion as a European research project, history of fusion research, European research facilities, ITER, future plans toward a power plant, technological, environmental and sociological aspects of this energy source etc.

During 2013 six events were organized: Big Bang Festival in London, Science centre Ahhaa in Tartu, Ecsite conference in Gothenburg, Science Days in Rust, Science week in Prague and fusion show in Antwerp. Additionally Fusion Expo contributed with the support action to the Sziget festival in Hungary.

IMPROVEMENT OF DIAGNOSTICS IN EDGE PLASMAS OF FUSION DEVICES

Tomaž Gyergyek^{1,2}, Jernej Kovačič¹, Milan Čerček¹

¹Jožef Stefan Institute, Ljubljana, Slovenia

²Univerza v Ljubljani, Fakulteta za elektrotehniko
e-mail: tomaz.gyergyek@fe.uni-lj.si

1 INTRODUCTION

Probe measurements remain an important diagnostic system in the SOL region of tokamaks and even beyond. Our group works on improvement of probe related diagnostics and generally on problems associated with potential profile formation in front of electrodes, an issue closely connected to probe physics as well as general edge plasma physics. We have continued our work on emissive probes/surfaces by estimating the effect of the secondary electron emission on the wall heat load. As explained below, we unfortunately did not manage to perform the measurements with an externally heated emissive probe in tokamak, although the final design of the probe head had been completed.

In 2013 we took part in two tasks agreements under EFDA, namely WP13-IPH-A06-P1-01 (SOL transport measurements by probes in L-mode, inter-ELMs and ELMs) and WP13-IPH-A06-P1-01 (Development of probe head with emissive probes for electric field measurements). Our main collaborators in these tasks were INRNE.BG, University of St. Kliment Ohridski, Sofia (USKOS), ÖAW-P1, University of Innsbruck (UIBK) and ÖAW-P5, UIBK.

2 WORK PERFORMED IN 2013

Emissive probe measurements

Electron emitting surfaces immersed in various plasma types remain an important part of our research. In the last few years we have been a part of a group in charge of investigating the feasibility of the use of an electron emitting probe in tokamak edge plasma. In the previous years we have constructed various theoretical and simulation models describing the behaviour of an emissive probe in plasmas including different specifics of tokamak plasmas, i.e. energetic electrons, various types of collisions, magnetic field. In this year we have helped in the final design of the emissive probe head, which will be constructed by our collaborators from UIBK. The probe head itself will be made for ASDEX tokamak and will also be useful for measurements in COMPASS tokamak because of the similarity of the probe manipulators. It will comprise of four

Langmuir probe (LP) pins and a single emissive probe in the middle, which will be made from a LaB₆ crystal.

Electron emitting surfaces

Due to the successful simulation modelling of an emissive probe in tokamak plasma [1], [Annual Report 2011], we have decided to use the model also to calculate the effects of the electron emission on the heat flux to the wall. For practical reasons, we can define the wall, e.g. divertor tiles, to be at a floating potential relative to the plasma potential. In theory, with an increasing emission current, the sheath should decay and the floating potential should become equal to the plasma potential, rendering all potential barriers between the plasma and the wall. Such is the case with ELMs, when the sheath heat transmission can be increased, due to the decrease of the sheath potential. This would mean that the surface would be directly exposed to plasma thermal electron and ion current. In this case, unlike for the emissive probe measurements, the fact that the emission regime changes from temperature limited to space-charge limited actually comes in handy.

The simulations were performed on HPC-FF and the model is identical to the one described in [1] with enhanced diagnostics. We have again used the fully-kinetic, massively parallel 1.5d3v particle-in-cell BIT1 [2].

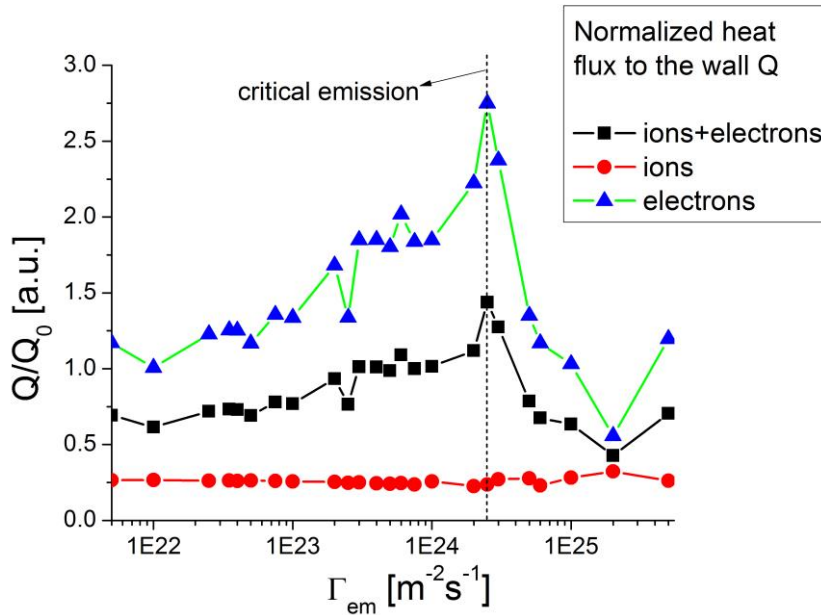


Figure 1: Electron (blue), ion (red) and total heat flux with dependence on the electron emission flux from the wall. The dashed line designates the point of critical emission.

In the figure 1 we present the decreasing of the sheath potential drop and the subsequent increase of the ion and electron heat flux normalized to the case of zero electron emission from the surface. We can see that up to the point of the critical emission at $\Gamma_{em,crit} \approx 3 \cdot 10^{25} m^{-2} s^{-1}$, which designates the transition from temperature limited emission to space-charge limited emission, the electron energy flux is increased

and reaches its maximum at the point of critical emission. At that particular point, it is approximately $Q_{e,heat}(\Gamma_{em} = \Gamma_{em,crit}) = 2.7 Q_{e,heat}(\Gamma_{em} = 0)$ higher than for the case of zero emission. Afterwards, with increasing emission the electron heat flux again drops even below the original value. Meanwhile, the ion energy flux tends to drop to a quarter of its original value and remains there. The net energy flux reaches its maximum at the point of critical emission and has a value of roughly $Q_{i+e,heat}(\Gamma_{em} = \Gamma_{em,crit}) = 1.4 Q_{i+e,heat}(\Gamma_{em} = 0)$ the value of energy flux at zero emission.

Non-Maxwellian electron energy distribution function measurements and simulation

In past couple of years our group had also been active in development and use of advanced methods for measurements of the electron energy distribution functions (EEDF) and its derivatives. The First derivative probe technique (FDPT), based on non-local kinetic theory, allows for plasma potential determination with accuracy of $\pm 10\%$ even in strong magnetic field of a tokamak, due to being able to take into account the suppression of the electron part of the I-V characteristic and also by handling of a non-Maxwellian EEDF assumption. We had already made several measurement campaigns utilizing the FDPT on our Linear magnetized plasma device (LMPD) [3, 4]. In 2013 together with our collaborators from University of Innsbruck we made the first fully-kinetic simulations of LMPD and double-plasma (DP) machine in Innsbruck in order to verify the EEDF obtained by the particle-in-cell code BIT1 code [5].

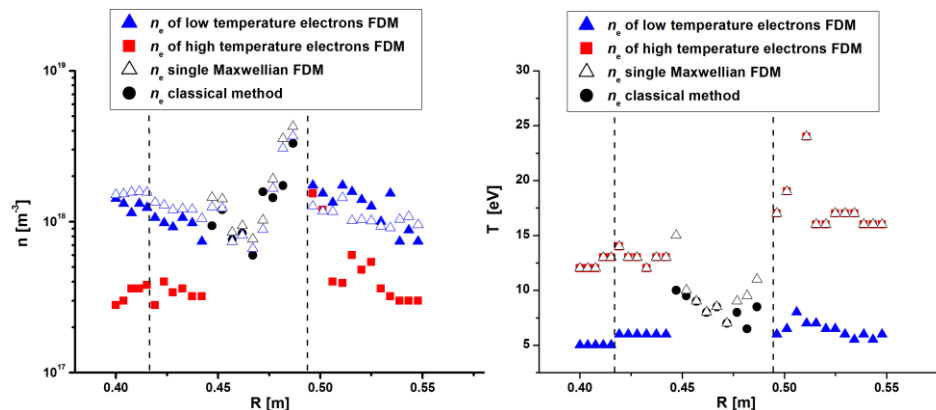


Figure 2: The density profile (left) and the temperature profile (right) for the divertor probe area in COMPASS tokamak shot #3912 (from [8]). Dashed lines designate the strike points.

Our group also took part in the evaluation of the LP measurements on COMPASS tokamak, where an experiment was made in order to study the EEDF in the SOL region. The experimental setup during the shot #3912 was a typical L-mode shot with $B_t=1.15T$ and plasma current $I_p=110kA$. In the experiment, led by our collaborators from University of Sofia (INRNE.BG), the following Langmuir probes were simultaneously used: horizontal reciprocating probe (HRP), vertical reciprocating probe (VRP) and the array of 39 divertor probes. This experiment was dedicated to an experimental evaluation of the deviation of the distribution function from Maxwellian in

the strong magnetic field of a tokamak. The FDPT models the deviation from Maxwellian distribution function by constructing a bi-Maxwellian distribution function with two separate electron species, a high temperature and a low temperature one.

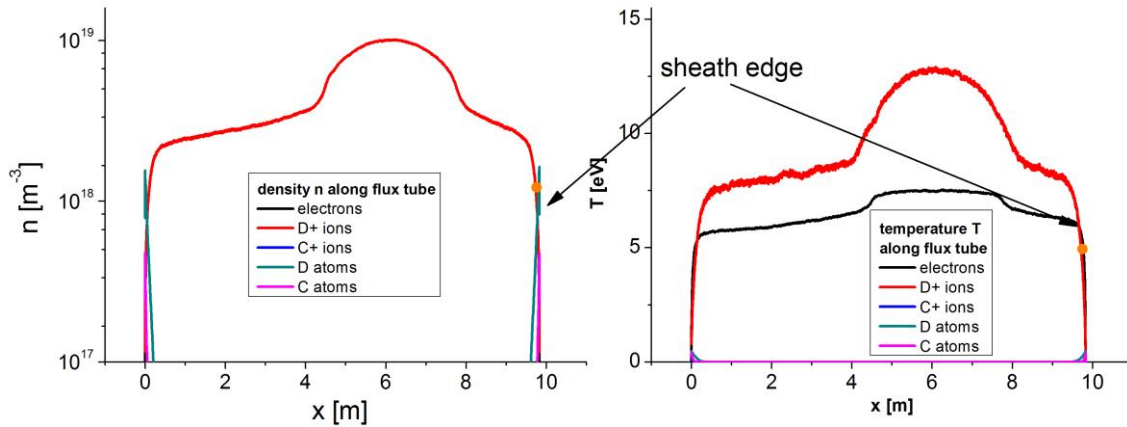


Figure 3: Density (left) and temperature (right) profiles of a single flux tube simulation. Orange circle designates the point of sheath entrance.

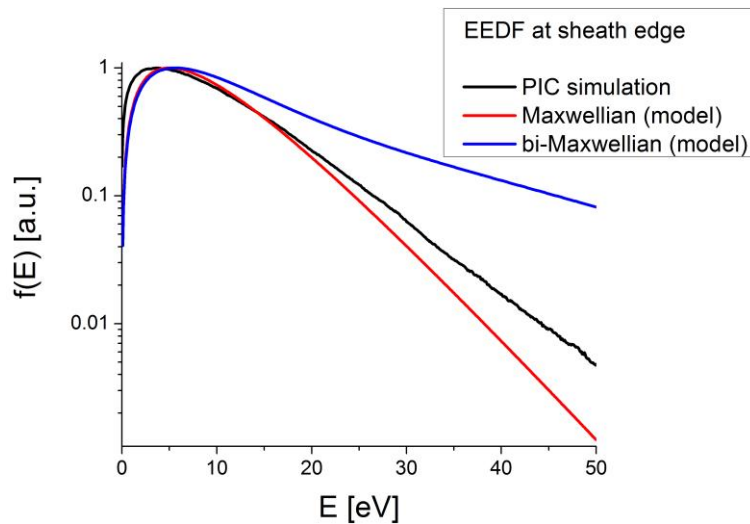


Figure 4: The normalized EEDF obtained at the sheath edge from the simulation (black), and comparable models of a single Maxwellian EEDF (red) and bi-Maxwellian according to the measurements.

In parallel with the experiment we were performing fully-kinetic simulation of the COMPASS SOL [6], again with the BIT1code. The simulation campaign was run under a dedicated project on HPC-FF. We tried to repeat the experiment using BIT1, to see the origin of the fast electrons by applying different collisionality regimes. In [7] it was shown, that for intermediate collisionality the possible discrepancies in temperature measurements at the divertor probes are caused by inelastic collisions that result in an enlarged high-energy tail of the Maxwellian distribution. The profiles of density and temperature of a case of intermediate collisionality are presented in Figure 3. In Figure 4 the plot shows the distribution function obtained at the point of the sheath edge in front of the divertor plate, mimicking the energy distribution function measured by the

divertor probe. The values of parameters for EEDF are written in Table 1. For comparison we have also presented a single Maxwellian model with temperature $T = 5$ eV and a bi-Maxwellian model with parameters obtained from probe measurements in COMPASS tokamak shot #3912 [8]: $T_l=5,0$ eV, $T_h=13,1$ eV, $n_l/n_h=5$. While we can see a high energy tail in the simulated distribution function, it is not very well pronounced. From the values of the obtained plasma simulation parameters in Table 1 we can see, why there is such a discrepancy in the two results. The simulation results, like for the case in [7], show for an order of magnitude smaller population of fast electrons than the measured one.

	n_l [m ⁻³]	n_h [m ⁻³]	T_l [eV]	T_h [eV]
Experiment (FDPT)	$\approx 1,5 \cdot 10^{18}$	$\approx 3,0 \cdot 10^{17}$	$\approx 5,0$	$\approx 13,1$
Simulation	$\approx 1,5 \cdot 10^{18}$	$\approx 0,4 \cdot 10^{17}$	$\approx 4,9$	$\approx 9,0$

Table 1: Comparison of plasma parameters at the sheath edge obtained by experiment and by PIC simulation

It was subsequently shown in the radial measurements of the EEDF that we had performed [9],

that the temperature of the slow electrons remains roughly the same in the radial profile of the SOL, while the temperature of the high energy electrons drops significantly. Effectively, the bi-Maxwellian distribution radially relaxes into a single-Maxwellian. Unfortunately, to simulate that, we need a full 2d3v kinetic code. Since the parallel transport does not seem to have a big influence on the shaping of the EEDF, this should be accounted to the radial transport.

3 CONCLUSIONS AND OUTLOOK FOR 2014

In 2013 we have continued our work in the field of the electric probe measurements in the scrape-off-layer of tokamaks. This work has been performed partly as a support in the evaluation and interpretation of the probe measurements and partly for development of new probe measurement techniques. We have participated in the evaluation of the COMPASS tokamak probe measurements and in design of the emissive probe for tokamak use. Using fully-kinetic PIC code we have also evaluated the effect of the secondary electron emission on the heat flux to the wall. PIC simulations have also been made to study the nature of the non-Maxwellian EEDF in SOL.

In 2014 we will continue our collaboration with INRNE.BG on the use of the FDPT in tokamaks and the interpretation of EEDF measurements. We are also continuing our work with ÖAW on the development of the emissive probe for tokamaks. Additionally, we are included in the development of a fully-kinetic 2d3v code under EUROFUSION Enabling Research project in 2014.

4 REFERENCES

- 1 J. Kovačič, T. Gyergyek, Simulation of a planar emissive probe in a mid-sized tokamak plasma., *Contrib. Plasma Phys.*, 51 (2011), 962-970.

- 2 D. Tskhakaya et al., PIC/MC code BIT1 for plasma simulation on HPC, Proceedings of the 18th Euromicro Conference on Parallel, Distributed and Network-based Processing, IEEE, (2010), 476-481.
- 3 Tsv. Popov, P. Ivanova, M. Dimitrova, J. Kovačič, T. Gyergyek, M. Čerček, Langmuir probe measurements of the electron energy distribution function in magnetized gas discharge, Plasma Sources, Sci. & Tech, 21 (2012), 1-10.
- 4 Tsv. Popov, J. Kovačič, T. Gyergyek, M. Čerček et al., Langmuir probe method for precise evaluation of the negative-ion density gas discharge magnetized plasma, Contrib. Plasma Phys., 53 (2013), 51-56.
- 5 J. Gruenwald, J. Kovačič, T. Gyergyek, M. Čerček et al., Comparison of measured and simulated electron energy distribution functions in low-pressure helium plasmas, Plasma Sources Sci. Technol. 22 (2013), 1-7.
- 6 J. Kovačič, T. Gyergyek, M. Čerček et al., Kinetic simulations in support of probe measurements of COMPASS scrape-off-layer, Proceedings of the 22nd International Conference Nuclear Energy for New Europe, Bled, September 9-12, 2013.
- 7 D. Tskhakaya et al., Interpretation of divertor Langmuir probe measurements during the ELMs at JET, J. Nucl. Mat., 415 (2011), S860-S864.
- 8 M. Dimitrova, J. Kovačič et al., Plasma parameters in the COMPASS divertor during ohmic plasmas, Contrib. Plasma Phys., 54 (2014), 255-260.
- 9 Tsv. Popov, J. Kovačič et al., Langmuir probe evaluation of the plasma potential in tokamak edge plasma for non-Maxwellian EEDF, Contrib. Plasma Phys., 54 (2014), 267-272.

PROCESSES WITH NEUTRAL HYDROGEN ATOMS AND MOLECULES

Sabina Markelj¹, Iztok Čadež¹, Primož Pelicon¹, Zdravko Rupnik¹, Anže Založnik¹,
Vida Žigman²

¹Department for Low and Medium Energy Physics, “Jožef Stefan” Institute, Jamova
cesta 39, SI-1000 Ljubljana, Slovenia

²University of Nova Gorica, Vipavska 13, SI-5000 Nova Gorica, Slovenia
e-mail: sabina.markelj@ijs.si

1 INTRODUCTION

The main goal of the project is to contribute to understanding and to provide quantitative data for processes with neutral hydrogen atoms and molecules which are relevant for the current efforts in EU towards developing the magnetically confined fusion. Processes on the surface and in the bulk of fusion relevant materials as well as collision processes in the gas phase are all of our concern. However, the emphasis is on the processes which are recognized by EFDA to be most relevant for preparation of efficient ITER construction and operation (ITER physics (IPH) program).

The first objective in project's work plan for 2013 (WP2013) was to continue the study of H and D interaction, with tungsten irradiated by high energy W ions (neutron-like-damaged tungsten) and with undamaged tungsten as a reference. The goal is to understand the influence of the neutron induced damage to deuterium retention in tungsten exposed to neutral deuterium atoms. To simulate n-irradiation, damaged samples are in our case produced by high energy W-ion irradiation, the so-called self-implantation. This work was conducted in collaboration with Max-Planck Institute für Plasmaphysik (IPP), Garching, Germany and is the subject of a task agreement within EFDA IPH WP2013. Second objective of our project in WP2013 was to study deuterium thermal desorption from tungsten exposed to deuterium ion beam under well-defined surface and exposure conditions. This was performed in collaboration with PIIM laboratory, University Aix-Marseille (CEA association) and was also subject of another task agreement within EFDA IPH WP2013. Third objective was to study the production of excited particles by interaction with hydrogen, seeding and impurity atoms/molecules with PFC materials at elevated temperatures.

2 WORK PERFORMED IN 2013

The research activities in 2013 are described below, following the above mentioned specific objectives as given in the work plan for 2013. Efforts were focused

on the first two objectives dealing with the problems clearly identified in EFDA tasks within IPH Topical Research A3 - P1 and P2.

Atomic hydrogen interaction with tungsten irradiated by high energy W ions (neutron-like-damaged tungsten) and with undamaged tungsten as a reference

Our goal is to contribute to the prediction of hydrogen isotope retention in undamaged and n-irradiated W. This is an important issue as it has significant implications for ITER and especially for future fusion reactors. We apply the self-implantation of W (self-damage) for simulation of n-irradiation because it generates dense cascade with large clusters which are typical for n-irradiation. The aim of our work is to determine the influence of self-damage on hydrogenic retention for different grade of tungsten exposed to thermal hydrogen atoms.

In 2013 the work on this subject has been performed by the new *in situ* Nuclear Reaction Analysis (NRA), which was set at the end of 2012. The new set up was developed at Jožef Stefan Institute (JSI) in analogy with earlier *in situ* Elastic Recoil Detection Analysis (ERDA) [1, 2]. The dynamics of deuterium retention in undamaged and damaged W exposed to atomic deuterium beam was investigated. The neutron-induced damage in tungsten is simulated by irradiating tungsten with high energy tungsten ions creating dense cascades with large clusters typical for tungsten subjected to the neutron irradiation. This method also does not introduce any chemical modification of sample.

The deuterium depth profile in the sample is obtained by analyzing the energy distribution of protons and alpha particles created by $D(^3\text{He},p)^4\text{He}$ nuclear reaction. The *in situ* NRA configuration set up is shown in Fig. 1, with new 1500 μm thick proton detector (NRA detector) at 135° and the α particle detector at 102° , used for D concentration determination within near-surface layer. In order to obtain the D concentration profile up to the depth of 7 μm , five different ^3He ion beam energies from 760 keV to 4.3 MeV were used: 766, 1555, 2580, 3399 and 4322 keV in our case. The size and shape of the ion beam at the target was defined by 2 mm diameter entrance orifice. A mesh beam current monitor is placed after the entrance orifice.

The atomic hydrogen (H or D) beam is created by thermal dissociation of hydrogen molecules in a hot capillary of a hydrogen atom beam source, HABS. For given conditions, distance between the sample surface and capillary exit being 80 mm and atom beam angle to the surface normal being 51° , the central D atom flux density at the sample was 5.2×10^{18} D/m²s. The ion beam spot size and position was determined by observing the burn trace after short exposure of a millimeter paper mounted at the location of the sample. The average D flux density at the probing ion beam position was

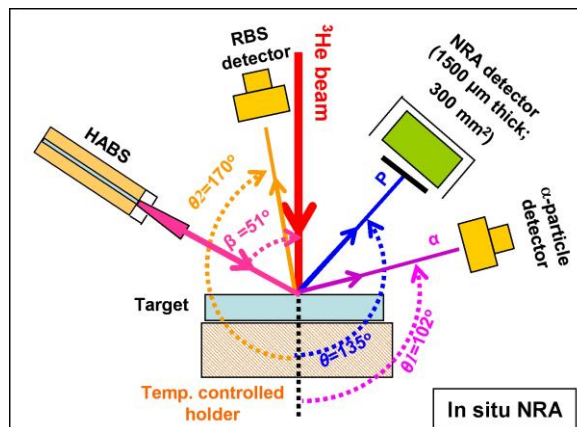


Figure 1: The set up for the present *in situ* NRA measurements. Incident ^3He beam is perpendicular to the sample surface.

$(4.5 \pm 0.1) \times 10^{18}$ D/m²s. The sample temperature was computer controlled and monitored by a thermocouple attached to the sample surface by a sample holding clamp.

The studied samples, 10×15 mm² in size and 1 mm thick, were made of polycrystalline tungsten manufactured by Plansee AG, with grains elongated perpendicular to the surface. They were mechanically polished to a mirror-like finish. Damaged samples were obtained by irradiation using different ion energies to create a flat damage distribution with 0.89 dpa damage concentration. The thickness of the damaged layer is 2.4 μm. Preparation of samples was done at IPP, Garching.

We have performed experiments with damaged and undamaged W exposed to D atoms at sample temperatures between 500 K and 700 K. The time evolution of D depth distributions were obtained by *in situ* NRA described above and results were presented at the PFMC 2013 (paper accepted for publication in Physica Scripta [3]). The *in situ* measurements gave direct information on the time development of D saturating the traps in W during the exposure to D atom beam. Good agreement was obtained for terminal D-depth profiles after exposure determined by present *in situ* experiment and *ex situ* D depth profiles on equivalently damaged and exposed W. In the case of undamaged W, the *in situ* data reveal considerably higher D retention during exposure as compared to the *ex situ* measurement. An indication of the influence of probing beam irradiation on D retention was observed. This observation appears to be due to the combined effect of dynamic retention and D decoration of damage produced by the analyzing He beam. Further studies are needed in order to clearly distinguish and evaluate individual contribution of the probing beam irradiation and dynamic retention to the observed phenomenon. This effect is not pronounced on the damaged W, what gives easier interpretation and comparison of the results. With these studies and the obtained results we have fulfilled the first milestone of our work program.

One example of the results of the present *in situ* NRA measurements on damaged W exposed to D atoms at 590 K is presented in Fig. 2. Typical measurement time to obtain one D depth profile (five different ion beam energies and four spectra with 1.25 μC accumulation dose each) was 1-1.5 h. The deuterium depth profiles were measured during D atom exposure of damaged W (3 h, 23 h, 28.5 h) and after the exposure was stopped (total exposure: 48 h) and are shown in Fig. 2a. The sample was subsequently analyzed *ex situ* by NRA at IPP five days after the end of the exposure,

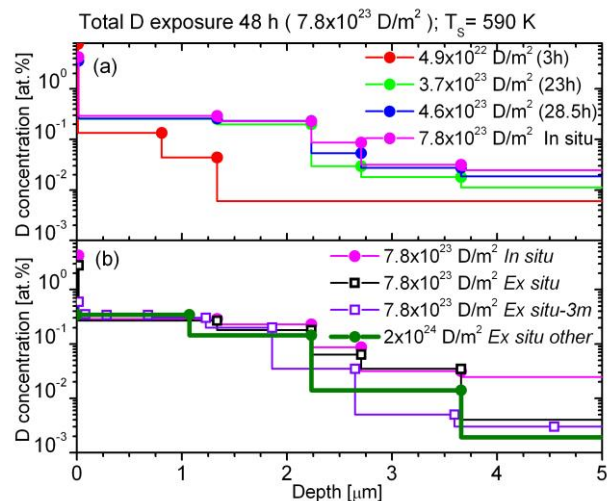


Figure 2: a) D depth profile obtained by *in situ* NRA during the exposure. b) NRA measured after stop of the exposure and *ex situ* 5 days and 3 months after exposure on the same sample. For comparison the depth profile of the previous *ex situ* NRA study is shown (“*Ex situ other*”). D atom flux density at the probing beam position is 4.5×10^{18} D/m²s.

(shown in Fig. 2b). For comparison, the depth profile of previous *ex situ* measurement (exposure at 600 K) is included as well in Fig. 2b. One can observe that after 23 h the traps produced by the damaging irradiation are already almost saturated. Small increase in the concentration is observed after 28.5 h and after 48 h. The increase is observed in deeper layers, between 2 and 3 μm . There is a good agreement between the depth profiles obtained after stop of exposure measured *in situ* or *ex situ*. The same sample was measured again after three months and the D content was found to decrease at depths below 2 μm .

The isotope exchange on damaged W was studied by the same *in situ* set up as for the above studies. The experiment was done on the following way: first the D exposure was performed at 700 K sample temperature and then the sample was subjected to the H atom beam at 500 K. Only small amount of D near the surface (few nm) was removed by H-atom exposure that lasted two times longer than D exposure. Sample was then left in vacuum for few days and then we have again exposed the sample to H atoms. The exposure lasted for a week and deuterium started to decrease in layer, up to 1 μm deep, but the concentration deeper in the sample stayed constant. The isotope exchange on damaged W was studied also at 590 K, where sample was first exposed to D atom beam and thereafter to H atom beam. Between the two atom beam exposures, the sample was for one night (20 h) left at 590 K in vacuum. The depth profiles were measured by NRA during D and H exposure and also after the sample was left in vacuum at 590 K for 20 h and results are shown in figure 3. Total isotope exchange was obtained at 590 K throughout the analyzed depth as can be seen in the figure 3. However, the D thermal desorption also contributes to the D decrease, as was observed by D decrease after one night at 600 K in vacuum without exposure. To separate the thermal desorption and isotope exchange further studies are needed. This was the first study of isotope exchange in damaged tungsten performed by *in situ* NRA. In the line of this work we have also published a paper where we have studied thermal dependence of D atom adsorption and isotope exchange on undamaged W and explained the observed results by modeling [4].

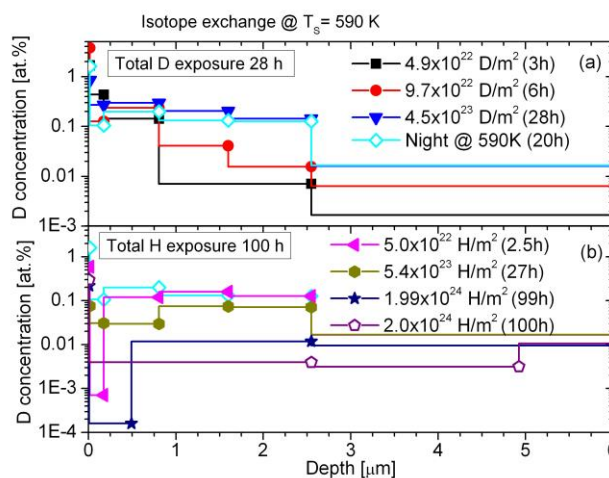


Figure 3: a) D depth profile obtained by *in situ* NRA during the D exposure and sample in vacuum after 20 h at 590 K. b) NRA measured during H exposure and after stop of H exposure. D and H atom flux densities at the probing beam position are $4.5 \times 10^{18}\text{ D/m}^2\text{s}$ and $5.6 \times 10^{18}\text{ H/m}^2\text{s}$, respectively.

We have also published a paper where we have studied thermal dependence of D atom adsorption and isotope exchange on undamaged W and explained the observed results by modeling [4].

We have performed first test measurement of dual beam experiment; high energy He beam irradiation and D atom beam exposure with subsequent NRA ^3He . Two Eurofer samples were irradiated by 1.5 MeV ^4He with simultaneous exposure to D

beam for 6 hours at 500 K and 800 K. The depth profile measurement by NRA using ^3He beam was performed after the ^4He irradiation. In order to perform this, a mesh dose integrator had to be removed from the beam line in order to allow for homogeneous irradiation by 1.5 MeV ^4He . Therefore the dose of irradiation was determined only from RBS spectra which were collected during entire time of irradiation experiment for each of two samples. Position and homogeneity of the irradiation beam was determined by optical record on the alumina target prior to the irradiation experiments. Entrance aperture on the beam line was of circular shape with 4 mm diameter for ^4He irradiation. For the immediate subsequent NRA measurement the ^3He beam was collimated by 2 mm diameter orifice and additionally focused by the quadrupole lens in the beam line. Quadrupole lens was switched off during ^4He irradiation for the sake of homogeneity. The samples were analyzed by NRA at IPP on different positions after irradiation in order to distinguish irradiated versus non-irradiated region – experimental results are under evaluation. The reconstruction of the NRA ion beam line is in progress allowing simultaneous high energy ^4He irradiation and D atom exposure and prompt subsequent ^3He NRA in situ analysis. For this purpose the mesh dose integrator has to be moved in the beam for the NRA measurements and out of it for irradiation.

This work was conducted within EFDA PWI WP13-IPH-A03-P1-01/PS/MESCS entitled: “Atomic and low-energy hydrogenic plasma interaction with damaged tungsten”. The work was performed in close collaboration with IPP, Garching by discussing the measurement plan as well as by joint first measurements with simultaneous irradiation by ^4He and D atom exposure. An article benchmarking of the data for sequential damaging of W and deuterium exposure is under preparation. By these activities we have fulfilled the objectives/milestones of our proposed work within possible and planned extent. The IPP side has also supplied all undamaged and damaged W samples studied in present task.

Deuterium thermal desorption from tungsten exposed to deuterium ion beam under well-defined surface and exposure conditions

The main subject of this objective is to improve the understanding of detailed microscopic mechanisms responsible for hydrogen retention. The main applied methods to achieve this goal is to perform systematic deuterium thermal desorption (TD) studies from W exposed to deuterium ion beam or plasma under well defined conditions and to check the quantification of D-retention by Nuclear Reaction Analysis (NRA). The purpose of this is to develop a well-controlled step-by-step procedure aimed to facilitate in-depth understanding of the adsorption, diffusion and desorption of D from W and the formation of defects by D removal techniques and their impacts on the re-adsorption process. The experimental work of TD was performed at PIIM laboratory, University Aix-Marseille (CEA association). The 2013 task was the continuation of a previous task where a close collaboration was initiated by the 9 month visit of S. Markelj through the EFDA mobility scheme. During her period of stay the set up for performing temperature programmed desorption studies on tungsten was upgraded and calibrated (doubly differentially pumped mass spectrometer) and as well as the cleaning procedure for tungsten was studied in detail by surface science techniques (Auger electron spectroscopy and High resolution electron energy loss spectroscopy). The TD system at

PIIM was reconstructed in 2013 to singly differential pumping in order to increase detection sensitivity. The report on the new mass spectrometer TPD system was completed this year.

In this year the PIIM team performed detailed studies on tungsten samples, (recrystallized by A.L.T.M. Co. and electropolished in lab) - task WP13-IPH-A03-P2-01/CEA_Ferro. Only an introductory summary of this work is presented here. Recrystallized and surface-cleaned tungsten samples were exposed to deuterium ion beam with energy of 500 eV/D₂⁺ under UHV (10⁻⁹ mbar) conditions at 300 K. After the exposure the temperature programmed desorption (TPD) was performed in the same chamber by differentially pumped mass spectrometry. The study was very detailed at different D-ion exposure fluence. For the first time the range from very low fluence (10¹⁸ D/m²) to fluence comparable to previous measurements (few times 10²¹ D/m²) was studied. A factor of 10 difference between present and other measurements is obtained. The thermodesorption signal as obtained from new measurements on polycrystalline tungsten with heating rate of 1 K/s had one broad low temperature D₂ thermodesorption peak at 470 K that is composed of three overlapping peaks.

It was found that the amount of D retained in tungsten is very low, about 5% of the implanted deuterium at low fluence and even decreases at higher fluence. At the highest possible fluence 10²¹ D/m² with 500 eV D₂⁺ ion bombardment 0.3% of the implanted deuterium was retained in sample (0,33x10¹⁹ D/m²), where also saturation was observed. The retention studies were mostly made on one sample and no memory effect was observed, meaning that re-saturation of deuterium by D ion implantation is the same in fuel depleted layers after thermal desorption. Therefore, the amount of the retained D in the sample is the same (within the error bars - 30%) between the first implantation and the last one, where in total 109 implantations was performed.

Before we could do deuterium concentration depth profile analysis by NRA, a study of the variation of the amount of retained deuterium with the storage time in vacuum and with air exposure was performed by TPD. This was important since i) we intend to study the impact of air exposure on retention ii) the total retention is low due to the low fluences studied and iii) the sample needs to be transported from France to Slovenia, meaning that there certainly will be few days between the exposure and analysis.

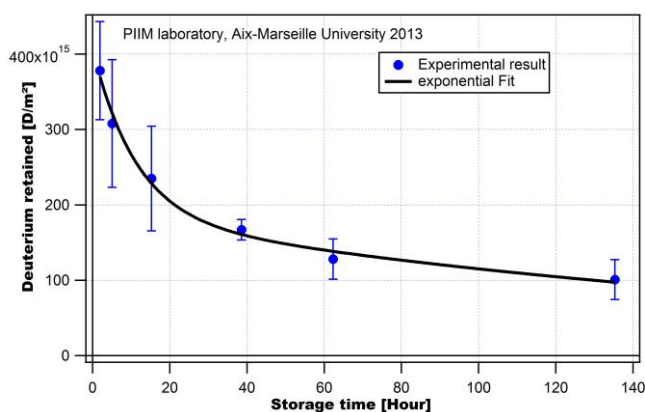


Figure 4: Deuterium retention as obtained by TD spectroscopy after sample irradiation with 500 eV D₂⁺ ions with fluence of 2.8x10¹⁹D/m² at different storage times in vacuum.

It was found that the total desorption signal decreased exponentially with the storage time in vacuum, indicating the room temperature D desorption. The retention

decrease as a function of storage time in vacuum for the sample bombarded by 500 eV D_2^+ ions with fluence $2.8 \times 10^{19} D/m^2$ is shown in figure 4. Desorption peak shifts slightly to higher temperatures with the storage time. This is direct proof of the dynamic retention for the W that was not exposed to air. Due to the low retention, fast deuterium decrease with waiting time and since the fluence can not be increased very much, we have performed first a test of NRA deuterium measurement on W sample that was exposed to 5 keV D_2^+ ions at fluence of $0.98 \times 10^{21} D/m^2$. It was found that the sample bombarded by 5 keV D_2^+ ions retained four times more deuterium than the sample bombarded by 500 eV D_2^+ ions after 135 h of waiting time in vacuum. The study was performed at lower fluence in the $10^{19} D/m^2$ range.

The deuterium depth profile in the sample was obtained by analyzing the energy distribution of protons created by $D(^3He,p)^4He$ nuclear reaction. The 1500 μm thick proton detector (NRA detector) was placed at 135° . In order to obtain the D concentration profile up to the depth of 7 μm , five different 3He ion beam energies from 760 keV to 4.3 MeV were used: 766, 1555, 2580, 3399 and 4322 keV in our case. The size and the shape of the ion beam at the target were defined by 2 mm diameter entrance orifice. The NRA measurement was performed about 120 h after the exposure and the obtained depth profile is shown in figure 5. It is seen that most of the deuterium is retained near the surface ($2.4 \times 10^{19} m^2$) and the total amount of deuterium detected by NRA is $5.3 \times 10^{19} m^2$, what is 5.4% of the implanted deuterium. The sample was send back to the PIIM laboratory and the TPD measurement was performed five days after the NRA measurement. It was found that the retention was 0.2%, meaning that about $2.3 \times 10^{18} D/m^2$ remained in the sample 10 days after implantation. This is much less than the 5% that was obtained by NRA and still less than was expected by the TPD measurement (1.2% after 5 days and 0.6% after 10 days) at the same energy but lower fluence. This is under the assumption that the difference in the retention behavior with the storage time between 500 eV and 5 keV ions is the same at low and high fluence. The discrepancy in the retained deuterium between the NRA and TPD could be due to the fact that some deuterium is, due to the air exposure, desorbed during TPD also as HD and deuterated water. Further studies are needed to see which species containing deuterium are also desorbing due to the air exposure. Moreover, an additional small peak was observed in the TPD spectra of mass 4 at about 850 K after the NRA analysis. This could be due to the trapping of D in the defects created by the analyzing 3He beam. After doing a TPD (from 300 K to 1300 K) on the NRA-analyzed sample (and seeing an additional peak $\sim 850K$), three cycles of "500eV D_2^+ implantation/TPD" on the same sample was made. The mass 4 desorption peak was observed in TPD spectra at about 800 K the first time but not the 2nd and the 3rd time.

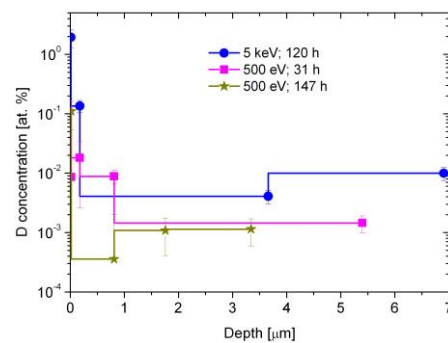


Figure 5: Deuterium depth profiles as obtained by NRA on W samples exposed to D_2^+ ions at 5 keV and 500 eV at fluence of $0.98 \times 10^{21} D/m^2$ after about 120 h for 5 keV case and after 31 h and 147 h for 500 eV case.

It could be that the TPD ramps annealed the defects induced by the NRA analysis. The amount of D retained in the NRA-analyzed sample was the same as for the previous TPD analysis for the 500 eV D_2^+ implantation. After the first test two samples exposed to 500 eV D_2^+ ions, fluence 0.98×10^{21} D/m² were analyzed by NRA at two different storage times 31 h and 147 h. The respective depth profiles are shown in figure 5. The total amount of D retained in the two samples were 0.96×10^{19} D/m² and 0.30×10^{19} D/m² obtaining of about 2-3 times difference in quantification between NRA and TPD. The depth profiles of the samples analyzed after longer storage times but exposed to different ion energies are very similar, with maximum concentration at the surface. On the other hand the depth profile for the sample analyzed at shorter storage time had still substantial concentration even 1 μ m below the surface. This means that with time, the deuterium in the bulk slowly diffuses to the surface where it recombines and desorbs.

This work was conducted within EFDA PWI WP12-IPH-A03-P2-01/PS/MESCS entitled: “D re-adsorption/re-saturation of W surfaces subjected to helium RF-discharge as a fuel removal technique” in collaboration with CEA, Cadarache and PIIM, Marseille, France. By these activities we have fulfilled the objectives/milestones of our proposed work within possible and planned extent.

Production of excited particles by interaction of hydrogen, seeding and impurity atoms/molecules with PFC materials at elevated temperatures.

We continued the work on study of production of excited particles, especially vibrationally excited hydrogen molecules, by hydrogen atom interaction with surfaces. The vibrational spectrometer was upgraded by installing additional turbomolecular pump ensuring differential pumping of the detection region and recombination/interaction region. The system is now further upgraded by new electron gun with trochoidal electron monochromator in order to improve the energy resolution.

In the previous years we have been experimentally studying reactions involving neutral atoms and molecules by operating a hydrogen reaction cell as a source for vibrationally excited molecules in a low pressure regime (to ensure the dominance of particle-surface interactions) [5]. In order to enable interpretation and detailed analyses of experimental data we were developing physics-based modelling of the relevant interactions and taking into account the particular cell characteristics [6]. The simple numerical model for determining particle concentration in partially dissociated low pressure neutral hydrogen gas in a metal reaction cell where flowing gas is partially dissociated by a hot tungsten filament was completed and made operational in 2013. Neutral hydrogen atoms and molecules in different vibrational states are taken into account. Available parameters for thermal dissociation, atom recombination, adsorption/desorption and vibrational relaxation are used as input parameters for the model. Calculated particle concentration distributions were compared to experimental data and qualitative agreement was obtained. Such a model is needed as a tool for in-depth understanding and interpretation of results from our specific experiment and thus in turn enabling checking and evaluating rates and cross sections for the above surface processes.

3 CONCLUSIONS AND OUTLOOK FOR 2014

We have performed first study of D retention in undamaged and damaged W exposed to D atoms by *in situ* NRA, where depth profile was measured during the exposure. *In situ* measurements gave direct information about the dynamics of D migration in W. The *in situ* measurements of terminal D concentration after stop of exposure are in good agreement with *ex situ* measurements on equivalently damaged W. The *in situ* NRA during D atom exposure on undamaged W gave higher retention compared to *ex situ* measurements. The results of these measurements appear to be due to simultaneous effect of dynamic retention and D decoration of damage produced by the analyzing He beam. Further studies are needed in order to analyze the influence of the probing He beam, since this is crucial for further *in situ* NRA studies and to clearly distinguish the contribution of the probing beam irradiation and dynamic retention for undamaged W.

The isotope exchange in damaged W was also studied for the first time by *in situ* NRA. Complete isotope exchange was achieved for 590 K sample temperature what was not for the case for 500 K, with D atom exposure performed at 700 K. Further studies are needed in order to see the efficiency of isotope exchange at other sample temperatures and to separate the deuterium bulk decrease due to the thermal desorption versus isotope exchange. Work on studies with damaged tungsten will be further stimulated in the coming years as we started participation in the IAEA CRP entitled “Plasma-Wall Interaction with Irradiated Tungsten and Tungsten Alloys in Fusion Devices” started in autumn 2013.

Initial measurements with dual beam irradiation (He ion + D atom) were performed confirming the concept for the measurement procedure. The beam line is now under reconstruction and first systematic studies will be performed in 2014. The dual beam irradiation could be in the future also extended to study simultaneous D ion exposure and damaging by energetic W ions on W samples afterwards analyzed by NRA *in situ* and also to study D retention in other fusion relevant materials exposed to atomic beam or to low energy D ion beam.

A detailed study of thermal desorption of D from W subjected to different ion fluences was performed and results compared to available data from other experiments. For the first time an extension to very low exposure fluences was made (10^{18} D/m²) as compared to other retention studies for W. A detailed study of the influence of the storage time in vacuum on decrease of the amount of retained deuterium was performed, showing that the dynamic retention is very large. The NRA study on samples exposed to 5 keV and 500 eV D₂⁺ ions was performed; showing that the deuterium was retained mainly at the surface for the long storage time, whereas increased concentration up to 1 μm below the surface was observed for short storage time. Further studies are needed in order to quantify the impact of exposure of D-containing samples to air on the amount of retained deuterium and to study the discrepancy between NRA and TPD results of D concentration measurements. The impact of He discharge on samples exposed to D ions is planned for the future.

Activities on production of excited particles on metal surfaces at elevated temperatures was proposed to the Enabling Research Program of EUROfusion but not approved for 2014. As the possibility for support in following years is expressed, we will continue this activity during 2014 at lower level as our voluntary program.

4 REFERENCES

- 1 S. Markelj, P. Pelicon, I. Čadež, T. Schwarz-Selinger and W. Jacob 2012 In situ study of erosion and deposition of amorphous hydrogenated carbon films by exposure to a hydrogen atom beam, *J. Vac. Sci. Tech. A* 30 (2012) 041601-1
- 2 S. Markelj, O. V. Ogorodnikova, T. Schwarz-Sellinger, P. Pelicon, K. Sugiyama and I. Čadež, Study of thermal hydrogen atom interaction with undamaged and self-damaged tungsten, *J. Nucl. Mater.* 438 (2013) S1027-S1031.
- 3 S. Markelj, O.V. Ogorodnikova, P. Pelicon, T. Schwarz-Selinger, P. Vavpetič, G. Kukec and I. Čadež, In-situ NRA analysis of D retention in undamaged and self-damaged tungsten under atomic D exposure, 14th PFMC conference, May 2013, Juelich, Germany ; accepted in *Physica Scripta*.
- 4 S. Markelj, O. V. Ogorodnikova, P. Pelicon, Th. Schwarz-Selinger, I. Čadež, Temperature dependence of D atom adsorption on polycrystalline tungsten, *Appl. Surf. Sci.* 282 (2013) 478-486.
- 5 S. Markelj and I. Čadež, "Production of vibrationally excited hydrogen molecules by atom recombination on Cu and W materials", *J. Chem. Phys.*, 134, 2011, pp. 124707-1-17.
- 6 V. Žigman, "Non-equilibrium kinetic versus Monte Carlo modelling of hydrogen-surface interactions", *Nucl. Eng. Des.*, 241, 2011, pp. 1272-1276.

REMOVAL OF DEPOSITS BY NEUTRAL OXYGEN AND NITROGEN ATOMS

Miran Mozetič, Alenka Vesel, Aleksander Drenik, Rok Zaplotnik, Gregor Primc

Jožef Stefan Institute, Jamova 39, SI-1000 Ljubljana, Slovenia

e-mail: miran.mozetic@ijs.si

1 INTRODUCTION

Despite moving away from the research topic described in the title of our project, there is still a common theme to our research activities: the interaction of neutral atomic species with solid surfaces. In a large part, this continues to be our research of interaction of atomic species with carbon deposits. This research is performed under the scope of the development of chemical methods of fuel removal. So far, we managed to develop very efficient methods of removal of amorphous hydrogenated carbon (a-C:H) deposits, which were based on the application of atomic oxygen. However, the use of atomic oxygen raised concerns of damage to surrounding plasma facing components (PFCs). In 2012, we started to develop an alternative method, based on the use of active species produced in NH_3 plasma. The initial experiments showed that the method was indeed effective in the removal of a-C:H. In 2013, we managed to demonstrate that it is possible to achieve removal of a-C:H deposits even without ionic species. The method relies only on the interaction of neutral species with the surface, and can thus replace oxidation by atomic oxygen in fuel removal application.

Carbon based PFCs, however, are being phased out of fusion devices, in favour of a full-metal first wall. As carbon is being phased out, new problems linked to a full-metal wall arise. Removal of carbon from a fusion device does indeed strongly reduce the problem of fuel retention, however it also means that in the absence of an intrinsic radiating impurity, the fraction of radiated power is considerably lower. At the same time, the metallic PFCs provide a narrower window of operation and lower resistivity to heat loads[1, 2]. In order to replace the carbon as a radiator, and to reduce the heat loads to divertor surfaces, nitrogen is being seeded into the plasma to promote radiation[3, 4]. While nitrogen was found to successfully replace carbon as a radiating impurity, the introduction of nitrogen gives rise to new physical and chemical processes which are not yet fully understood. The main concern is the formation of ammonia, which could pose as a serious issue to ITER operation[5]. The formation of ammonia is a surface process, involving hydrogen and nitrogen atoms. Since the dissociation threshold of the ammonia molecule is considerably lower than that of nitrogen, the molecules produced in plasma-wetted regions are very likely to be dissociated. Therefore, stable molecules are most likely produced in areas which are not in direct contact with the plasma.

Accordingly, the species that take part in the formation of ammonia are only neutral atoms. The assessment of ammonia production is a fusion relevant topic, as it is being researched at JET and ASDEX-U, however, the technological and operational restraints of the tokamak environment, along with the presence of various hydrogen isotopes and other contaminants make in situ tokamak assessment of ammonia production a very difficult task. In support of the fusion device based research, we have begun the research of ammonia production in laboratory plasmas in hydrogen-nitrogen mixtures.

2 WORK PERFORMED IN 2013

The year 2013 marked an important milestone for our group as we have, for the first time, expanded our research from purely laboratory experiments to participation at fusion devices. Through our involvement in the JET experimental campaign, we are addressing the problem of ammonia formation both from the “real-world” side, as well as by performing isolated studies of the underlying phenomena in a controlled environment of the plasma laboratory. Our involvement at the COMPASS tokamak represents the application of fuel removal methods, that were developed in the laboratory, to deposits from an actual fusion device and finally, to the fusion device itself. Beside these activities, we continue our laboratory based research, such as laboratory experiments with nitrogen-based plasma-surface interaction in collaboration with CIEMAT, Madrid, and dusty plasma experiments at CNRS LAPLACE, Toulouse, however, with the aim of applying the developed methods in the environment of fusion devices as well.

Scavenger Effect Research

The scavenger effect has so far proven to be a promising technique for preventing the formation of a-C:H deposits in carbon-walled fusion devices. It is based on the introduction of nitrogen-based species into carbon-depositing plasmas. The nitrogen species react with the carbon-based species in the plasma volume and form products with a significantly lower sticking coefficient, thus reducing the deposition rate. The efficiency of the method has been proven in the laboratory, however in the environment of a fusion device, it is difficult to distinguish between the reduction of the deposition rate and the erosion of already deposited a-C:H layers by nitrogen plasma species.

The aim of experiments is to determine the erosion rate of a-C:H deposits by N-H plasma radicals. This will aid the evaluation of the efficiency of the scavenger effect in fusion devices. Additionally, the favourable erosion rates indicate that erosion by N-H plasma radicals could also be used to remove a-C:H layers, either during the fusion plasma pulses or in subsequent conditioning.

In 2012, we have conducted an experiment in collaboration with CIEMAT, Madrid, in which we exposed samples of a-C:H deposits to NH₃ plasma, created in an inductively coupled radiofrequency generator. In 2013, we studied the erosion of a-C:H by neutral radicals coming from NH₃ plasma. This was achieved by placing the samples not within the discharge region (i.e. the plasma volume) but further downstream of the plasma, in the late afterglow region. In those conditions, the density of charged particles

is negligible and the active species that take part in the a-C:H erosion are neutral plasma radicals.

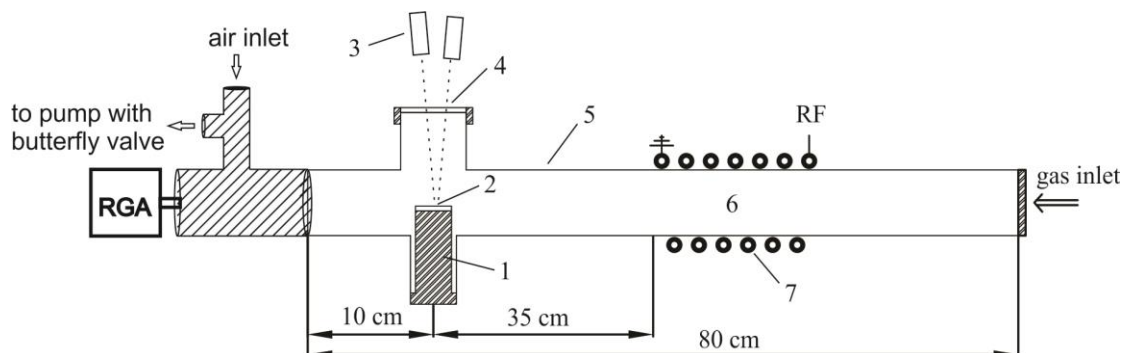


Figure 1: Experimental setup for erosion of a-C:H in the afterglow of NH_3 plasma. Samples (2) are mounted on a temperature controlled sample holder (1). A quartz window (4) allows for the in-situ monitoring of the erosion with a laser interferometry system (3). Plasma is generated in the discharge region (6), with an inductively coupled radio frequency generator (7).

Apart from that, the experimental set up, shown in Fig. 1, was identical to the one used in the experiments in 2012. The plasma was created by an inductively coupled RF generator, in pure NH_3 at the pressure of 50 Pa. The erosion of a-C:H was monitored in-situ with a laser interferometry system. The discharge was characterised with a residual gas analyser (RGA). As the working pressure is an order of magnitude above the pressure limit of RGA operation, the RGA was differentially pumped and connected to the experimental system through a flow-reducer. As a result, the active species formed in the discharge (N, H, NH and NH_2) recombined before they could reach the detector, and only stable molecules (N_2 , H_2 and NH_3) could be detected. However, on the glass surface of the vacuum vessel, H and N atoms recombine in H_2 and N_2 molecules with a significantly greater probability than into the NH_3 molecule. Therefore, the conversion of NH_3 into N_2 and H_2 in the measured mass spectra is a good estimate of the degree of dissociation in the reactor volume. Based on the behaviour of NH_3 conversion versus generator power, we identified two regimes of operation: low dissociation mode (30 % conversion) and high dissociation mode (near 100 %) conversion. The erosion of a-C:H was studied as a function of surface temperature in both modes of plasma operation.

The measured erosion rates, shown in Fig 2, exhibit an exponential dependence on the surface temperature.

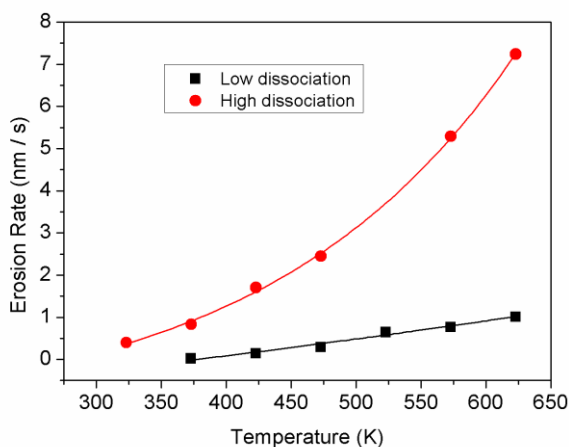


Figure 2: Erosion rates of a-C:H in the afterglow of NH₃ plasma

In the high dissociation mode, the measured erosion rates are an order of magnitude higher than in the low dissociation mode. In the high temperature end, they reach the value of 7 nm/s. At the same temperature, the erosion rate in the low dissociation mode is about 0.8 nm/s. The measured erosion rates are considerably lower than those achieved in the afterglow of O₂ plasma, however a higher density of active species and thus higher

erosion rates could be achieved with higher pressures of NH₃.

Assessment of NH₃ production in plasmas of N₂/H₂ mixtures

Nitrogen puffing into the divertor region is being tested as a way to cool down the edge plasma and thus reduce the heat load on the divertor plasma facing components.

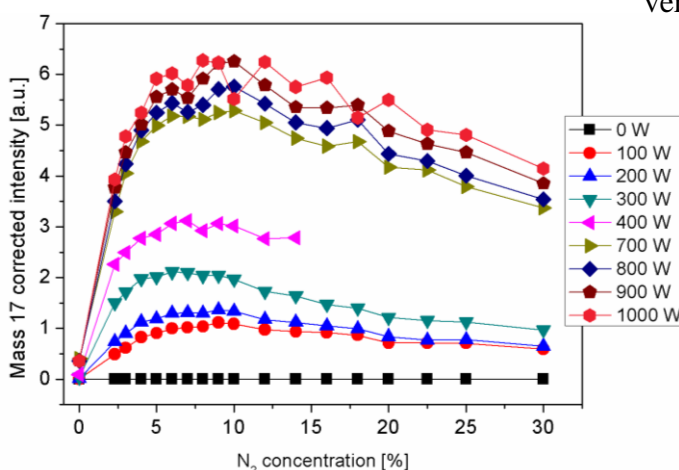


Figure 3: Intensity at 17 AMU in nitrogen – hydrogen plasma. The intensity signifies relative amount of ammonia.

While this is a very efficient procedure, the introduction of nitrogen into reactor vessel gives rise to new physical and chemical processes which are not yet understood. The biggest concern is the formation of tritiated ammonia, which in a D-T fuel mixture would become tritiated ammonia. Because of the relatively high boiling point of ammonia and its affinity to adsorb on metal surfaces, a significant production of stable molecules of ammonia could strongly contribute to fuel

retention in the reactor vessel.

Past experiments at ASDEX-U have confirmed the production of NH₃ during N₂ seeded plasmas, while the results obtained in N₂ seeding experiments at JET have

proven to be inconclusive in the regard of assessment of ammonia production. Because the “real life” environment of a fusion device is too restrictive, the mechanisms of ammonia production have to be studied in controlled laboratory experiments.

Working in collaboration with CIEMAT, we have studied the formation of ammonia in nitrogen – hydrogen plasmas at the Jožef Stefan Institute of Ljubljana. The experiments were performed in a plasma reactor powered by a 1 kW inductively coupled radiofrequency generator. The vacuum chamber which encompassed both the discharge and the afterglow region comprised of a borosilicate glass tube with the inner diameter of 36 mm. Plasma was created in a mixture of N₂ and H₂ with variable ratios. The pressure in the discharge chamber was kept at 50 Pa. The ammonia was detected with a residual gas analyser (RGA) connected to the plasma system.

Figure 3 shows the production of ammonia as a function of N₂ concentration, at different generator powers. The maximum of NH₃ production occurs at approximately 10 vol % of N₂. The concentration of NH₃ in the residual atmosphere of the discharge was two orders of magnitude lower than that of N₂ which indicates that the production of NH₃ on glass walls is rather low. This is further illustrated in Figure 4 which shows the concentration of NH₃ in the residual atmosphere of a discharge created in pure NH₃, at the same discharge parameters as in the N₂ – H₂ mixture. At higher generator powers, the ammonia is completely dissociated into N and H atoms. The N and H atoms subsequently recombine into stable molecules. As the partial pressures of N₂ and H₂ molecules are significantly higher than of NH₃ molecules, we can safely conclude that on a glass surface, the recombination that results in the formation of ammonia is far less likely than the formation of N₂ and H₂.

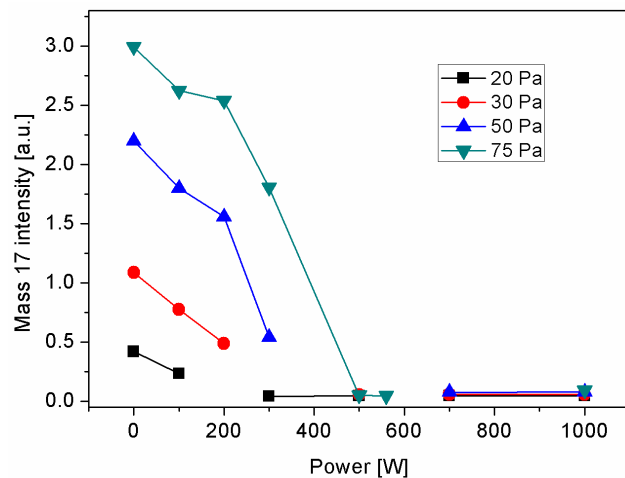


Figure 4: Intensity at 17 AMU in a NH₃ plasma versus generator power. The intensity signifies relative amount of ammonia. At powers above 500 W, almost all NH₃ is converted to N₂ and H₂.

In addition to laboratory experiments, in 2013 we were involved in the research of NH₃ production also in the framework of the C31 and C32 experimental campaigns at JET. Formation of ammonia was studied under designated Task: T13-15: Application of Residual Gas Analysis for nitrogen seeding and Experiment M13-27: Quantification of N retention and ammonia production in nitrogen seeded discharges, however other experiments with nitrogen seeded discharges also provided data.

The main instruments in these studies were residual gas analysers (RGAs) that are operating in the JET subdivertor region and in the pump ducts. However, while the RGAs have been installed and operating at JET for a while, they were not included in the automatic data acquisition system prior to the start of the experimental campaigns. Thus, a considerable effort was exerted in integrating the existing RGAs into the

automatic data acquisition system. While this task is still not yet completely finished, the automated data acquisition is now operational and RGA data is available through the standard methods of data display at JET.

Because JET operates with a D-H gas mixture with a high D concentration, the identification of the ammonia molecule in the mass spectra is difficult as the masses of the molecular fragments overlap with the masses of methane and water fragments. To allow for a more straight forward interpretation of the mass spectra, the experiment M13-27 was performed with the ^{15}N isotope. This way, the fully deuterated ammonia molecule would result in a peak at 21 AMU in the mass spectra which is otherwise unpopulated. However, during the seeded discharges, there was no increased intensity at 21 AMU. The reason for the absence of increased intensity could be in the fact that the rate of seeding was relatively low, but also because the D/H ratio in the ammonia molecule can be heavily influenced by the isotope exchange processes that take place on the surfaces between the area of ammonia formation and the position of the RGAs.

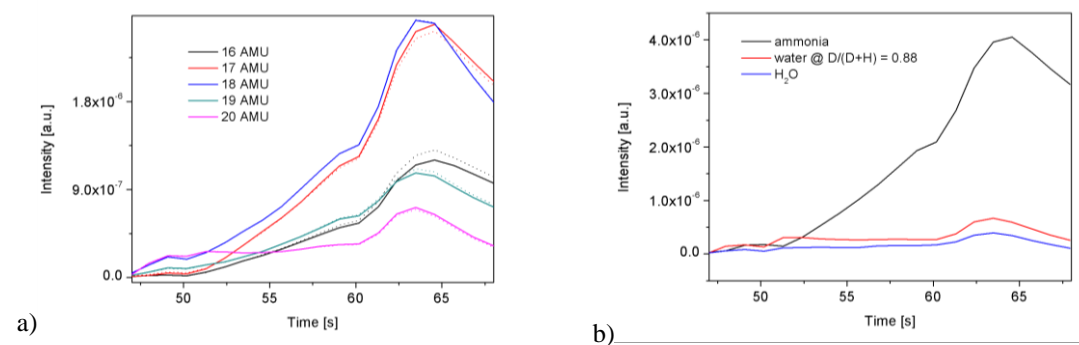


Figure 5: a) JET sub-divertor RGA recording of discrete masses during discharge #84889 (solid lines) and the simulated intensities (dashed lines), b) simulated relative intensities of water and ammonia.

To interpret the RGA data, a method of de-convolution of the mass spectra was developed. It is based on a least-squares fit of candidate molecules to the recorded mass spectra. An example of the de-convolution is shown in Fig 5. The measurements (time traces of intensities at discrete masses) were recorded during a seeding experiment where large quantities of ^{14}N were introduced in the plasma. Despite the high D/H ratio, the nitrogen seeding gives rise to intensities predominantly at 17 and XX AMU, indicating that the D/H ratio in the detected ammonia molecules is considerably lower. The full data analysis is still underway and is expected to be finished in 2015.

*Assessment generation of dust
by chemical methods for
removal of co-deposits*

In 2012, we performed experiments in collaboration with CNRS LAPLACE in Toulouse to assess the generation of dust by chemical methods for fuel removal. In order to simulate a worst-case scenario, we developed a method of depositing a large scale model dusty deposit (MDD). The MDD was produced by deposition with dusty C_2H_2 plasma. It was composed of hard graphite-like grains, embedded in a soft a-C:H matrix. Additionally, the adhesion of the matrix to the surface was poor, making the deposit prone to flaking and cracking at exposure to plasma.

During the deposition of the MDD, we monitored the floating potential. By performing frequency analysis of the floating potential, we found a broad peak at approximately 20 MHz that corresponded with the appearance of dust in the plasma volume, shown in Fig 6. In 2013, we performed additional experiments to further study the behaviour of the peak in frequency spectrum in the floating potential, in the scope of the EFDA ITER Physics Support Task WP13-IPH-A03-P2-02-MESCS-BS.

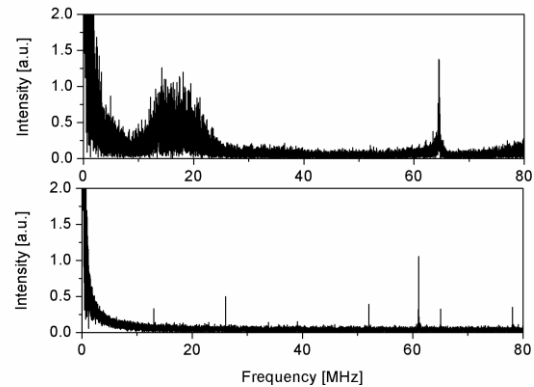


Figure 6: Top: Signature of the dusty discharge in the frequency spectrum of the floating potential – broad peak at 18 MHz; Bottom: The signature does not appear in dustless C_2H_2 plasma.

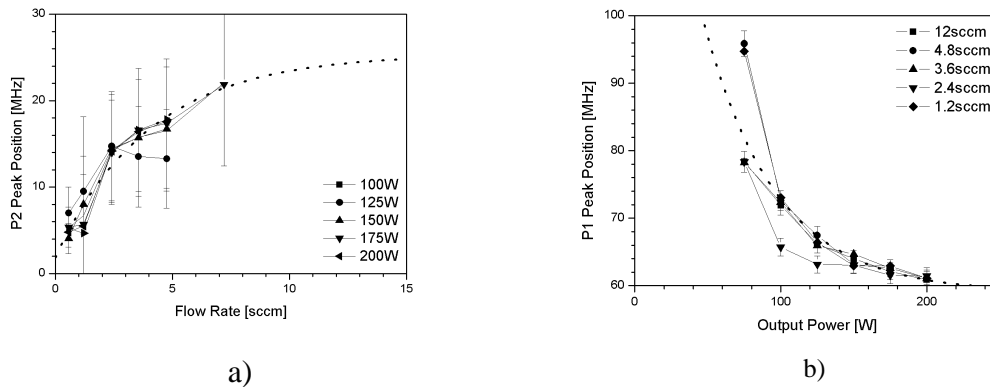


Figure 7: Evolution of a) the broad, 5 – 25 MHz peak and b) the narrow, approx. 60 MHz peak positions with the output power and the acetylene flow rate.

The floating potential was recorded through a scan of discharge parameters (acetylene flow rate and microwave generator power). The central frequency of the broad peak, along with an additional, sharper peak around 60 MHz is shown in Fig 7. The sharper peak is associated to lower hybrid oscillations of hydrogen ions, while the broader, lower frequency peak is associated to oscillations of dust particles in the magnetic field. More data analyses are currently underway, and additional experiments are planned in the following years. However, if the broad peak is indeed linked to the

oscillations of dust particles, the spectral analysis of the floating potential could provide information about the density and charge-to-mass ratio of the dust particles, and could thus be developed into a simple and effective method of dust detection in magnetized plasmas.

Chemical fuel removal methods for use in the COMPASS tokamak

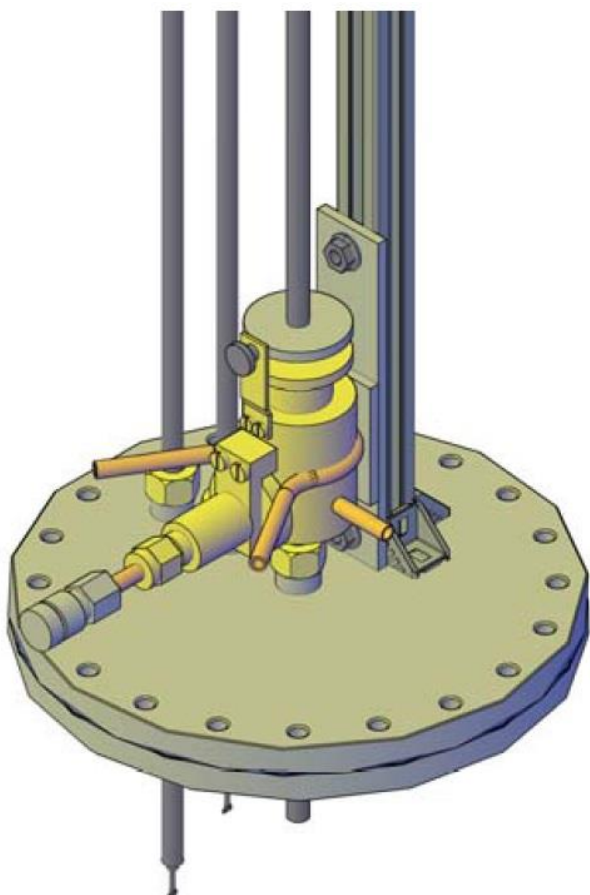


Figure 8: Remote atom source fitted to the flange, developed for use at COMPASS.

In the second half of 2012, we obtained a graphite tile from the COMPASS tokamak limiter. Samples from three regions the tile surface, chosen by visual estimates of a-C:H deposit thickness, were prepared for analyses and fuel removal experiments.

The unprocessed samples were analysed by Auger electron spectroscopy (AES) depth profiling, by X-ray photoelectron spectroscopy and by scanning electron microscopy (SEM). The AES results revealed that samples from all three regions were covered by approximately 200 nm thick boron – carbon layer. The sample from the region with the estimated thickest a-C:H deposit was covered with approximately 100 nm thick carbon layer. Analysis by XPS revealed similar concentrations of B and C on samples from all three regions (approximately 50 at % C and 20 at % B). High resolution XPS spectra showed that carbon was

bound predominantly as graphite and to a lesser extent boride. Boron was bound predominantly as boride with only a small contribution from the B-oxide peak. SEM analyses showed flake-like and layered deposits.

Samples were processed with chemical methods of fuel removal, previously tested on laboratory prepared a-C:H samples. They were exposed to the afterglow of O₂, NH₃ and N₂ ICP plasmas, at the surface temperature of 350 °C, for a total time of 4 minutes. Subsequent analyses revealed that the B concentration at the surface was diminished, however B was still present, indicating that the B-C layer was not completely removed. The most aggressive method (afterglow of O₂ plasma) would result in the removal of approximately 1 µm of laboratory prepared a-C:H deposit, whereas the deposits on the COMPASS samples were reduced by no more than 150 nm.

The topmost a-C:H layer was removed, but the boronisation layer persisted on the surface, indicating that the B-C layer is chemically significantly more resistive than pure a-C:H. In the SEM images, the surfaces of processed samples featured porous structures which indicate selective erosion.

In order to apply the neutral-atom based fuel removal methods at the tokamak itself, we developed a remote atom source, based on a surfatron microwave discharge. The atom source is mounted on a specially prepared CF 150 flange, shown in Fig 8. The

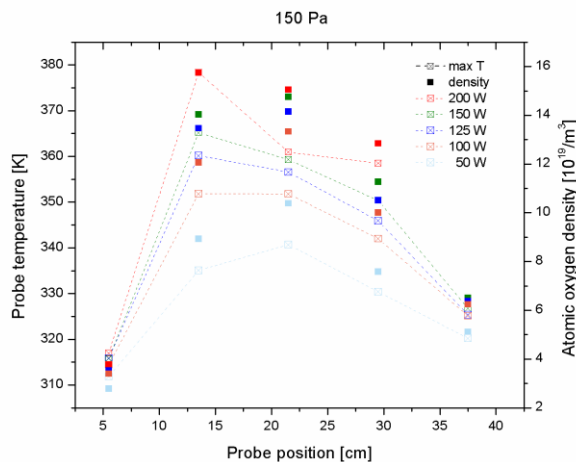


Figure 9: Density profile of atomic oxygen in the large reactor vessel

flange allows for the mounting of a movable catalytic probe, which will be used to measure the density distribution of the oxygen atoms inside the COMPASS reactor vessel. The initial experiments at COMPASS are yet to be performed, however the atom source was tested in the laboratories at IJS. The flange was mounted on a large stainless steel vacuum chamber, pumped by a two-stage rotary pump with the maximum pumping speed of 28 m³/h. The atom source was operating with pure oxygen at different flow rates which resulted in the chamber pressure between 20 and 150 Pa. An example of a measured atomic oxygen density profile is shown in Fig 9. The maximum density achieved by the atom source was $1.6 \times 10^{20}/\text{m}^3$. This is somewhat lower than the densities usually achieved in our laboratory reactors, which bodes lower erosion rates as well. In order to achieve higher atomic oxygen densities, experiments in Ar – O₂ mixtures are planned in 2014.

3 CONCLUSIONS AND OUTLOOK FOR 2014

In 2013, we have for the first time, extended our research of the interaction between neutral atomic species and solid surfaces to the environment of a “real life” fusion device by participating in an experiment of quantification of ammonia production at JET. In parallel to that, we have approached the problem through the isolated study of the ammonia formation in a controlled environment of the laboratory plasma reactor.

Ammonia was also the subject of another experiment we performed in 2013. In continuation of our research began in 2012, we studied the removal of a-C:H with neutral species formed in ICP NH₃ plasma. We managed to show that neutral species alone can be efficient in the removal of a-C:H and could thus be an alternative to atomic oxygen in the application of chemical methods of fuel removal.

Working in collaboration with CNRS LAPLACE, Toulouse, we continued our dusty plasma research. Departing from the original research topic, we studied the frequency spectrum of the floating potential of the C₂H₂ ECR plasma at different values of the discharge parameters. While more data analysis and additional research is needed to fully explain our findings, the initial results indicate that observing the frequency spectrum of the floating potential could be a basis to develop a new, inexpensive and robust method of dust detection in magnetised plasmas.

Our activities linked to the COMPASS mark another instance of the application of laboratory-developed skills, knowledge and techniques to the environment of the fusion device. The application of our fuel removal methods to the samples from a graphite tile from the COMPASS limiter is an important assessment of the efficiency of techniques that were previously tested only in the laboratory environment.

The changes in the European scheme of fusion development funding will inevitably reflect on our future research activities. The research of removal of carbon deposits will be significantly curtailed, dusty plasma research is not foreseen for 2014, nor are there foreseen any laboratory experiments of ammonia formation in the scope of the PFC work package. While we do plan to continue our research, some of them will likely have to be put on hold in the upcoming year.

On the other hand, we will continue to participate at ammonia studies in fusion devices. Besides taking part in the JET experimental campaigns, in 2014 we will participate at experiments of ammonia formation at ASDEX-U in the scope of the MST1 work package. We are planning on analysing and processing more samples from fusion devices and linear plasma devices from fusion research centres, as well as applying some of our laboratory-developed techniques in fusion devices and linear plasma devices. Time has now come to sum up the knowledge gained in the safety of the laboratory and use it in the real world.

4 REFERENCES

- 1 L. Horton and E.-J. Contributors, The JET ITER-like wall experiment: First results and lessons for ITER, *Fusion Engineering and Design*, 2013. 88(6-8): p. 434-439.
- 2 F. Romanelli and J.E. Contributors, Overview of the JET results with the ITER-like wall, *Nuclear Fusion*, 2013. 53(10).
- 3 C. Giroud, G.P. Maddison, S. Jachmich, F. Rimini, M.N.A. Beurskens, I. Balboa, S. Brezinsek, R. Coelho, J.W. Coenen, L. Frassinetti, E. Joffrin, M. Oberkofler, M. Lehnen, Y. Liu, S. Marsen, K. McCormick, A. Meigs, R. Neu, B. Sieglin, G. van Rooij, G. Arnoux, P. Belo, M. Brix, M. Clever, I. Coffey, S. Devaux, D. Douai, T. Eich, J. Flanagan, S. Grunhagen, A. Huber, M. Kempenaars, U. Kruezi, K. Lawson, P. Lomas, C. Lowry, I. Nunes, A. Sirinnelli, A.C.C. Sips, M. Stamp, S. Wiesen, and J.-E. Contributors, Impact of nitrogen seeding on confinement and power load control of a high-triangularity JET ELMY H-mode plasma with a metal wall, *Nuclear Fusion*, 2013. 53(11).
- 4 G. Tardini, R. Fischer, F. Jenko, A. Kallenbach, R.M. McDermott, T. Putterich, S.K. Rathgeber, M. Schneller, J. Schweinzer, A.C.C. Sips, D. Told, E. Wolfrum, and A.U. Team, Core transport analysis of nitrogen seeded H-mode discharges in the ASDEX Upgrade, *Plasma Physics and Controlled Fusion*, 2013. 55(1).
- 5 D. Neuwirth, V. Rohde, T. Schwarz-Selinger, and A.U. Team, Formation of ammonia during nitrogen-seeded discharges at ASDEX Upgrade, *Plasma Physics and Controlled Fusion*, 2012. 54(8).

APPLICATION OF ION BEAM ANALYTICAL METHODS TO THE STUDIES OF PLASMA-WALL INTERACTION IN TOKAMAKS (IBAF)

Primož Pelicon, Iztok Čadež, Zdravko Rupnik, Primož Vavpetič, Sabina Markelj, Matjaž Kavčič, Zvone Grabnar, Mirko Ribič, Anže Založnik

Department for Low and Medium Energy Physics,
Jožef Stefan Institute, Jamova cesta 39, P.O.B. 3000, SI-1000 Ljubljana
e-mail: primoz.pelicon@ijs.si

1 INTRODUCTION

Ion Beam Analytical (IBA) methods are extensively used for diagnostics of plasma facing materials (PFM) and components (PFC) both in various laboratory studies as well as for the post mortem analyses of samples extracted from fusion plasma devices after general or dedicated experimental campaigns (see [1] as a recent example). They are also extensively used for material analyses after its exposure to high density plasma in linear plasma devices and similar high heat load experiments. All this efforts are aimed to enhance understanding and predicting of fuel retention in PFM, PFC modification and life-time determination under realistic conditions, new material development, material erosion and transport to core plasma, material migration and formation of deposits. This last problem is especially important for plasma devices with mixed material composition of PFC such as for ITER-like wall experiments at JET and especially for predicting material migration in ITER.

The goal of the present project is to perform IBA measurements on the samples of interest for EU fusion research program, to continuously upgrade the methods for fusion research at 2MV tandem accelerator at Jožef Stefan Institute (JSI). During this continuous process we have developed and later started systematic use of ^7Li Elastic Recoil Detection Analyses (ERDA) for H and D depth profiling in fusion relevant materials, and recently Nuclear Reaction Analysis (NRA) with ^3He ion beams for deuterium depth profiling by $\text{D}(^3\text{He},\text{p})^4\text{He}$ nuclear reaction. This method has been recently implemented at the chamber for in-situ measurements with broad beam (beam diameter of 1 or 2 mm) as well as on micro-beam (beam diameter in the order of 5 μm). Particle Induced X-ray Emission (PIXE) and Rutherford Back Scattering (RBS) are used in parallel to extract auxiliary information on the sample.

2 WORK PERFORMED IN 2013

Main project objective was to study deuterium depth profiles in samples obtained through the collaboration with CEA and PIIM, France and MEdC, Romania. The objective

was included in two EFDA priority supported tasks and correspondingly represents the main activity within the project in 2013. In addition, application of micro-NRA for the analysis of deuterium in the deuterated flakes / dust was conducted within the project in collaboration with CEA, France.

Temperature dependence of deuterium retention in mixed thin layers relevant for ITER operation.

Mixed material deposits are formed on various surfaces during the operation of fusion devices. Fuel retention in these deposits during their formation and also later after subsequent exposure to discharges is important for predicting the overall fuel balance. Materials used in the largest fusion device ITER are beryllium for the inner wall and tungsten in the divertor area, so the mixed material deposits will mostly consist of these two metals and possibly of seeding (e.g. nitrogen) and intrinsic (e.g. carbon) impurities. The formation of mixed material deposits and deuterium co-deposition is extensively studied by *in situ* and post mortem analyses in tokamaks but also by depositing such layers using laboratory plasmas (e.g. magnetron sputtering) with addition of deuterium.

The main effort during 2013 within the present project was devoted to studies of mixed material layers within priority supported task »Analyses of the deuterium trapping in mixed materials«, WP13-IPH-A01-P3-01/MESCS/PS in EFDA's Work Program for 2013. This activity was performed in close collaboration with MEdC, Romania. The goal of this work was to contribute to the quantification of the influence of seeded and intrinsic impurity species on D-retention/release. In addition, the investigation on Al as a proxy for Be was undertaken. The goals were:

- a) Quantification of the mixed layers (including also Be mixed layers) provided by MEdC and the depth profiles of D retained in these layers by RBS and NRA at JSI,
- b) Determination of temperature dependence of D release by *in situ* NRA in W:C and W:C:Al based mixed layers and bi-layers. Further on, similar study extended to W-based layers containing Be and the influence of seeding (N) and intrinsic impurity (C) species on D retention.

We have experimentally studied mixed material samples (Al used as a Be proxy in some samples) by two kind of experiments. The first is thermal desorption (TD or TDS, S for spectroscopy) of deuterium from samples with co-deposited D using *in situ* NRA and RBS. In the second approach, the deuterium free samples were exposed to deuterium atomic beam and deuterium uptake (DU) was quantified *in situ* by combination of NRA and RBS. Sequentially, TDS was applied at the end of experiment. In both types of measurements vacuum composition was monitored by mass spectrometry.

The following measurements were performed:

- i) Deuterium thermal desorption from mixed materials C-W (D₂), C:W:Al (D₂), and from Be (D₂) layer on C and Si substrate by *in situ* NRA and mass spectrometry.
- ii) Deuterium uptake by multilayer C:W:C film (200 nm of C on 500 nm of W on C substrate), and mixed materials W:Al/Si, W:Al(N₂)/Si, W:Be(N₂)/Si under exposure to D-atom beam and subsequent TD.

All samples studied in the present task were prepared at MEdC by depositing thin layers on C or Si substrate by Thermionic Vacuum Arc (TVA) method [2]. Co-deposition of D or N in the layers was achieved by performing layer deposition under the low pressure D₂ or N₂ atmosphere in the vacuum chamber.

Deuterium thermal desorption during linear sample heating was monitored *in situ* by Nuclear Reaction Analysis (NRA) and by mass spectrometry. The depth profile was measured (five ion energies of ³He beam) before and after the thermal desorption. For deuterium measurement the ³He ion beam is used inducing nuclear reaction D(³He,p)⁴He [3]. The deuterium depth profile is obtained by analyzing the energy distribution of protons created by this nuclear reaction. For the detection of protons a 1500 μm thick proton detector (NRA detector) was mounted at the angle of 135° in the vacuum chamber with 24 μm Al absorber placed in front of it in order to stop the backscattered ³He ions and to block the visible light. Second detector was placed at the angle of 170° for detecting the backscattered projectile particles (RBS detector), giving the information about species in the material that are heavier than ³He. The elemental concentration depth profiles are obtained from NRA and RBS spectra by using SIMNRA program [4]. During the linear sample heating, used for TD, the NRA spectra were recorded using 2.5 MeV ³He beam. This energy was chosen due to several reasons: i) the beam goes through the layer, providing an integral signal from D, ii) proton peaks from nuclear reaction between ³He and ¹²C are also visible in the NRA spectrum, giving the information about C content in the layer and iii) the Rutherford Backscattering signal is well resolved. The sample was heated by a heater (Boralectric heater) and its temperature was computer controlled and monitored by a thermocouple attached to the sample surface by a sample holding clamp.

Mass species, desorbed from the sample, were detected by a mass spectrometer (PrismaPlus, Pfeiffer, 1 - 100 amu/q) during approximately linear sample heating. During the heating, concentrations of several masses were followed including masses 2, 3 and 4 which correspond to H₂+D, HD and D₂ ions, respectively. The base vacuum pressure in the vacuum chamber was about 1×10⁻⁷ mbar.

The atomic hydrogen (H or D) beam was used in the case of deuterium uptake studies. Atoms are created by thermal dissociation of hydrogen molecules in a hot capillary of a hydrogen atom beam source. The average D flux density at the probing ion beam position was (4.5 ± 0.1)×10¹⁸ D/m²s.

An example of thermal desorption study is shown on C:W mixed layer, 1.5 μm thick on Si substrate, with deuterium co-deposited during sample preparation. We made two experiments with two almost identical samples #1 and #2. The mixed layer in both samples had approximately 6 atomic % of W and 93 atomic % of C as measured by RBS, yielding approximately 1:1 mass ratio. The concentrations of C, W and D are not homogeneous over the layer's depth. The deuterium depth profile was measured by NRA before and after the sample heating. The comparison of the deuterium concentration in samples #1 and #2 before the heating is shown in Fig. 1, having almost identical deuterium concentrations depth profiles. Mean deuterium concentration in the pristine layer is about 1 atomic %. This is not typical for W, where deuterium concentrations below 1 at. % are usually obtained in different tungsten grades exposed to plasma. On the other hand, the hydrogen (deuterium) content in plasma-deposited amorphous hydrogenated carbon layers may exceed 30 at. % .

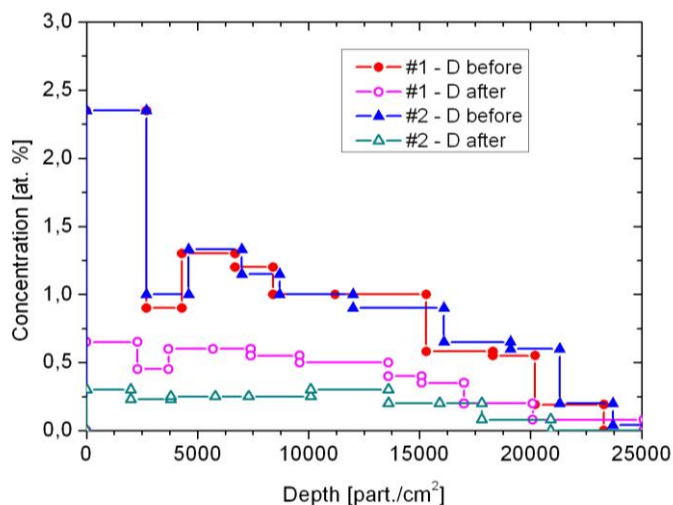


Figure 1: Deuterium depth profile measured in C:W mixed layer for two samples (#1 and #2) before and after the linear heating.

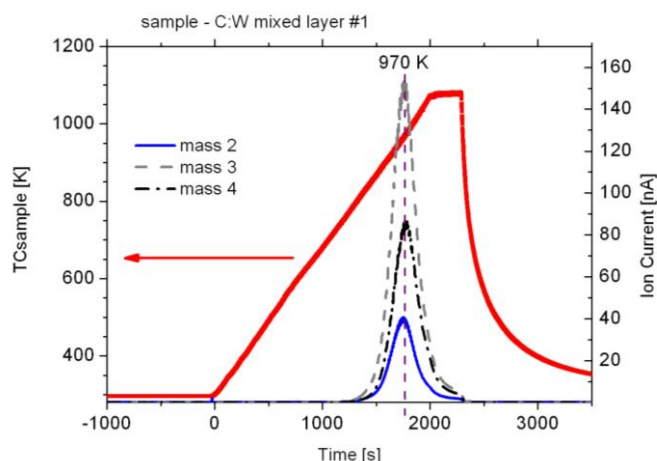


Figure 2: Linear heating of the sample C:W #1, heating rate 23 K/min. Time variation of the sample temperature and ion signal for M/q 2, 3 and 4 measured by the mass spectrometer.

After the depth profile analysis the sample #1 was heated linearly with constant heating rate of 23 K/min. During the heating several masses were followed with the mass spectrometer. Ion current at M/q equal 2, 3 and 4, attributed to H₂/D, HD and D₂ ions and the sample temperature are shown in Fig. 2 as a function of time. The main desorbing specie was mass 3, followed by mass 4 and 2 all having one main desorption peak at 970 K. Since desorption is similar for all three masses one could doubt that the signal is coming from the sample. Mass 3 (HD) had the highest desorption peak, meaning that there is beside deuterium also hydrogen in the layer. After the heating, the deuterium depth profile was measured again, shown in Fig. 1. About half of deuterium still remained in the layer, being distributed over the whole layer. We have repeated the experiment on sample C:W #2, that had the same properties as the first sample. The experimental procedure was somehow modified with respect to the first sample and during the sample heating the NRA signal was recorded at single ³He ion energy, 2.5

MeV. The integral of the proton peak from the nuclear reaction gives information about the total content of the deuterium in the layer. At first the sample was heated to 970 K very fast, heating rate 120 K/min, and then again with slower heating rate of 15 K/min up to 1170 K. There were two main NRA signal decreases, which can be also correlated to the desorption peaks measured by the mass spectrometer. First decrease was during the first ramp, where maximum of desorption was at 930 K, and the second one was during the second ramp with peak maximum at 1040 K. The temperature of the desorption peaks for samples #1 and #2 are in good agreement, where the difference in temperature could be due to the different heating rates. The NRA signal decrease is 32% of the initial signal during the first ramp and during the second ramp the remained signal drop is 60%. The depth profile for C:W sample #2 after the thermal desorption is shown in Fig. 1. The deuterium concentration is approximately half smaller than in the case of sample #1, but still about 0.25 at. % of deuterium remained in the sample.

Another experiment is shown in figures 3 and 4. Here a TD from mixed material sample C:W:Al with co-deposited deuterium is shown. Here one can observe that some amount of D remain in the sample even after heating above 1000 K (figure 4) and time evolution of deuterium release during heating as monitored by the integral signal from NR protons at 2500 keV ^3He beam energy is shown in figure 5.

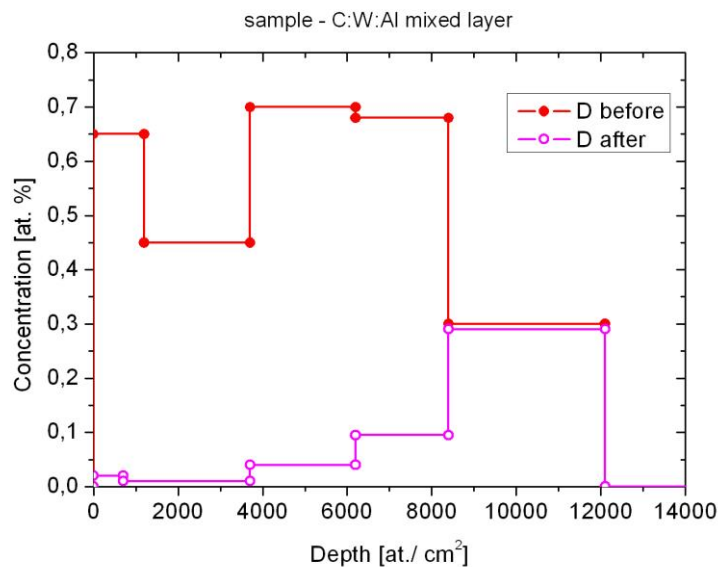


Figure 3: Deuterium depth profile measured by NRA in C:W:Al mixed layer before and after the linear heating.

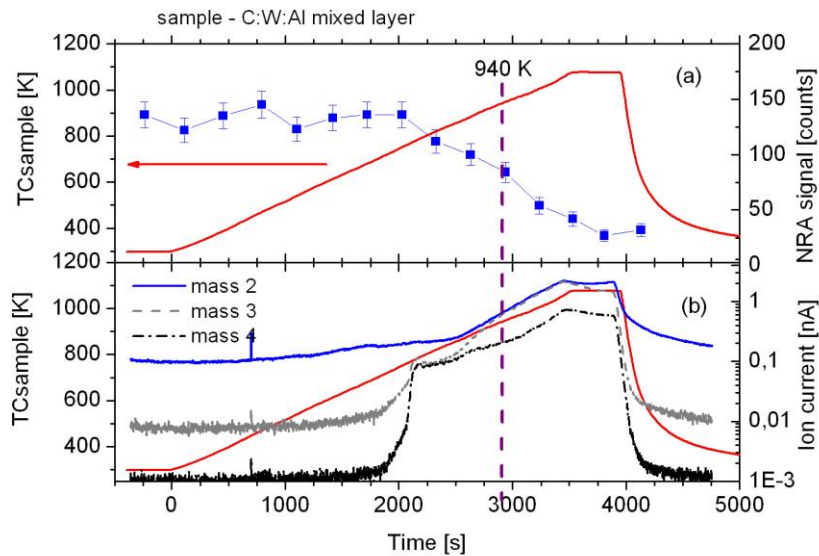


Figure 4: Heating of the C:W:Al mixed layer. a) Integrated NRA signal at 2.5 MeV ^3He beam energy and b) ion signal of masses 2, 3 and 4 are shown as a function of time. On both graphs sample temperature is also shown, heating rate 13 K/min

In an attempt to examine the influence of nitrogen as a probable constituent in mixed layers and compare Al as a proxy for Be we have studied three, initially deuterium free, samples of mixed materials deposited on Si:W:Al (1 μm thick), W:Al(N₂) (1 μm) and W:Be(N₂) (100 nm). These samples were first characterised by RBS and then exposed to D-atom beam for 20 hours. Sample temperature was 100°C during exposure in order to minimize possible impurity build-up. After exposure the D depth profile was determined by NRA using the above described procedure.

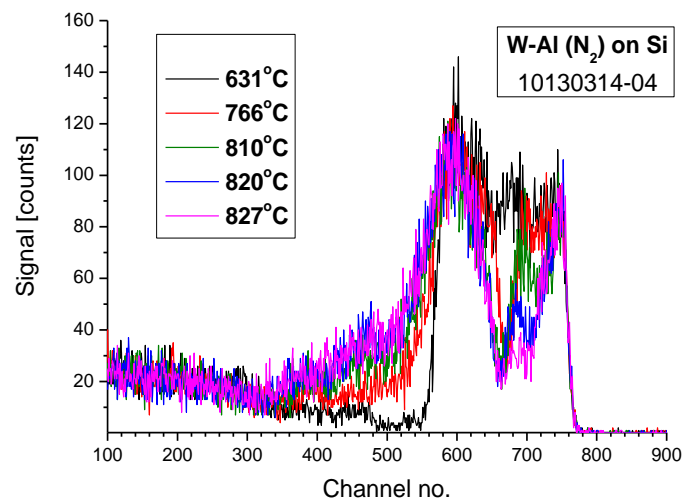


Figure 5: RBS spectra showing important modification of W-Al (N₂) layer during TD following sample exposure to D-atom beam.

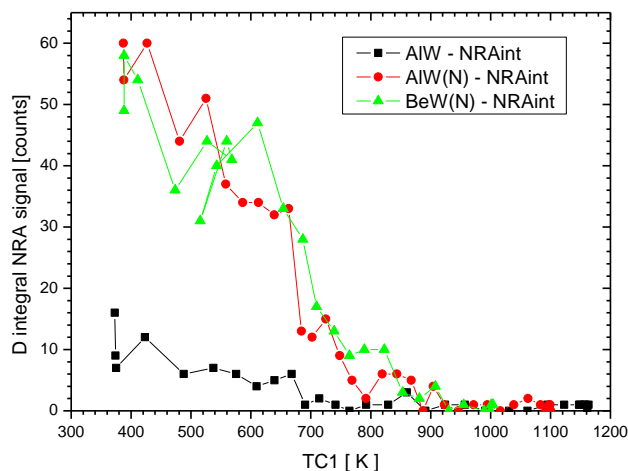


Figure 6: Deuterium TD signal (integral signal over the NRA proton peak using 2.5 MeV ^3He beam energy) following 20h exposure to the D-atom beam for three sample layers on Si substrate. Samples produced in nitrogen atmosphere are labelled with (N).

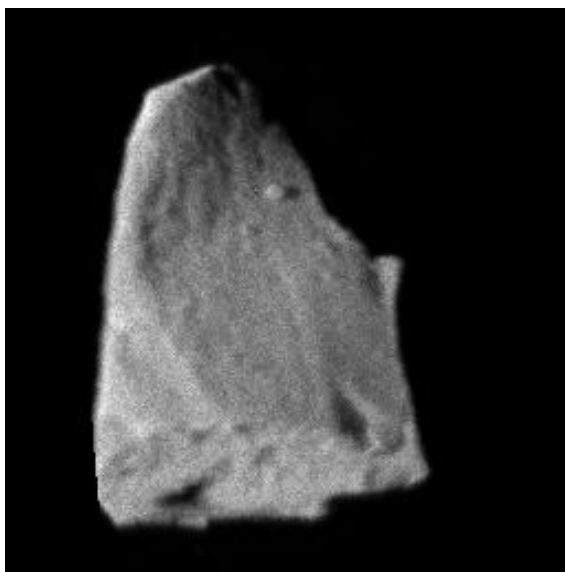
After this the in situ TD was performed by sample heating with the rate of about 13 - 15 °C/min. NRA and RBS spectra were sequentially accumulated using 2.5 MeV ^3He beam and set of mass peaks were monitored during temperature ramping. Examples of the results for these layers are shown in figures 5 and 6. From RBS spectra presented in Fig. 5 one can observe strong modification of the structure of mixed layer during heating after its exposure to atomic deuterium. This modification is evident even by its visual appearance. Another important observation is increased deuterium uptake of the samples deposited in the presence of nitrogen, Al:W vs. Al:W(N) in Fig. 6. The third shown case corresponding to Be:W(N) cannot be directly related to the other two due to its smaller thickness but it is indicative of the presence of high D-content. For all three cases similar thermal release is obtained.

All the planned work within the WP for the described EFDA task was done with part of NRA and RBS spectra remaining to be analysed and results published. A part of these results was presented at a conference and published in conference proceedings [5]. More studies with symmetrical layers containing Al and Be is needed to draw firm conclusions on usefulness of Al studies as proxy for Be.

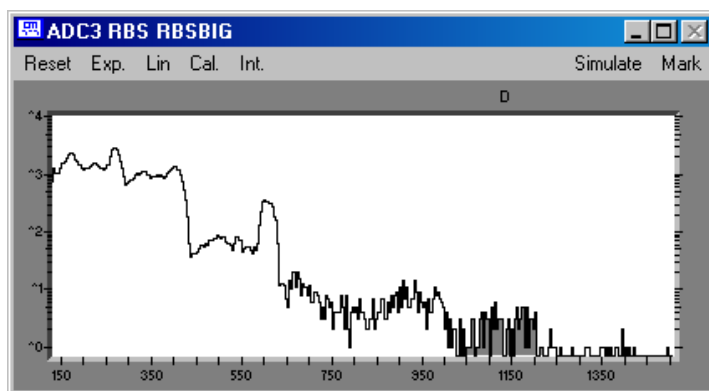
Application of Micro-NRA for the analysis of deuterium in the deuterated flakes / dust

The above mentioned NRA method based on the $\text{D}(^3\text{He},\text{p})^4\text{He}$ nuclear reaction was applied also at micro-beam experimental station at another beam-line of JSI Tandatron accelerator. The initial narrow ion beam well defined by two slits is focused by strong triplet lens to the micrometer sized probing beam which is directed to a studied sample. By proper bending system beam can be scanned over the sample so that detailed 2D maps can be obtained using various available detectors. Using this technique with ^3He incident ion beam and thick Si detector for high energy protons we have studied deuterium content in small particles and flakes. Measurements were performed of deuterium concentration on tungsten micro-particles deuterated in plasma reactor Casimir at CEA using 4.5 MeV incident beam energy. Image of the tungsten

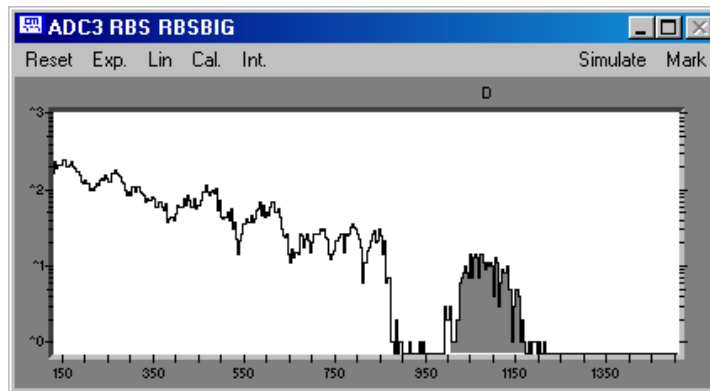
distribution in studied particle is obtained by detecting characteristic W $L\alpha$ X-rays induced by ^3He ion impact – (3HIXE technique). Such image is shown in Fig. 7a and it provides information on overall shape of the studied sample (dominantly W). The integral NRA spectrum recorded simultaneously with 3HIXE image recording is shown in Fig. 7b. The contribution in the spectrum due to deuterium is shaded. In order to enable quantification of the NRA signal the standard a-C:D thin film is used and corresponding spectrum recorded under identical conditions is shown in Fig. 7c.



a)



b)



c)

Figure 7: Micro-NRA analysis of tungsten particle deuterated in Casimir reactor using 10 micrometer dia. 4.5 MeV ^3He ion beam at JSI. a) Image generated from ion-induced W La X-rays. The size of the frame is $2 \times 2 \text{ mm}^2$. b) Simultaneously recorded spectrum obtained by NRA detector -deuterium signal is shaded. c) NRA spectrum recorded under identical conditions using reference a-C:D on Si used for calibration of NRA spectra –deuterium signal is shaded.

The reconstruction of the deuterium retained in the particle needs to take into account the particle topography, which is demanding task and currently in progress.

Other activities

The upgrading of the beam line for broad beam NRA/RBS/ERDA experimental chamber was initiated in order to enable homogeneous sample irradiation by high energy ions in order to allow studies of synergic effects of helium on the hydrogen retention.

3 CONCLUSIONS AND OUTLOOK FOR 2014

In previous years we have done substantial progress on development of experimental techniques based on IBA methods enabling efficient studies of material properties related to fusion development. Particularly important qualitative breakthrough was done in 2012 when system upgrades provided highly efficient use of ^3He beam for NRA, bringing the associated costs connected with the price of ^3He gas to sustainable level. This is the reason that in 2013 a high fraction of total accelerator beam-time was dedicated to the fusion-related studies. These were mainly performed on the broad beam NRA/RBS/ERDA experimental station also described in report on the project 1.4.1. What concerns new development of the accelerator facility for future studies we have undertaken modification of the broad-beam beam-line in order to allow dual beam irradiation of the sample. This is needed for studies of ion damage of materials and its influence on hydrogenic retention.

Our work in 2013 was mainly dedicated to the second objective from project's WP which was supported by EFDA through preferentially supported task »Analyses of the deuterium trapping in mixed materials«, WP13-IPH-A01-P3-01/MESCS/PS. We have well developed experimental procedures for systematic studies of deuterium release from mixed material samples using powerful *in situ* NRA-thermal desorption

technique. On this way we have studied release of deuterium from layers with co-deposited D: C:W(D)/Si, C:W:Al(D)/Si, Be(D)/C, Be(D)/Si in order to evaluate the influence of layer composition to deuterium retention. In addition the D-uptake by initially D-free mixed layers (C:W/C, Al:W/Si, Al:W(N₂)/Si, Be:W(N₂)/Si) was studied by *in situ* NRA during exposure to D-atom beam and subsequent thermal desorption. Pronounced influence of nitrogen impurity on D-uptake was observed. All mixed material samples were provided by MEdC. Objectives for this task as defined in the WP2013 were accomplished and further activities well prepared. Continuation of close collaboration with MEdC and other laboratories is foreseen. There was no particular activity on static NRA measurements of deuterium in tungsten as no special interest for this was expressed by EFDA and other partners. NRA studies on micro-beam performed in 2013 have shown the possibility of this powerful method and also its limitations due to the low NRA signal. Such studies, being very demanding regarding measurement time and data analysis, have to be well targeted to particular cases of high importance.

We plan to extend *in situ* D-retention studies by TD and DU methods applied for the first time in 2013. Extension of such studies on isotope exchange is very promising. Systematic studies on standardized sets of mixed material layers relevant for fusion experiments deposited with or without presence of seeding impurities are planned to be performed in 2014. This work will be continued within the new framework of EUROfusion program.

4 REFERENCES

- 1 M. Rubel et al., "Tungsten migration studies by controlled injection of volatile compounds", *J. Nucl. Mater.* **438** (2013) S170 – S174; H. Bergsaker et al., "Microanalysis of deposited layers in the divertor of JET following operations with carbon wall", *ibid.* S668 - S672.
- 2 C. P. Lungu et al., "Beryllium coatings on metals for marker tiles at JET: development of process and characterization of layers", *Phys. Scr.* **T128**, 2007, pp. 157–161.
- 3 V. Kh. Alimov, M. Mayer and J. Roth, "Differential cross-section of D(3He,p)4He nuclear reaction and depth profiling of deuterium up to large depths", *Nucl. Instr. and Meth. in Phys. Res. B* 234, 2005, pp. 169-175.
- 4 M. Mayer, SIMNRA User's Guide, Report IPP 9/113, Max-Planck-Institut für Plasmaphysik, Garching, Germany, 1997. <<http://www.rzg.mpg.de/~mam/>>.
- 5 S. Markelj, I. Čadež, P. Pelicon, P. Vavpetič, C. Porosnicu, C. Lungu, "Deuterium Thermal Desorption From Mixed Layers Relevant for ITER", Proceedings from 22nd Int. Conf. on Nuclear Energy for New Europe (NENE2013), Bled, Slovenia 9.-11.9.2013, Paper no. 1405.

PERMEATION MEASUREMENTS OF MIXED Be/W LAYERS ON EUROFER

Vincenc Nemanič, Marko Žumer

Jožef Stefan Institute, Jamova 39, 1000 Ljubljana, Slovenia
e-mail: vincenc.nemanic@ijs.si

1 INTRODUCTION

Beryllium and tungsten will be used for the first wall of ITER. Thermal load and ion impact will induce tritium retention in mixed deposits of tungsten and beryllium. So far, as follows from a literature survey, a few reported data on investigation of such mixed layers exist, [Skinner 1, Doerner 2]. Mixed materials were also investigated as Be films on W substrate, but they have rarely been investigated as mixed layers as may be formed in ITER during the operation. The missing knowledge of their possible interaction with hydrogen isotopes is thus searched by using various experimental techniques.

Hydrogen in metals represents a complex two element interaction system as the lattice may have any form extending from a well-structured mono-crystal to nano-crystalline metal. It is known that stable tungsten beryllides Be_2W , Be_{12}W , Be_{22}W can be formed, but generally non-stoichiometric alloy is supposed to be formed in fusion reactors. Accordingly, hydrogen (H/D/T) may occupy a single-energy-type interstitial site of the mono-crystal or any type of defects which represent sites for a single H atom with different binding energy. Beside single occupation interstitial or defect-induced sites, metal vacancies may be present in the disordered lattice. Each may be occupied by several H atoms and the term super-abundant vacancy (SAV) was launched in theory. Their role influencing metal properties has also been calculated recently. Grouping of vacancies into clusters was also predicted which further complicates experimental evidence of SAV. In general, sophisticated experimental techniques are needed to determine contribution of defects and SAV on observed hydrogen mobility. Classic permeability measurement of gaseous hydrogen through bulk specimens is a suitable complementary method to determine its mobility. Unfortunately, macroscopic sizes and thicknesses of samples with low hydrogen diffusivity result in extremely low permeability which is beyond the detection limit of present day experimental technique. The same technique using a “duplex membrane” simplifies the experiments as thin W or Be/W films with desired micro-structure can be prepared on a highly permeable substrate much easier than bulk W samples [3,4,5]. Fortunately, Be/W deposits will be formed as thin and disordered layers which makes our data even more relevant, initially mainly for JET as well as later on for ITER.

In 2013, precise hydrogen permeability measurements combined with long term outgassing rate measurements were continued from 2012 for pure tungsten and Be/W films, both deposited by thermionic vacuum arc (TVA) method in the laboratory of dr. Cristian Lungu at National Institute for Laser, Plasma and Radiation Physics, NILPRP, Romania. This deposition method gives a specific film microstructure and morphology which was characterized by various techniques, AFM, SEM, XPS and XRD. Most of experimental data points for permeation measurements which lasted at least 24 hours were obtained at 400 °C.

2 WORK PERFORMED IN 2013

Hydrogen outgassing followed by permeation through pure W films deposited by thermionic vacuum arc (TVA) technique on Eurofer substrates was investigated as this data was required to get a reference in the sense of the expected range for Be/W films deposited by the same method. Pure Be films, deposited also by the TVA method, have been investigated previously. The correlation between permeation flux and W film morphology was searched first. W surface was characterized by various surface sensitive techniques while the XRD was applied for determination of average grain size. The results were then applied in further studies for Be/W films, deposited by the TVA technique. Complementary SEM, XPS, XRD, AFM methods were applied for characterization. This report is related to 4 samples on pure W films and 8 samples with Be/W films. As the complex and mutual dependence of film nanostructure and additionally beryllium high chemical activity on overall observed permeation properties, all samples were deposited with the same thickness of 8 µm and in atomic ratio Be:W = 3:1.

2.1. Experimental

Sample preparation and experimental procedure

The base substrate material on which we applied the coating was the reduced-activation tempered martensitic steel Eurofer with the chemical composition (wt. %): 0.11 C, 8.7 Cr, 1.0 W, 0.10 Ta, 0.19 V, 0.44 Mn and 0.004 S, balance Fe. The steel was supplied in the form of a 100-mm diameter bar by Forschungszentrum Karlsruhe GmbH, Karlsruhe, Germany, in the normalized plus tempered condition, i.e., 980 °C/110 min plus tempering at 740 °C/220 min/air-cooled. The reason for selecting this special grade of steel are: a) it is well characterized in the last few years for interaction with hydrogen and b) it has extremely high permeability for hydrogen at elevated temperature and c) good mechanical properties which enabled simple machining as smooth substrates had to be prepared for this study.

All films were prepared by means of TVA at stated conditions: anode-cathode voltage; 1400V, anode-cathode current: 1.90 A, substrate temperature: 400°C, substrate bias related to the ground; -400 V. Four equally prepared substrates were deposited by pure tungsten: **Sample 1** was deposited in 14.5 h, with the film thickness equal to 4.1 micrometers. **Sample 2** was deposited in 16.75 h with the film thickness equal to 2.7 micrometres. **Sample 3** and **Sample 4** were deposited in the same run in 25.5 h, with the film thickness equal to 4.2 micrometres. The last value implies a medium deposition

rate of ~ 0.0457 nm/s. Pressure in the chamber was $\sim 1 \times 10^{-5}$ mbar. Be/W films were prepared at similar conditions from two different sources simultaneously.

Membranes were sealed in the permeation cell by two Au 0.6 mm thick O-rings. The resulting hydrogen exposed area was 8.4 cm^2 . The film was oriented into the upstream chamber. The setup is assembled from all-metal UHV components applying gas accumulation technique described elsewhere [3].

The initial phase in both measurements was a slow warm-up stage to reach $400 \text{ }^\circ\text{C}$ in 2 hours and the next 4 hours were allowed to expel hydrogen from the membrane and the cell. The downstream chamber was then valved-off for 10 to 30 minutes to accurately record the background pressure rise slope. Then, the upstream chamber was valved-off too and hydrogen was rapidly introduced. Accumulated gases were analyzed by the QMS in the separate chamber each time just before they were pumped out. Hydrogen represented the main species with traces of CO and CO₂. In addition, transients of hydrogen kinetics at the downstream side after upstream pressure changes were followed directly by the QMS.

For all measuring campaigns with the tungsten coated membranes, the time to reach a steady permeation flux was substantially longer than 6.5 s, which is the characteristic time of bare membranes [3]. In our former studies, we found out that processes on the surfaces and within the tungsten film caused some further slow drift of the permeation flux value. For this experiment, the hydrogen permeation flux was recorded for 24 h while keeping the upstream pressure at 1 bar and $400 \text{ }^\circ\text{C}$ when films had been stabilized. After hydrogen removal, the membrane was pumped on both sides for 1 h, the valves were closed and pressure dependence of the permeation flux was recorded.

The response of the permeation rate to the step change of the upstream pressure may give some additional data about the mechanism of hydrogen transport through the film. This information is important since the formalism to apply experimental data assumes that the diffusion is the rate limiting process of the permeation. The first experimental proof is made by plotting recorded steady flux density values j versus the square root of the upstream pressure. The relation should give a linear dependence of j vs. $p^{0.5}$, which is called the Sieverts law. The second proof is obtained by comparing the time response. Each new steady j should be achieved within the same time after the upstream pressure had been changed. For even higher accuracy, besides recording dp/dt by the capacitance manometers in suitable time intervals, hydrogen signal for some samples was measured continuously also by the calibrated QMS.

Four new samples of Be/W films were investigated by the same hydrogen permeation technique, each sample required 2 days of UHV system conditioning, while the permeation evaluation lasted at least 24 h at 400°C and for some samples additional 48 h.

Complementary sample investigation methods

The X-ray photoelectron spectroscopy (XPS) measurements were performed in the XPS spectrometer PHI-TFA XPS with monochromatic X-ray source. Survey and

high energy resolution spectra were acquired on as-received sample 2 in order to identify elements on the surface and to evaluate the oxide layer thickness.

Atomic force microscopy (AFM) was conducted by the AFM microscope model Solver PRO P47 produced by the MTD-NT company. Surface morphology was recorded in semi-contact mode over an area of 5 x 5 micrometers on different locations across the same sample. After proper background subtraction the roughness parameter Ra was calculated.

Scanning electron microscope (SEM) JSM6500F was used for an additional imaging the W surface at various locations across the same sample.

3 RESULTS

Results of XPS, AFM and SEM on pure W surface

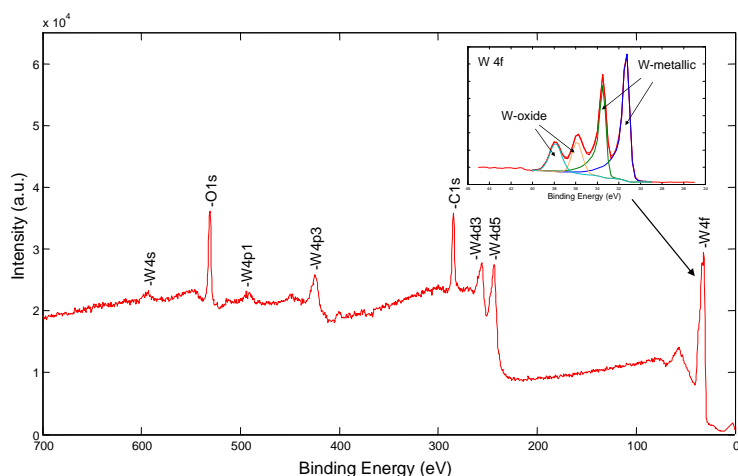


Figure 1: XPS survey spectrum of the W coating. Inset in the figure shows the W 4f peak which is composed of two doublets originating from W-oxide layer and W-metallic coating.

The XPS spectrum (Figure 1) obtained on the surface of the W-coating shows peaks of O 1s, C 1s, W 4f, W 4d and W 4p. From detected peaks the surface composition was calculated to be 46 at.% of C, 31 at.% of O and 23 at.% of W. Carbon C 1s signal originates from adsorbed carbon based contamination. Oxygen O 1s signal may be also partially related with the adsorbed layer but its main origin is a thin W-oxide layer. Inset in Figure 1 shows high energy resolution spectrum of W 4f in which doublet with W 4f_{7/2} peak at 35.9 eV is related with W(6+)-oxide layer and a doublet at 31.3 eV is related with metallic W atoms. In order to determine the thickness of W-oxide layer we compare intensities of these two doublets using the regular procedure. In this way we determined that the W-oxide layer is (0.4 ± 0.2) nm thick, what means that oxide layer is in the range of a monolayer.

Morphology of the W-coating deposited on the Eurofer substrate, which was characterized by FM and SEM, shows similar features. Corresponding images are shown in Figure 2. The surface is uniformly composed of small plate-like crystallites of three angular shapes. From AFM image we calculated the Ra roughness to be (30 ± 3) nm measured over area of 5 x 5 microns.

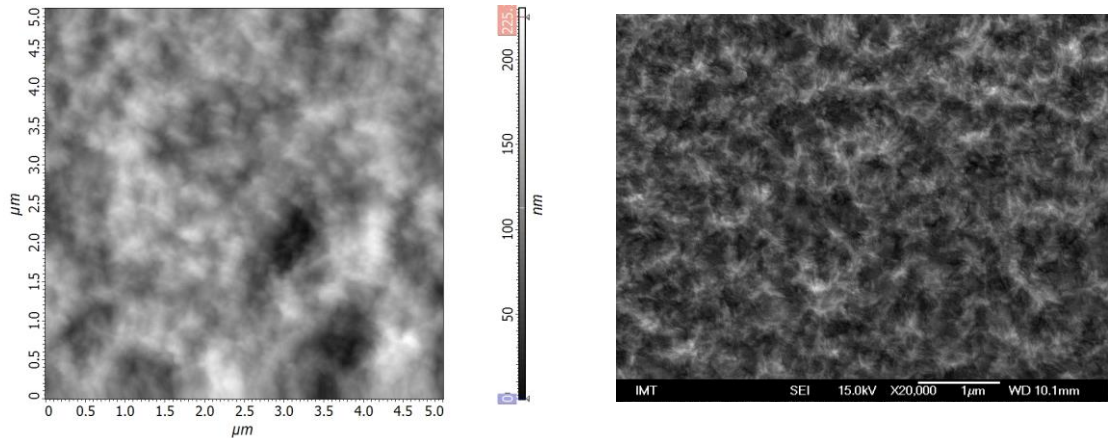


Figure 2: AFM (left) and SEM photo (right) of W surface of sample 2 show very similar texture.

Results of XPS,AFM and SEM on Be/W surface

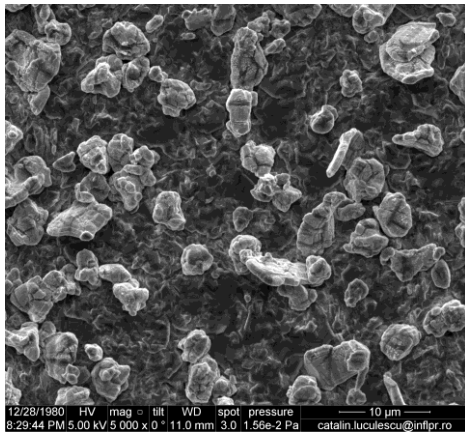


Figure 3: Be/W surface exhibits different morphology than pure W in Fig.2. The contrast on grains is related to poor sample conductivity and does not express different grain composition.

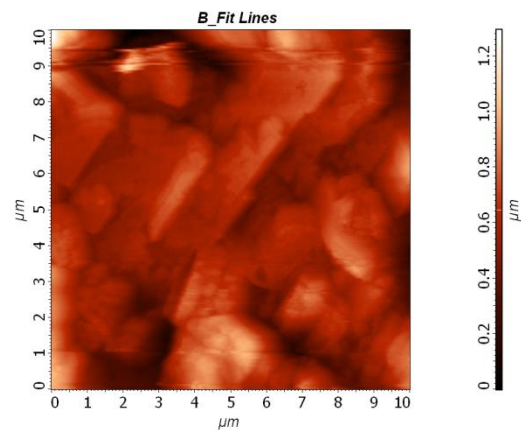


Figure 4: A detail of Be/W film on Eurofer as recorded by AFM.

Results on permeation measurements on pure W films

Identical bare 0.5 mm thick Eurofer membranes have been formerly investigated since a good reference for evaluation of W films was needed [1]. The high diffusivity and permeability of clean bare membranes is manifested in fast response to hydrogen exposure; high steady flux $\sim 1.12 \times 10^{-5}$ mol H₂/m²s is established at 400 °C at 1 bar. This value allows evaluation of the PRF of all coated samples. Time-lag for bare substrate was ≈ 6.4 s. Both these data were recorded after the sealed membrane had been outgassing for some hours at 400 °C. The results on Sample 1 and sample 2 at 400 °C are presented in Table 1.

	thickness	PRF	L_2	P_W (24 h)*	D_W	S_W
	μm	24 h	s	$\times 10^{-15} \text{mol H}_2 / (\text{m s Pa}^{0.5})$	$\times 10^{-15} \text{m}^2/\text{s}$	$\text{molH}_2/\text{m}^3 \text{Pa}^{0.5}$
sample 1	4.1	5.9	40	32	213	0.085
sample 2	2.7	96.1	500	1.1	2.2	0.55
sample 3	4.2	31.5	50	5.2	103	0.047
sample 4	4.2	33.7	60	4.9	32.2	0.075

*the value of the Eurofer substrate in eq. 3 is $P_E = 1.9 \cdot 10^{-11} \text{ molH}_2/\text{m s Pa}^{0.5}$, [3]

Table 1: The value of PRF recorded after 24 h, time-lag L_2 , calculated permeability P_W , diffusivity D_W and solubility of hydrogen in tungsten S_W on four samples at 400 °C.

The only difference between samples deposited at similar, but not identical conditions is the resulting size of micro and nano-crystallites within the film as revealed by XRD. Sample 1 has larger crystallites than Sample 2 and consequently higher permeability. This is in agreement with theoretical predictions and this important detail is needed also for evaluation of Be/W films. By XPS analysis and pressure dependence of permeation flux it may be confirmed that thin tungsten oxide layer does not influence hydrogen permeability. The situation may be substantially different in Be/W films where BeO is supposed to have extremely low hydrogen diffusivity.

Results on permeation measurements on Be/W films

Be/W films with stated composition (75 at.% Be, 25 at.% W) exhibit even less predictable behavior after hydrogen exposure compared to pure W films deposited by TVA method. The actual nanostructure of the film is always influenced by slight modification of true deposition parameters which are not fully controlled. An important parameter was substrate temperature which influenced coalescence of grain. Unless the temperature was increased to 400 °C, Be/W films, films were not dense enough to enable measurements. Another problem was high Be affinity to water as it could result in BeO formation during deposition as well as during the permeation rate measurements. We realized hydrogen purity is extremely important in experiments with Be, but a few ppb level purity, trusted to be maintained in present experiments, might not be enough [6,7]. It seems that water desorption from hot surfaces of the cell contribute the uncontrolled conditions. Moreover, the role of BeO layer grown on pure Be has not been reported to influence hydrogen permeability, except in our report [7]. Even its bulk solubility and diffusivity for hydrogen is lower than in Be and it may not suppress the permeation flux as it may have porous structure like FeO which also does not influence permeation rate through Fe. In 2013 better controlled experimental parameters enabled us to obtain more reliable and stable values in permeation rate measurements. At present, we have no explanation for the difference on two simultaneously deposited samples, sample 10 and sample 11. They both were very stable, but the difference is almost tenfold. Our prime goal, to distinguish between two parameters: film nanostructure and Be/W ratio on permeability and hydrogen retention has not been realized completely.

	tested	thickness	<i>PRF</i>	<i>PRF</i>
		µm	1 h	24 h
sample 1	2011	8	fail	
sample 2	2011	8	1-2	1-2
sample 3	2011	8	260	155*
sample 4	2011	8	100	420**
sample 5	2011	8	fail	
sample 6	2012	8	78	150
sample 7	2012	8	21	
sample 8	2013	8	52	45
sample 9	2013	8	67	85
sample 10	2013	8	3.5	3.6
sample 11	2013	8	33	32

* Unstable readings at fixed hydrogen pressure

** Repeatable achieved anomaly of hydrogen flux increase and decrease at constant upstream pressure

Table 2: Permeation reduction factors (*PRF*) and calculated permeability for Be/W films achieved in 1 h and in 24 h. All numbers for 24h are approximated as all values still drift.

4 CONCLUSIONS AND OUTLOOK FOR 2014

Knowledge of the properties of diffusion, permeability and solubility of H in Be/W alloys is very poor today and further research is definitely required. Since both W and Be films were rarely measured in relation to fusion, we have an advantage that we have more than 3 years of collecting our own experimental data on both material in form of films, Be and W, both relevant to ITER. It is thus important to determine first the parameters that govern the permeation process at known film structure and composition and achieve proper understanding of the influence of material morphology, structure and high temperature loads on H/D/T retention in films made of Be/W alloys with different Be/W ratio.

Besides this knowledge, our data may contribute complementary data to predict the upper limit for D/T accumulation in Be/W deposits or dust formed in JET or ITER. Permeation properties of nano-crystalline W films on Eurofer, produced by different techniques, exhibit substantial differences which can be attributed to the size of crystal grains and their orientation. Our technique is unique in this sense as formerly published data on W rely on bulk material and very high temperature. The aim of study in 2013 was to determine primarily the permeation properties W films deposited by the TVA which enabled direct comparison to Be/W films. Unfortunately, the influence of crystal size in pure W seems to compete Be reactivity with traces of water at the upstream side may result in BeO formation. This detail requires some improvements of the experimental setup, particularly cryo-cooling of tubes delivering hydrogen to the upstream side. As these improvements have been tested, even more relevant data will be extracted from experimental data in 2014.

The final remark of this report is that the program was realized successfully and besides this report, the scientific output is almost prepared for two papers in fusion related journals.

1 REFERENCES

- 1 Skinner CHetal, *Fus. Sci. & Technol.*, 54 (2008) 891–945.
- 2 Doerner RP, Baldwin MJ, Causey RA, *J. Nucl. Mater.*, 342 (2005) 63–67.
- 3 Zajec B, Nemanič V and Ruset C, *J. Nucl. Mater.*412 (2011) 116 – 122.
- 4 Zajec B, *Int. J. of Hydrogen Energy* 36 (2011), 7353–7361.
- 5 Nemanič V, Zajec B, Dellasega D, Passoni, *J. Nucl. Mater.*,429 (2012) 92–98.
- 6 Nemanič V, Zajec B, Žumer M, Porosnicu C, Lungu C, *Fus. Eng. Des.*, 86, (2011) 2421–2424
- 7 Zajec B, Nemanič V, Žumer M, Porosnicu C, Lungu C, *J. Nucl. Mater.*, 443 (2013) 185–194
- 8 Kirscheim R, *Phys.Scripta*, (2001), T94, 58–67.

PLASMA DEPOSITION OF H:C-METAL COATINGS

Peter Panjan, Miha Čekada, M. Panjan, Darinka Kek Merl, Damjan Matelič

Department for Thin Films and Surfaces, Jožef Stefan Institute, Jamova 39, 1000
Ljubljana, Slovenia
e-mail: peter.panjan@ijs.si

1 INTRODUCTION

In fusion devices with carbon based plasma facing components the accumulation of amorphous hydrogenated carbon deposits may present a very serious safety issue as it is a strong contribution to in-vessel fuel retention. To ensure a safe and uninterrupted operation of the reactor, the carbon deposits should be regularly removed. One proposed method is removal by neutral oxygen atoms. The efficiency of the method will strongly depend on the density of neutral oxygen atoms in the vicinity of the surface deposits. The density of neutral oxygen atoms will in turn strongly depend on the recombination on solid surfaces. We have determined the recombination coefficient of amorphous carbon deposits for neutral oxygen and hydrogen atoms.

Within the Euratom project our task is the synthesis of hydrogenated carbon deposits, which should be as similar as possible to real impurity deposits in a fusion reactor. For this experiment we prepared a set of samples coated with hydrogenated carbon films (W-C:H). Work Programme 2013 included three topics: a) deposition of multilayered Cr/W/W-C:H/a-C:H films, b) high power impulse magnetron sputter deposition (HIPIMS) of carbon based coatings and characterization of HIPIMS plasma c) arcing problems in magnetron sputtering.

2 WORK PERFORMED IN 2013

W-C:H coatings prepared by sputtering in Sputron deposition system

Sputter deposition system with thermoionic arc was used for preparation of W-C:H films on stainless steel substrates. The stainless steel samples were finally polished with diamond paste to $R_a=10-14$ nm, ultrasonically cleaned and degreased in bath of hot alkali solution, de-ionized water and then dried in hot air before mounting on the substrate holders. One part of substrates were in situ cleaned by ion etching prior to coating deposition. Metal interlayers (Cr, W) were used to improve the adhesion. Altogether 2 deposition runs were done using the above mentioned technique. The deposition parameters of films which compose a multilayer structure of typical sample are presented in Table 1. These samples are designed for removal test of a-C:H with neutral oxygen atoms. On samples prepared in such a way we performed an experiment

to determine the recombination coefficient of amorphous carbon deposits by measuring the spatial distribution of neutral oxygen and hydrogen atoms in a closed side-arm of the reactor lined with amorphous carbon samples /Ref 1/.

	Cr	W	W-C	a-C:H
target purity	99,95	99,95	99,95	C2H2
background pressure (mbar)	5×10^{-7}	5×10^{-7}	5×10^{-7}	5×10^{-7}
argon pressure (mbar)	2×10^{-3}	2×10^{-3}	2×10^{-3}	2×10^{-3}
flow rate C2H2 (a.u.)				800
target voltage (V)	1700	1700	1700	1700
target current (A)	0.6	0.6	0.6	0,6
substrate temperature (°C)	120	120	120	120
Deposition time (min)	7	1	33	33
deposition rate (nm/min)	10	8	9	

Table 1: Deposition parameters of W-C:H films

Characterization of plasma in high power impulse magnetron sputtering

HIPIMS deposition technique was used for deposition of carbon based coatings. In collaboration with the co-workers from Lawrence Berkeley National Laboratory (USA), we published several papers /Ref 2-5/, where we proposed a model for transport of ions in high power impulse magnetron sputtering. The model is based on the discovery of plasma structures called ionisation zones which rotate in the magnetron plasma in the direction $\mathbf{E} \times \mathbf{B}$. In this model they proposed that inside the ionization zones the electron and ion densities are spacially separated therefore the electric field forms in azimuthal direction. Thus the electric field rotates in line with the zones. The ions primarily form within the ionization zones therefore they acquire the kinetic energy of the rotating electric field which accelerates them in azimuthal direction up to the energy of 100 eV or more. This model is supported by experiments, conducted using mass and energy spectrometry in the scope of the post-doctoral stay of dr. Matjaž Panjan in Berkley. Experiments with high-speed camera imaging have recently demonstrated that in the high power impulse magnetron sputtering plasma becomes self-organized in more or less periodic structures. Such structures are called ionization zones and rotate in the direction of $\mathbf{E} \times \mathbf{B}$ electron drift at about 7 km/s. In this study a high speed imaging was used to observe plasma structures from the side of the magnetron. Images revealed that ionization zones are accompanied by “plasma flares”, which expand perpendicularly to the target surface. It was proposed that plasma flares are formed by electrons which drift in the direction normal to the magnetron due to magnetic and azimuthal electric field formed within the ionization zones. From the images and proposed model of plasma flare formation it was estimated that flare velocities reach about 20 km/s, while the azimuthal electric field was estimated to be around 2000 V/m. Recent experiments by mass spectrometry and ion/electron collector showed that ionization zones and plasma flare play a major role in the asymmetrical transfer of ions in High Power Impulse Magnetron Sputtering (HiPIMS) discharge.

These studies contribute to the understanding of fundamental process in HiPIMS plasma and have practical significance for understanding spatial transfer of ions contributing to the growth of thin films.

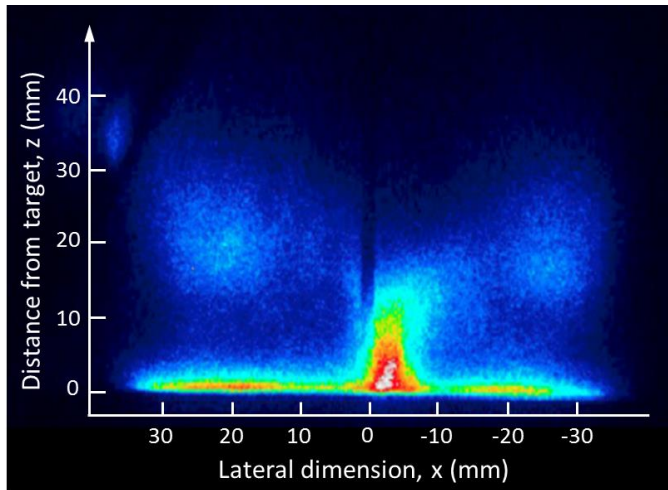


Figure 1: Top-view of HiPIMS plasma showing ionization zones with arrow-like shape rotating in $E \times B$ direction

Arcing in magnetron sputtering

In the framework of this project we focused our research activities on problem of arcing in unbalance magnetron sources we used for deposition of carbon based coatings. We found that on the magnetron target two types of arcs can be distinguished with respect to the location of an arc: arcs on the racetrack and those on the perimeter (the poisoned part of the target). In the former case the electric field is perpendicular to the magnetic field which forces arc to travel along the racetrack. The energy is spread over a larger area and such arcs are less dangerous for macroparticle transport. On the perimeter of target the electric field is approximately paralel with the magnetic field. Arcs are stationary and the energy is concentrated in one point, therefore such, arcs are more explosive. Regarding to droplets and other particle formation an arc on the perimeter is much more dangerous due to easier transport of macroparticles to the substrates. Arcs are spatially localized and sporadic, while their intensity is very different.

After sputter deposition a lot of arc traces are visible on the targets as well as on the table and anodes. Arcs on targets cause emission of microdroplets, while those on the shields and fixtures (which are coated with a thick deposit) can cause delamination of fine nanosized particles. Some of these droplets and particles can be incorporated into the growing coating forming nodular defects. The formation of such defects is also spatially localized and sporadic.

We tried to find any correlation between the defect density and the number of arcs (on sputter sources and substrate table during the etching and the coating phases), but we did not find any correlation. The reason could be related to the fact that the arcs are not distributed uniformly over the vacuum chamber. For this reason, substrates were not uniformly exposed to arc-formed macroparticles, which would give a clear statistical correlation between the arc formation and the defect density.

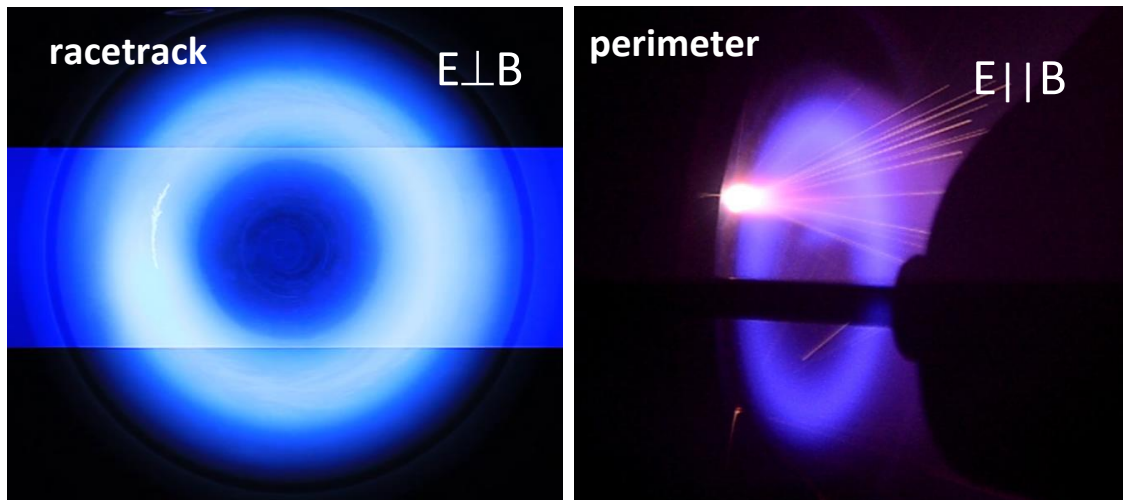


Figure 2: Arcing on racetrack and perimeter of poisoned target during reactive sputter deposition of carbon based coatings using unbalanced magnetron source

3 CONCLUSIONS AND OUTLOOK FOR 2014

Different deposition techniques (sputter deposition using thermoionic arc, unbalanced magnetron sputtering and high power impulse magnetron sputter deposition (HIPIMS)) were successfully used for preparation of metal containing carbon coatings.

4 REFERENCES

- 1 Drenik A, Vesel A, Mozetič M, Panjan P, Recombination of atomic oxygen and hydrogen on amorphous carbon, *J. Nucl. Mater.*, 442, no, 1/3, suppl. (2013), p. 751-754.
- 2 Anders A, Panjan M, Franz R, Andersson J, Ni PA, Drifting potential humps in ionization zones : the propeller blades of high power impulse magnetron sputtering. *App.Phys.Lett.*, 103, (2013), pp. 144103-1-144103-4.
- 3 Andersson J, Panjan M, Franz R, Anders A, Potential humps accelerating ions in high power impulse magnetron sputtering plasmas. In: *ICPSA 2013, International Conference on Plasma Science and Applications*, 4-6 December 2013, Singapore. Book of abstracts, 2013, p. 70.
- 4 Panjan M, Anders A, Asymmetric distributin of ion and electron fluxes measured near the target plane in HiPIMS and DCMS discharges. In: *19th International Vacuum Congress, September 9-13, 2013, Paris, France*. [S. 1.]: IUUVISTA, 2013. Wunderlich, Wilfried (Ed.). Ceramic materials. Rijeka: Sciyo, 2010, 99-114.

VISUALIZATION SUPPORT WITH KEPLER ACTORS AND VISIT UAL PLUGIN WITHIN ITM ADVANCED VISUALISATION TOOLS

Leon Kos

Association EURATOM/MESCS, University of Ljubljana, Slovenia
e-mail: leon.kos@lecad.fs.uni-lj.si

1 INTRODUCTION

Diverse visualization approaches are used within integrated fusion simulations in the frame of by the European Integrated Tokamak Modeling Task Force (ITM-TF). In an effort to provide diversity and at the same time universality of visualizations for different backends, ITMVis library provides a common description of the specialized plots contributed by users. Besides specialized dedicated plots many "standard" plots are used and are described within ITM-TF database via XSD schema that contains plot representation tags. From the representation tags one can generate standard plots for a specific computer language and visualization tool in use. Such approach is used for the VisIt visualization tool, where a C++ code for all possible plots in the database is generated with XSLT transform. It was soon realized Given that the same translation is needed by other tools within different languages to provide standard visualizations, . To lower the burden of translation for different tools we introduced an intermediate plot description with XML that, which is easily interpreted, was introduced. With such unified approach standard and custom plots are available for different backends such as VisIt and matplotlib.

2 WORK PERFORMED IN 2013

The European Integrated Tokamak Modelling Task Force (ITM-TF) is developing a framework to enable coupling of physics codes in order to allow flexible modeling, simulation (both interpretative and predictive), verification and validation for fusion research. The approach taken by the ITM-TF is to couple codes via well-defined data structures [1] that consistently describe different physical aspects covered in simulations. These Consistent Physical Objects (CPOs) are used for data storage and interchange between codes in the ITM simulation framework. The collection of CPO descriptions form together a complete data model for diverse simulations that can also contain imported experimental data. This approach enables a direct comparison of results with the experiment and/or use experimental data as an input. The implementation phases and continuous development of the ITM-TF framework are simplified by the fact that the CPO data structures are described by an XML schema

definition (XSD), which can be easily modified. This semi human-readable description allows rigorous validation, creation of data bindings and translations for different purposes.

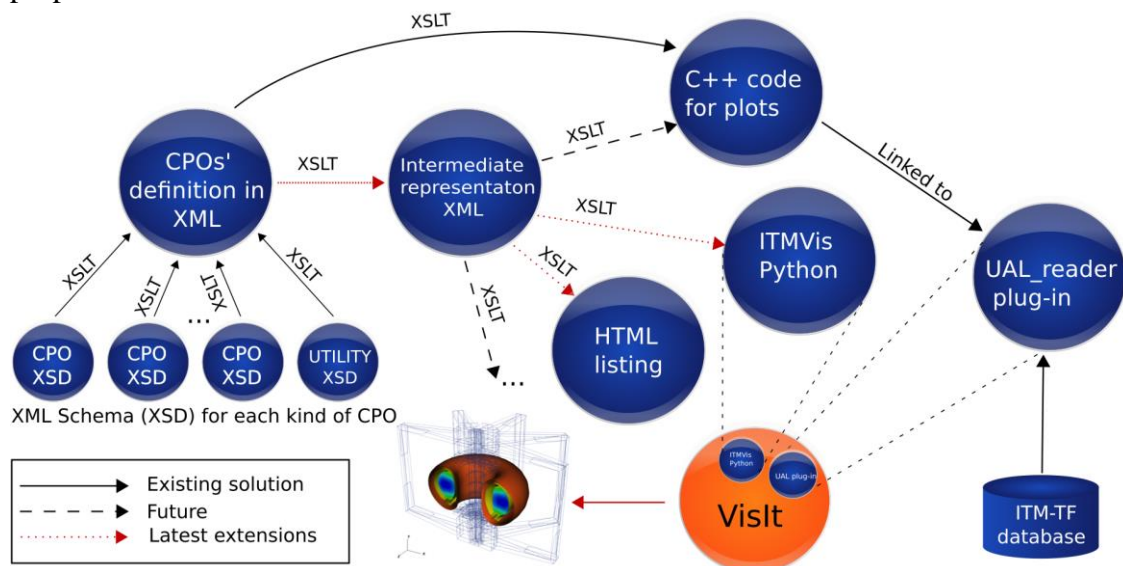


Figure 1: XSLT flowchart for standard representation transformations used for visualization.

The XSD datastructure description is mainly used to generate CPO definitions in an XML format obtained by applying the XSL translation (XSLT) language. Consistency of CPO definitions is assured by the XSD description, so that the derived CPO definitions in XML are consistent too. Additionally, the XSDs allow the use of custom complexType data-structures that are reused in different CPOs. The resulting CPODef.xml database description thus contains expanded and complete information about the ITM-TF data model. From this starting point all other code can be generated through XSLT processing. Figure 1 on the left shows this initial transformation from many CPO definitions into single CPOs' definition in XML. The fundamental purpose of CPODef.xml is a description of the ITM-TF persistent storage database, where actual data is stored. Storage can also be in-memory only (i.e. cached) for fast data exchange between coupled codes. CPODef.xml is used for the ITM-TF database creation and for describing access to data fields in the database by a variety of programming languages. The multi-language library that interfaces access to CPOs in the ITM-TF database is called Universal Access Layer (UAL) and includes definitions of CPOs in each supported programming language. The included definitions are then used in physics codes for data access with a small set of the UAL subroutines responsible for retrieving and storing CPOs during the ITM simulations. The UAL thus interfaces codes with storage in the hierarchical formats, which are commonly used in high performance computing (HPC) and the fusion community. The UAL extends these technologies by allowing cached parallel and distributed access to data between the ITM-TF users that are organized into several Integrated Modelling Projects (IMPs). The ITM-TF adapted existing simulation codes to use the UAL and developed new codes that will allow detailed simulations of present and future device scenarios.

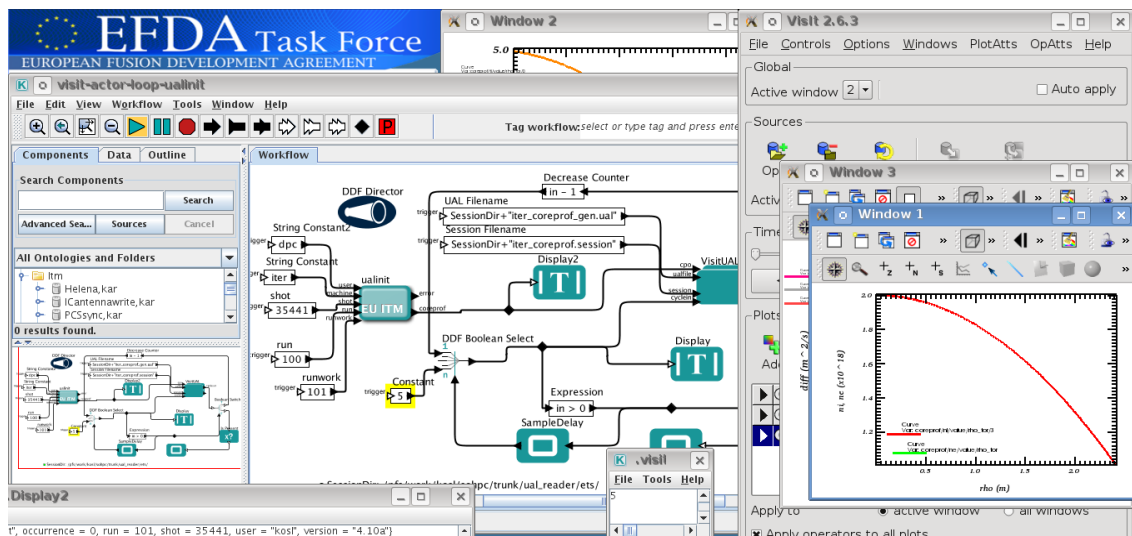


Figure 2: The VisIt Kepler Actor – VisItUAL in a workflow within a loop reading data through the Universal Access Layer.

As most of the CPOs are time dependent, the ITM-TF database stores slices of each CPO during simulation iterations or experiment sampling. Slicing occurs at different time scales for each CPO depending on the physics involved. To support the diagnostic of the time-dependent data in CPOs, several visualization tools are used depending on the scales and representation of the data that is regularly used in simulations. For many simulations, custom visualization are created using general-purpose graphics libraries. To avoid such custom approaches and to provide standardized sets of visualizations, the ITM-TF infrastructure support team (ISIP) aims to provide tools that can be used for visualizations without the need for scientists to manually program each plot. The ITM-TF selected the Kepler scientific workflow engine which enables graphical programming of workflows. Data flow between processes (called actors) is modelled by wires. Through wires only small amount of data (signals) are passed, usually just single numbers, strings and structures with CPO names, which identify database entries. The Actual data exchange between ITM actors encapsulating fusion codes is then implemented by direct access to the “real” data through the UAL library.

ITM-TF visualization tools

The ITM aims to provide complex visualizations for fusion codes that are adapted to the ITM framework. To provide scientists with general visualization tools in the ITM framework, the EUFORIA/JRA4 project has developed a plugin for the VisIt 3D visualization software that allows reading CPOs from the ITM-TF database directly. For inclusion of VisIt in the Kepler workflows the VisIt Kepler Actor (VKA) was developed. VKA has been recently upgraded to allow visualizations of multiple CPOs and now includes its own graphical user interface (GUI) written in Java. VKA provides seamless inclusion of VisIt into scientific workflows with UAL data access. Figure 2 shows use of the VKA named *VisItUAL* in a workflow that iterates in a loop through all time slices of a database retrieved through the UAL. VisIt is launched from the workflow itself and gets *fired* at each loop iteration to show the data for the *cycle*

specified as an input to *VisItUAL*. *VisIt* has a possibility to save a *session* describing plots that are saved in a *session file* for later reuse for similar visualizations where only the input database changes. Before starting the iterations, the actor *ualinit* copies the requested input CPOs into a local *runwork* from the distributed ITM-TF database. For this, the “tuple” *user*, *machine*, *shot*, and *run* identifying the database has to be specified. Copying and specifying the input CPOs provides *data provenance*. This means that the source is well known and not destroyed by modifications. Workflows prepared in this way can be easily shared and reproduced. *Provenance* is a feature of scientific workflows that is often overlooked; omitting it brings the risk that results cannot be easily verified.

Other ITM/ISIP visualization tools are mainly based on the Python language, where *matplotlib* is used for creating 2D *plots*. JRA4 developed the Python Kepler Actor that in contrast to the Java based *Jython* Kepler actor can import *matplotlib* for creating custom non-blocking plots in Kepler workflows. Another approach developed by the ITM to provide *standardized* plots is the *ITMVis* visualization library that aims to provide several output *backends* for custom plots scripted in Python. The *ITMVis* code snippets can be shared between users or put into a collective database of custom visualizations. Many of such snippets were translated from other languages like IDL, which is still used in many codes for visualization.

These visualization tools can be used within workflows or standalone. Most visualization tools are diagnostic and reporting tools used standalone and offline. If data is available during the simulation, they can also be used for monitoring of simulations. *VisIt* as a standalone tool needs an input file (with *.ual* extension), containing *tuples* pointing to database entries. The capability of *VisIt* to allow code instrumentation through its *SIMlib* was used to couple UAL and *VisIt* through the *ualconnector* (with possibility to access th ITM Grid Service Library) CPO server capable of serving complex unstructured meshes, which are used e.g. in the 2D edge transport code (SOLPS). *VisIt* as a general 3D scientific visualization tool can be used for many purposes as it builds on top of the Visualization ToolKit (VTK) that has an established visualization pipeline. Another useful visualization principle used in *VisIt* is data callback separation that a plugin needs to provide for visualizations.

Standard representations for visualization

The *ITMVis* library tries to follow the *VisIt* data description by splitting visualizations of CPOs into meta-data and plot data. This separation is a natural choice for all tools that want to prepare a list of possible visualizations depending on data availability. It should be noted that not all CPOs are filled with data when running a particular simulations. The *ITMVis* library presently concentrates on *custom plots*, while the UAL reader plugin works with *standard representations*. A representation is, in fact, a description of the visualization. There can be multiple representations of the same data. The *UAL reader* plugin for *VisIt* (see Fig. 1) utilizes *representation tags* that are included in the XSD files describing the CPOs. This means that ITM-TF data structure “knows” how it can be visualized. This is similar to the concept of *views* in SQL, which are stored in a database directly (except that these would be stored directly in the database). Representation tags are just a description that does not enlarge storage but facilitates views on data.

Listing 1: A representation tag provides name, type and links for a visualisation. The tag is added as an `xs:annotation/xs:appinfo` XSD element as shown in the following lines marked with a plus sign.

```
<xs:element name="imp" type="vecflt_type">
<xs:annotation>
<xs:documentation>Implicit source term [s^-1.m^-3]. Time-dependent.
    Vector (nrho)</xs:documentation>
+ <xs:appinfo>representation name=rho_tor; var=scalar; meshtype=curve0;
+ link1=/rho_tor;</xs:appinfo>
+ <xs:appinfo>representation name=rho_tor_norm; var=scalar; meshtype=curve0;
+ link1=/rho_tor_norm; </xs:appinfo>
</xs:annotation>
</xs:element>
```

An example of updated XSD with two representation tags is shown in Listing 1. The representation name is arbitrary and is shown as the last name in the VisIt path when adding plots. The attribute `var` can be either a scalar or a vector and describes the kind of data mapped on the mesh represented by one or more links. Several meshtypes exist:

- `curve0` Curve as a polylines plot.
- `axis1D0` X axis given as a link1 vs. a bunch of curves from a matrix.
- `mesh1D0` Contours (closed curves) as a (2D) surface mesh.
- `rectilinear0` or `curvilinear0` Meshes in 2D and 3D.

Meshtype describes the type of variable mapping in space. Each meshtype can have a variable number of links (`link1`, `link2` and/or `link3`) and thus different kind of visualizations that are constructed as VTK objects in VisIt. Links provide axis mapping to corresponding vectors or matrices that constitute a mesh. The topology name at the end of the meshtype means (0D points, 1D lines, 2D surface, 3D volume). The number at the end distinguishes variations of the same meshtype (0, 1, ...). If no topology is given, a general description is assumed (2D and 3D).

Depending on the type of data mapped on the mesh, given links are expanded to the proper hierarchical position within the CPO (called a *path*). When a `xs:complexType` is represented, then links are expanded with a local path of the CPO during generation of *CPOdef.xml* from the XSD files. For example `<xs:complexType name="rz0D">with link1=r; link2=z get expanded to link1=eqgeometry/geom_axis/r and link2=eqgeometry/geom_axis/z and thus adding the (missing) relative path from CPO to the link. In other words, complexTypes are relocatable as they are reused in many representations without absolute reference to fields in the same CPO. When an element specifies complexType (e.g. <xs:element name="position" type="rz2D">), then the representation in complexType is used and not in the element itself. Simple elements (scalars, vectors, matrices) can be directly linked within a CPO by specifying the absolute path to them. There are also compound elements that are reused (expanded) as a whole (e.g. <xs:element name="coord_sys">) in many CPOs. To distinguish between them, one has to describe links with absolute or relative paths. This is done with leading "/ for absolute`

references and any other as relative to a compound or *complexType* that is reused in many CPOs.

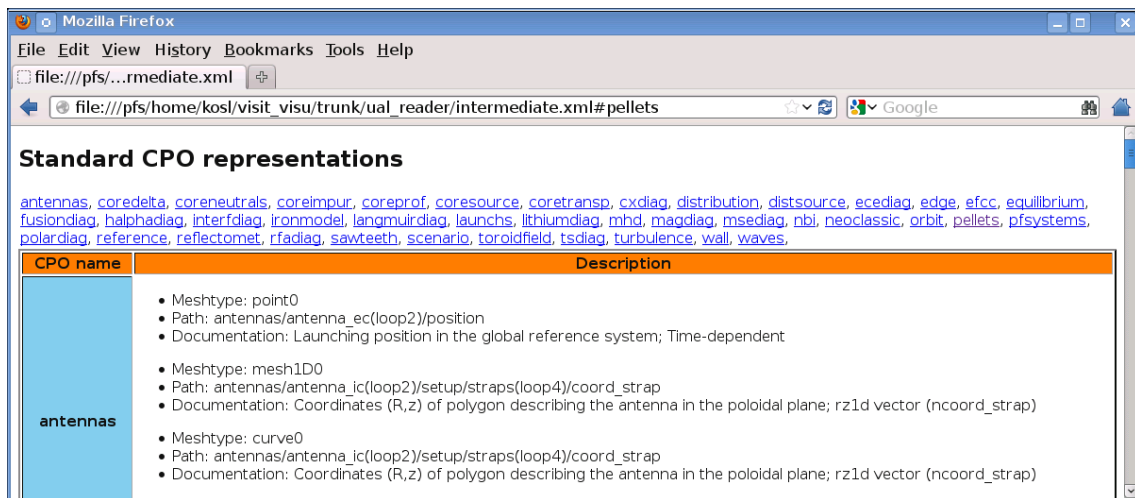


Figure 3: The Visit Kepler Actor – VisitUAL in a workflow within a loop reading data through the Universal Access Layer

Intermediate representation layer

Standard representations are currently used for data visualization within some CPOs, where the structure of the data fields allows this. For visualizations using data from multiple CPOs, the *ITMVis* approach provides scripting/post-processing capabilities that can combine results and output them through different backends. Visit combined with the *UAL reader* plugin allows both representations (standard and custom) by embedding a Python interpreter in the plugin itself. Standard representations were not included in *ITMVis* so far, although this was possible by direct interpretation of *CPOdef.xml* or by Python code generation as in *UAL reader* (where C++ code representing plots is generated from *CPOdef.xml* directly). The process of XSL translation shown in Fig. 1 with solid lines could be repeated for *ITMVis* too. From the experience gained in developing templates for C++ code used in *UAL reader*, where 220000+ source lines are generated, we came to a conclusion that introducing an *intermediate XML description* that extracts representation data from the *CPOdef.xml* will reduce the complexity of the XSLT process when applying it to several programming languages. This intermediate description is still in XML, except that it contains the standard representations described more naturally in a custom XML schema that is easily converted further with XSLT. The complexity of the XSLT code is thus reduced and distributed among XSL translations to and from *intermediate.xml*. Such an approach unifies standard CPO representations and can be extended with additional fields in the intermediate XML format for easier translation as required.

The primary goal of the proposed visualization unification shown in Figure 1 flowchart was to bring standard representations to the *ITMVis* library via an intermediate XML description. To facilitate this, the intermediate XML description was initially generated by adapting existing templates taken from the *UAL reader*. As the output is XML, the translation process is similar to *CPOdef.xml* in terms of XML

attribute and element specification. Additional complexity occurs where representation links XPath are used to derive linked information. The red dotted lines in Fig. 1 show the implemented XSL Translations. The simplest and most useful translation is generating documentation for standard representations. Instead of using command line XSLT tools, one can translate them into HTML via an XSL translator that is now built into all modern web browsers. All what is needed in the intermediate XML description is to specify the XSL stylesheet in the XML header and open the file in a browser. XSL and XML are then translated on the fly as shown in Fig. 3. The HTML output lists all representation tags within each CPO that are listed on the top of the page. Standard representations were generated by XSLT from intermediate XML directly into Python scripts that *ITMVis* can easily include into its library of available plots. Python is sensitive to source code indentation so the XSL templates were required to carefully generate the code. As the CPOs are hierarchically described with structures that are often generalized into arrays of structures one needs to specify required indexes of the structure. Required indexes are described in representation *path* by parentheses (loop#) in Fig. 3. It should be noted that probing for data availability in CPOs is required for VisIt that builds *metadata* information of available (valid) “plots”. To prepare valid metadata one needs to scan CPO by “looping” through all available arrays of structures for which data might be available. Such “scanning” can take great deal of time, so it is advisable to know in advance available data ranges in arrays of structures. Figure 4 shows an example *matplotlib* plot with the corresponding generated code snippet in Listing 2 that was used within *ITMVis* for the plot. Metadata is returned only if plot is valid (when data for the plot is available). Metadata provides plot description, axes names and units. *Plotdata* prepares required data for plot creation. For field data this means also preparing mesh information on which values are mapped. Further processing to produce visualization is backend (VisIt, matplotlib) dependent. Currently 38 CPOs are supported with 639 standard representations, not including time-dependent representations that can be produced by expanding the plot along the time-axis. For example, curves over time can be represented as rectilinear meshes.

```
def itmvis_coreprof_te_value_rho_tor_metadata(coreprof):
    '''Signal value; Time-dependent; Vector (nrho)'''
    if field_filled(coreprof.cpo.te.value) \
    and field_filled(coreprof.cpo.rho_tor):
        md = dict()
        md["type"] = ITMVIS_PLOTTYPE_XY
        md["axes"] = ("Toroidal flux coordinate (not normalised,
        equivalent to rho_tor norm) [m]", "Signal value")
            md["axes_units"] = ("m", "eV.")
            md["axes"] = md["axes_units"]
        md["legend"] = ["Signal value"]
    return md
else:
    return None
def itmvis_coreprof_te_value_rho_tor_plotdata(coreprof):
    data = {}
    data["x"] = coreprof.cpo.rho_tor
    data["y"] = coreprof.cpo.te.value
    return data
```

Listing 2: XSLT generated Python code from intermediate.xml.

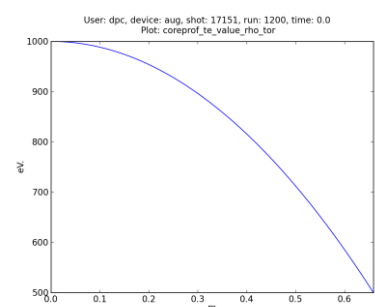


Figure 4: The coreprof CPO electron temperature *ITMVis* plot generated from standard representations via intermediate.xml

3 CONCLUSIONS AND OUTLOOK FOR 2014

Splitting the implementation of standard visualizations into two parts resulted in an intermediate layer that can be easily used for further translation into target libraries used for visualization. Including information about standard visualizations in the data structure descriptions allows to efficiently propagate information on how to represent the data to various visualization tools. The use of XSL translation assures correct resulting code during, even when changing the XSD schema files defining the data structure. This is an advantage over custom visualizations as e.g. implemented in ITMVis, which can require updates when the schemas are changed. Standard and custom visualizations are now both possible within the ITMVis and VisIt approach[2]. The introduction of an intermediate description layer simplifies the XSL templates and reduces template replication required for the target languages. This unified approach to visualizations in ITM-TF framework now leads to the availability of diverse visualization tools supporting both standard and custom representations.

Our introduction of intermediate *visualization schema* unifies and reduces efforts required to develop visualization tools. Such approach enables users to browse through available *standard* visualizations. In cases of custom requirements, scripting for plots can be used by *ITMVis* library that was embedded in VisIt UAL database reader. How to provide more sophisticated (algorithmic) mappings in the schema is ongoing question. Requirements for visualization tools in integrated modelling where GUI and Viewer can be attached from workflow and opposite attachment from VisIt to Kepler is a starting point for future work. Additionally, initiative for collaboration from CCFE on Kitware tools (VTK, ParaView) will start in 2014 under EUROfusion consortium.

4 REFERENCES

- 1 F. Imbeaux, J. B. Lister, G. T. A. Huysmans, W. Zwingmann, M. Airaj, L. Appel, V. Basiuk, D. Coster, L.-Goran Eriksson, B. Guillerminet, D. Kalupin, C. Konz, G. Manduchi, M. Ottaviani, G. Pereverzev, Y. Peysson, O. Sauter, J. Signoret, and P. Strand, "A generic data structure for integrated modelling of tokamak physics and subsystems," *Computer Physics Communications* 181, 987–998 (2010).
- 2 L.Kos, H.-J. Klingshirn, P.L.Garcia Muller, F. Imbeaux and EFDA ITM-TF contributors, *Unified Approach to Visualizations within the European Integrated Tokamak Modelling Framework*, 22nd Int. Conf. Nuclear Energy for New Europe, Bled, Slovenia, 9–12 Sept. 2013, 1402.1–1402.8

UPGRADE OF THE 360° MODEL OF JET – CALCULATIONS TO SUPPORT NEUTRON YIELD CALIBRATION

I. Lengar, L. Snoj

Jožef Stefan Institute (IJS), Reactor Physics Department, Ljubljana, Slovenia
e-mail: igor.lengar@ijs.si

1 INTRODUCTION

The aim of the project was the further upgrade of the MCNP model for JET, previously expanded in order to fill the whole torus. Another goal was the support of the experimental programs at JET with transport calculations of the relevant neutron and gamma fluxes. The calculations are focused also on the diagnostics needs.

The original MCNP models for JET comprised only one quarter of the torus since practically all MCNP calculations are performed for a circularly symmetric plasma source, what can be performed by modelling only one (symmetrical) portion of the torus by a section model. The symmetry brakes down in the rare case, where the neutron source is not circularly symmetric, i.e. during detector calibration with a ^{252}Cf point neutrons source, used at JET for. The model was previously expanded into a 360° model, the final adjustments were made in the frame of the present project in order for the model to be used for calculations of the correction/calibration factors during the calibration.

After these adjustments the model was used for calculation support during the Cf-source calibration in order to calculate the detector responses and correction factors for individual detector positions for many effects, e.g. corrections which originate from the undesired shielding of the source by the mascot robot arm holding the source. The task has in parallel been performed with a simplified and quick-running 360° model of the JET torus in its torus hall, but with a torus of rectangular cross-section. The model, developed in the frame of this project is of larger detail and helped in studying effects of the simplification of the calculations with the former model.

During the source calibration all together more than 200 calibration points were measured. All correction factors were calculated also with the detailed 360° model for comparison with results obtained from other models.

The three steps automatic procedure of insertion of the transformation matrices into the MCNP input file and its usage are presented in Figure 2.

The visualisation of the boom inside the torus is presented in Figure 4, using the visualisation module of the automatic conversion tool MCAM [2]

The original model comprised only a 90° sector of the torus. A 45° sector of this model was then used in order to fill the whole torus [3]. The previous step was a model of the torus, filled with eight identical sectors, i.e. eight equal octants (Figure 3 (a)).

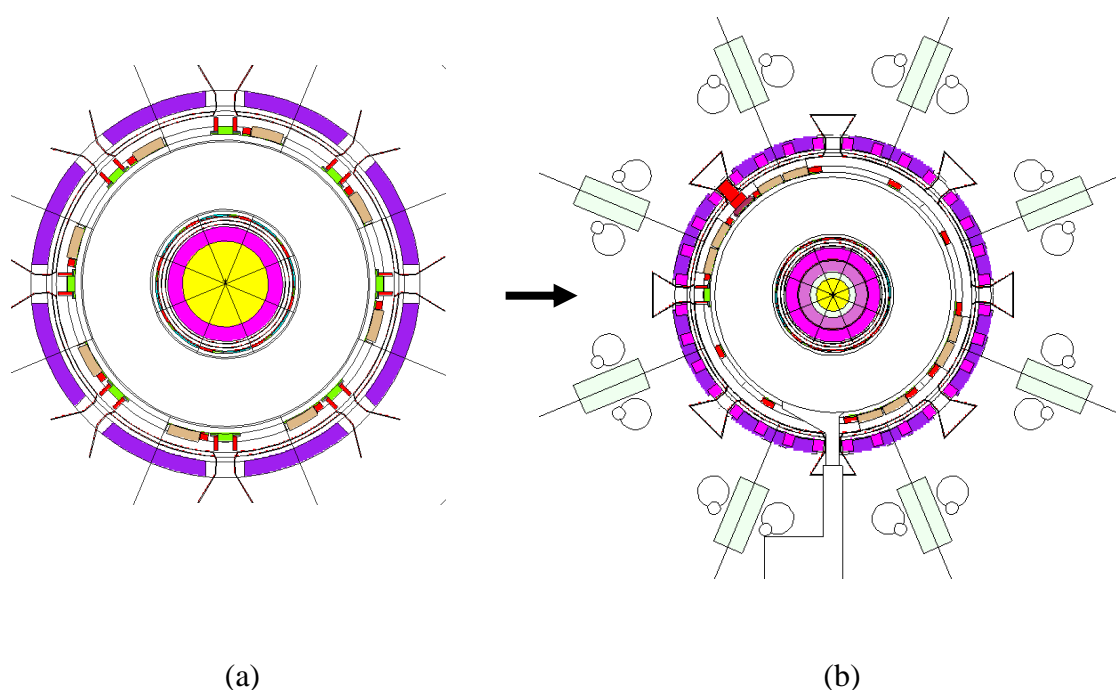


Figure 3: Graphical presentation of the change from the torus model composed of 8 identical sector models to the model, in which in-vessel components are modelled individually. The later model is also adapted to insertion of the boom (from below) and includes some ex-vessel structures.

In the frame of the present project the individual sectors were filled with according components. For this reason the structure of the whole torus was broken down into the vacuum vessel, which is duplicated 8 times, and into the components inside the vacuum vessel, which are individually modeled. These components are:

- ILW antenna
- lower hybrid
- wide poloidal limiters
- narrow poloidal limiters
- different sets of inner limiters

Each of these components was modeled in its own universe and positioned into the right place, possibly several times replicated as in the case of poloidal limiters. The obtained model is pictured in Figure 3 (b)).

Additionally some ex-vessel structures as the transformer limbs and torus hall were inserted.

A visualization of the last model including the boom inside the torus is presented in Figure 4. The vessel is removed from the picture for the in-vessel structures to be visible.

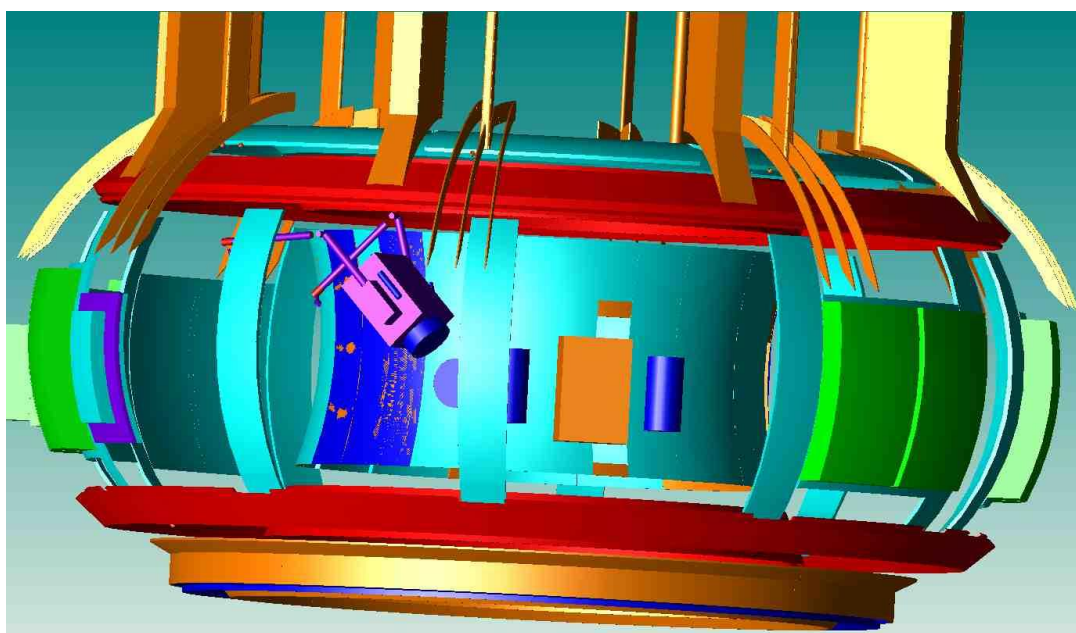


Figure 4: Presentation of the major in-vessel structures and the boom, inserted into the model. Graphics by MCAM [2].

Calculation of correction factors for KN2-3U and KN1

The calculation of correction factors using the MCNP Monte Carlo program is computationally a demanding task. For each configuration two runs with the ^{252}Cf source have to be performed; one with the remote handling boom in the model and one without the boom. The results are then compared in order to estimate the correction due to the boom. Each single run takes from one week to over a month to run on a single processor. Usage of larger computer clusters is thus necessary in order to perform the calculations in a reasonable time.

Before performing the main runs of the correction factors, optimization of the model was performed in order to achieve results with satisfactory good statistical accuracy in the shortest time. For this reason the changes were introduced into the model in order to study the results and observe the statistics/time at the KN1 and KN2-3U positions. The following steps were performed:

- a) changing importance of individual cells

- b) changing number of toroidal surfaces
- c) changing the number of sub-universes in the model

The model, which performed best in respect to a) was adopted. It was found, that the number of toroidal surfaces, studied in b) does affects the speed of calculations, but it was found unpractical to reduce their number, since this would affect the geometrical accuracy of the model. The level of sub-universes, studied in c), was found not to represent a notable difference in the speed of calculations.

The model has been subsequently used for calculation of calibration/correction factors. During the neutron source calibration, two neutron detector systems are measured – the KN2-3U in-vessel activation system and the KN1 ex-vessel fission cell system. The current MCNP model was originally optimized for calculation of the first system; by insertion of the ex-vessel structures and the torus hall, the KN1 response can, however, also be calculated. During the actual calibration of detector systems with the Cf source the large majority of calibration points, more than 200, was chosen to calibrate the KN1 system, only three locations were chosen for dedicated calibration of the KN2-3U system. In view of this, the computer time, needed for calculations for both systems, was shared in similar proportions. The results of calculation of the response and corresponding calibration/correction factors for both systems are presented in the continuation.

KN2-3U calculations

The calculated response including the calibration factors for three dedicated points, are presented in Table 1. Each calibration factor is presented in the form of the ratio of the corresponding response (activations of Indium atoms for the KN2-3U system and counts of the fission counter for the KN2 system per 109 source neutrons) for two cases: response (boom present)/ response (boom absent), i.e. the introduced perturbation due to the boom.

location	absoutle source position			response (no. of activated atoms, boom absent)	correction factor
	x	y	z		
midplane	-288.5	-58.3	30.2	35.1	1.02
middle position	-290.9	-59.1	104.7	97.7	1.00
upper position	-315.6	-63.6	159.6	744.8	0.99

Table 1: Calculated KN2-3U response (boom absent) and corresponding correction factors for three source points (presented in absolute numbers relative to the torus coordinate system).

It can be observed from the table that the remote handling system for the three configurations does not present a significant influence on the calibration. The absolute values for the response have been confirmed by calculations with a MCNP model for JET by Sean Conroy. The model is suitable for KN2-3U response and calibration factors calculations.

KN1 calculations

The number of calculations performed for the KN1 correction factors was significantly larger than for the KN2. In order to achieve the necessary statistical accuracy the time for a single Monte Carlo run was 12 CPU days. Altogether 2 x 200 runs had to be performed (for each calibration point two runs with/without boom), totalling the computer time to cca. 14 CPU years. The locations of the three KN1 fission chambers are presented in Figure 5.

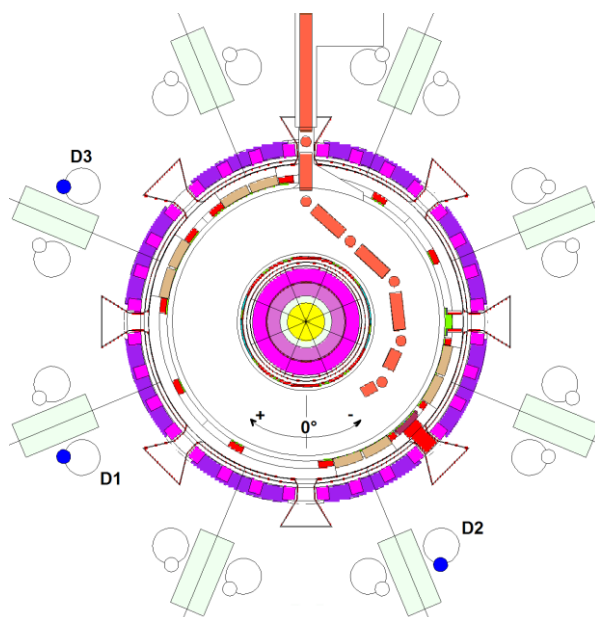


Figure 5: Locations of the three KN1 fission chambers, presented with blue colour.

The correction factors were calculated for each of the fission cell locations; D1, D2 and D3 (and also for the hypothetical fission cell locations on other limbs, another 13 locations, visible in Figure 5) and for all calibration points*: total of 200 points, 40 for each of the rings – central, lower, upper, inner, outer. In figure 6 the response for the fission chambers D1, D2 and D3 is presented for the central ring and in Figure 7 the corresponding correction factors. The location of individual calibration point can be determined from Figure 5.

* The locations of the Cf source – calibration points – used for calculation, were the planned locations. It was found after the calibration that actual positions differed from the planned ones. The locations of the latter were, however, not available in numerical format and the long-lasting calculations of the calibration factors were performed with the planned locations.

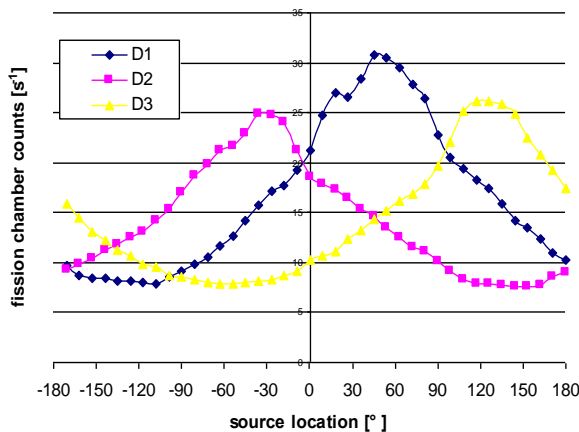


Figure 6: Response of fission chambers D1, D2 and D3; location of the source on 40 positions in the central ring; boom present.

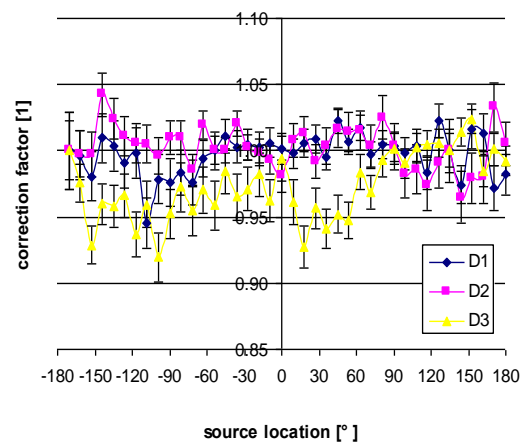


Figure 7: Correction factors for D1, D2 and D3; central ring.

The above results were compared to calculations with a MCNP model from Sean Conroy (CCFE, UU), also calculating KN1 correction factors [1]. That model was to a fair amount adjusted in order to fit the measured data. In addition Sean Conroy uses a low density Inconel ring on the outer side of the torus structure in order to mimic the many components, found around the torus, which can not be modeled explicitly for MCNP calculations.

The comparison shows, that lacking these ring of low density Inconel around the torus increases the value of the response of fission chambers by a factor of a few. In addition the peaks in Figure 6 are broader. The conclusion is that the model is not suitable in the present form for quantitative calculations of the detector response, it can however be used for qualitative estimation of the response and for calculation of correction factors for the KN1.

The values for the detector response and calibration factors for the current model (all together 6400 values – 16 detector positions, 200 calibration locations, 2 types) are available.

3 CONCLUSIONS AND OUTLOOK FOR 2014

The 3D MCNP model of JET was further upgraded in order to be optimized for calculation of correction factors, needed for the neutron source calibration. The new boom was inserted into the upgraded 360° MCNP model, the correctness of the insertion was examined.

Individual components (limiter, RF, LHCD ...) have been modeled each in own universe. Identical components have only to be modeled once and are replicated on all occurrences. The model is optimized for the automatic insertion of the boom to the necessary more than 200 positions (automatic insertion of transformation cards).

The correction factors in the frame of the calibration of JET neutron detector systems with a Cf source were performed with the final model. The calculations for the calibration points for the KN2-3U were found to be adequate and that the detector response and calibration factors can be used.

A large effort in computer time was invested for the calculation of the correction factors for the 200 calibration points of the KN1 system. Analyses shows that due to the lack of a low density Inconel ring in the surrounding of the torus, which approximates the many ex-vessel components, a too high detector response is obtained with regards to the model by Sean Conroy, using this approximation. The calibration values can thus not be used quantitatively but a qualitative estimation of the correction factors is possible.

In the frame of the present task, the MCNP model was further upgraded. It will be used in the future for calculations of the detector responses, in particular of the KN2-3U, needed as support for experimental work. In the year 2017-2018 a DT campaign is planned at JET, which will be preceded by a DT calibration. The model is planned to be used for the calculation of correction factors in support of this calibration and for the subsequent DT plasma measurements.

4 REFERENCES

- 1 Luka Snoj, Igor Lengar, Neutron studies for neutron calibration – calculations to support JET neutron yield calibration, JET TF-FT report, JW12-FT-5.41, 2012.
- 2 Y. Wu, FDS Team, CAD-based interface programs for fusion neutron transport simulation, Fusion Engineering and Design 84 (2009) pp 1987 – 1992.
- 3 Igor Lengar, Expansion of the Be-wall JET MCNP model to 360° and transport calculations, JET TF-FT report, JW11-FT-5.36, 2013.

NEUTRON STUDIES FOR NEUTRON CALIBRATION - CALCULATIONS TO SUPPORT JET NEUTRON YIELD CALIBRATION

Luka Snoj, Igor Lengar, Aljaž Čufar, Andrej Trkov

Jožef Stefan Institute (IJS), Reactor Physics Department, Ljubljana, Slovenia
e-mail: luka.snoj@ijs.si

1 INTRODUCTION

As the JET neutron calibration is critical in determining the fusion yields, the JET Operator performed a new calibration in 2013 to update and improve upon the old one. The preparations, results and interpretation of this calibration are clearly of interest to other major fusion devices requiring similar calibrations, in particular for ITER.

As in all such calibrations, neutronic calculations are required to support the physics, safety and engineering efforts. These cover 3 main requirements given below:

- 1) Validity of Calibration & Planning, e.g. counting rates, statistics, position & energy dependencies and any relevant JET model updates for both Fission Chamber and Activation System methods.
- 2) Corrections, e.g. scattering from source encapsulation, holder, or robot and other neighbouring items or edge and ‘real world’ effects such as open octants, items outside torus
- 3) Safety, e.g. dose rate estimates for various operating conditions, shields etc. to help decide which operations are manual or remotely handled.

Different models and calculations must be available during the 3 project stages of planning and design, actual physical calibration and post calibration phase. Particular models or variants may be used to examine special phenomena. Many calculations are based on Monte Carlo modelling using the advanced Monte Carlo transport codes, such as MCNP. We now have developed 3 types of MCNP model which have been/will be useful in different aspects of the calibration:

1. The first type is an updated version of M. Loughlin’s homogenised 1-sector model ‘JET C Wall 2000’, to allow comparison with the earlier calibration results in a consistent way for the new JET conditions. The two updated models, made by I Lengar, MESCS, between 2008 and 2010, in tasks JW9-FT-5.32 and JW10-FT-5.34, reflect the more recent configurations of JET geometry and materials, i.e. the more recent Carbon wall (1999) and the new ITER-like Wall (Be main chamber and W divertor) which was installed in 2011. Only the major internal items were updated, the models are now called: JET C Wall 2000, JET C Wall 2009, and JET Be Wall 2011, respectively. Outputs from running these models have allowed assessment of the effect of JET major changes on the predicted activation calibration value and on the same

modelling basis as the original. (About +3% change for the newer C wall and about -10 % for the ITER-like Wall changes).

2. The second type of model is a simplified but quick-running 3 dimensional model of the JET torus in its torus hall, but with a torus of rectangular cross-section (L Snoj, MESCS). This has allowed rapid, early evaluation of particular issues, e.g. the prediction of the toroidal dependence of the Fission Chambers' response with source position in the torus and the use of flagging to show that the response comes via the ports, and their relative importance. The optimisation of the source baton design for low neutron scattering and the prediction of corrections for such effects is another example. Both these points have been important in experimental planning. In addition this model was used in studies of the effect of the JET remote handling system on the external neutron monitor (KN1) response.

3. The final type of model is a new more-detailed 3-dimensional model of the JET torus in its torus hall (In progress, S Conroy, VR, 2010-2011). This model is more complex and potentially slower, but it has been built to optimise running time. Such a model is necessary to properly calculate the Activation System Response for the new direct point source calibrations, to provide good corrections for the external Fission Chamber data analysis and to deal with the wider range of scan information which will be provided by the new, more extensive calibration data. An early version of this model was used for the important task of estimating dose rates from the source in various shields and in the torus, for the purpose of evaluating the limitations to manned access in various operational situations.

Due to the large number of calculations needed to support the JET neutron yield calibration and to understand various effects, the so called "quick model" is indispensable in the JET neutron yield calibration project. This report describes the work performed to support JET neutron yield calibration by using the so called quick model. Most of the proposed tasks are strongly related to JW11-FT-5.35 and JW12-FT-5.41 Neutron studies for neutron calibration – calculations to support JET neutron yield calibration.

Within this task, another activity is performed, which is relevant to the development of neutron based plasma position monitoring system in DEMO. As DEMO will most probably lack neutron profile monitors, there is a possibility to monitor plasma vertical position with simpler neutron detectors. The purpose of the study proposed within this task is to perform preliminary computational analysis to support testing of such a system at the JET tokamak.

JET is already committed to the neutron yield calibration experiments as part of the 2012 JET Tile Exchange Intervention. Good neutron yield measurements will allow more reliable operation within set operational limits and support improved analysis and interpretation of JET pulses. In view of the planning for future tritium operations, it is especially important that the fusion yield measurements are well verified, starting with the current plans for D-D relevant calibrations. The deployment, measurement and calculational methods developed now will be extended to cover JET's D-T operations in the foreseen future. The proposed work will contribute to the foreseen JET-related activities.

The whole process of understanding & improving the knowledge of the neutron yield calibration for JET is of great interest for ITER, where the methods and

procedures for calibrating the neutron yield monitors have yet to be finally defined, but the requirement is for 10% accuracy in the fusion yield determination, as it is in JET. In addition, the results of the preliminary calculations to support the development of a neutron-based plasma position monitoring system with single detectors (i.e. without neutron profile monitors) are intended to lead to an evaluation of the potential of such a system on the proposed FC detectors on ITER.

2 WORK PERFORMED IN 2013

Work in 2013 was focused in three main tasks:

1. Analysis and evaluation of the JET neutron yield measurements after the experimental campaign – comparison of measurements and calculations
2. Analysis of Neutron flux anisotropy due to neutron source baton
3. Assessment of the use of neutron detector for plasma position monitoring system

A brief description of the abovementioned activities and major results are presented below.

Analysis and evaluation of the JET neutron yield measurements after the experimental campaign – comparison of measurements and calculations

Based on the remote handling coordinates we calculated the neutron source (NS) positions for the KN1 calibration points and compared them with the real ones, which are almost equal to the planned points. The difference in target vs planned NS point positions is presented in Figure 4. It can be observed that the agreement is relatively good, i.e. around 2 cm - 3 cm, which is acceptable, except for one point, where the discrepancy is around 4 cm - 5 cm.

We also analysed the measurements of KN1 response versus neutron source position. The results for central ring are presented in Figure 5. The results were compared to the calculations performed with Sean Conroy's (SC) model and some discrepancies were observed, mainly in Oct 5, 2 and 3. This led to fine tuning and improvement of the model by improving the models of some massive components ŽĆ, such as ITER-like antenna, Lower Hybrid antenna, Oct 6 limiter support frame, Oct 8 Beam scraper (on Oct 1+7 side) and the trolley of the JET RH system. This led to some improvements of the calculations, however some discrepancies remained due to limited information about the composition and size all components as well as due to limited capabilities to model all components around JET.

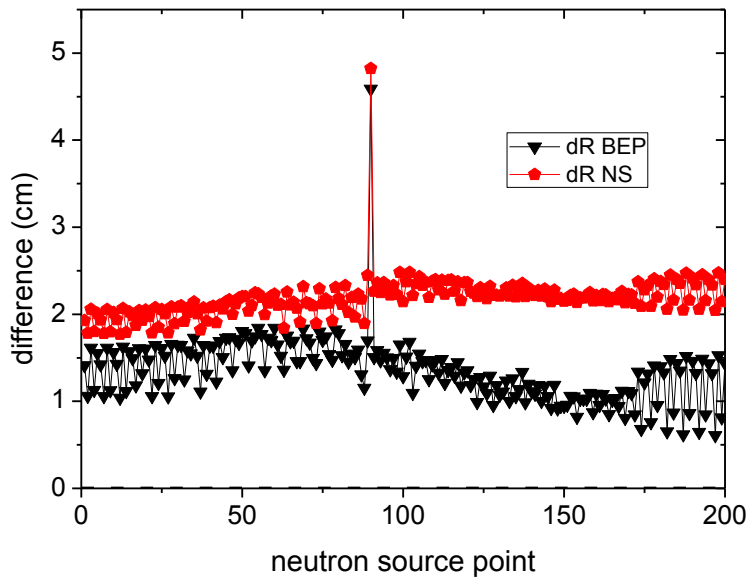


Figure 4: Difference in the target and planned neutron source positions. BEP refers to the baton end point and NS refers to the centre of the actual neutron source capsule position

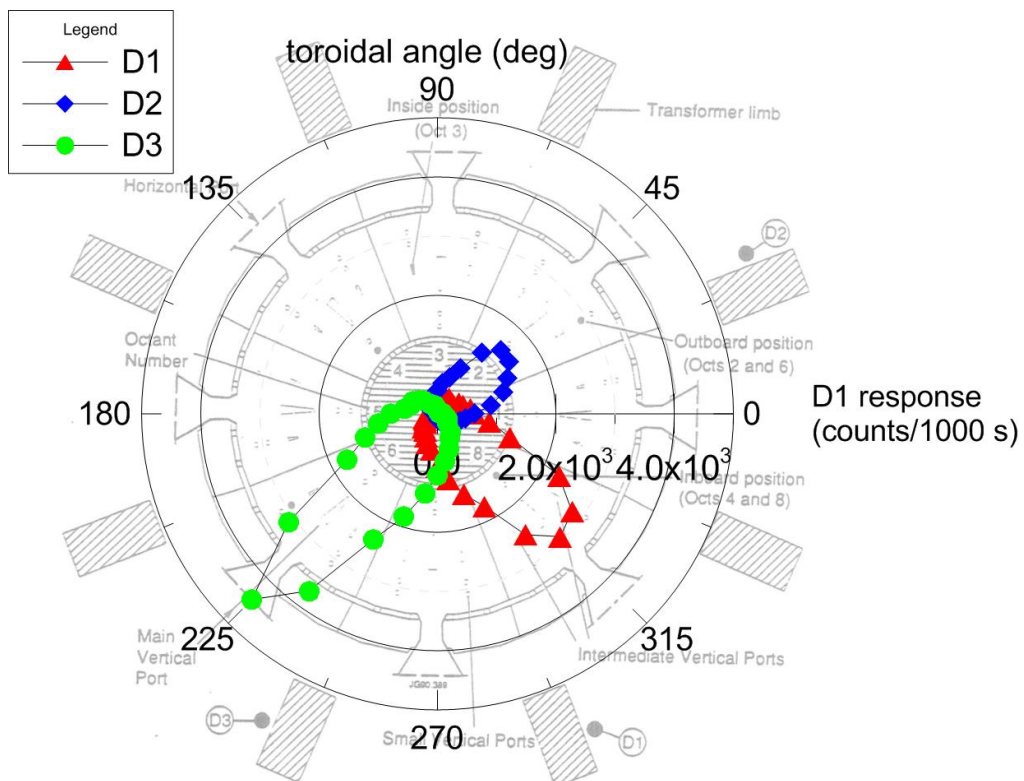


Figure 5: KN1 detector response versus neutron source position.

Based on the remote handling coordinates we calculated the neutron source (NS) positions for the KN2 calibration points as well. The positions were then used in Igor

Lengar's and Sean Conroy's JET model to calculate the model predicted calibration coefficients for the KN2 activation system. In this case we compared the target NS positions and the calculated ones based on the actual remote handling move files (see D3 for further explanation). It was observed that for KN2 lower and middle the differences in the two positions are below 2 cm, which is acceptable. For the KN2 upper, however the calculated differences are 10-14 cm. As a special tool was used to exactly position the NS to the KN2 upper position, we did further investigation. We had long discussions with the RH team and found the following:

- our script (RH2MCNP) correctly predicts the NS position/coordinates in the virtual reality (VR) world
- in the VR world the KN2 upper position (which was accurately determined in the real world by a special device) is 10-14 cm higher than in the real world, indicating that the VR world coordinates are not the same as the real world coordinates. Please see enclosed figure showing the position of the NS in VR in comparison with the positioning tool. The source of this bias might be stretched cables in the K joint (wrist of the mascot robot) of the remote handling system, due to relatively large torque of the relatively heavy baton, which was placed horizontally for all KN2 calibration positions.

In order to make appropriate corrections, the RH system was recalibrated outside the torus hall in order to estimate the systematic uncertainty due to stretched cables. The corrections were then applied to the final calculations of KN2 activation coefficients.

Analysis of neutron flux anisotropy due to neutron source baton

The calibration of the neutron detectors will be performed by moving a standardized ^{252}Cf point neutron source inside around the vacuum vessel and observing the detector response.

The neutron source will be deployed on the JET Mascot robot. In order to safely manipulate the neutron source with the robot, the source will be placed in a specially designed tube (source baton), which will connect to the mascot robot via a longer tube, called the mascot baton. The two batons approach is needed in order to ensure adequate separation of neutron source from the robot body, to reduce neutron scattering from the mascot robot, to reduce activation of the robot and to limit the dose on the robot cameras. The source baton has to be short enough to allow source transport inside it and inside the normal Transport Flask.

The baton is subject to several design constraints; it should be robust, the connection of the source and mascot baton should be fail-safe and the baton should not significantly disturb the spatial neutron flux distribution and energy spectrum of the neutron source. The latter point is especially important for accurate calibration. Hence a set of neutronic calculations is needed to support the baton design. The neutron flux anisotropy calculations were then compared to the measurements in order to independently verify the calculations. The comparison of calculated and measured anisotropy factor is presented in Figure. The results show relatively good agreement between the calculations and measurements. As some information about exact geometry and material composition of the neutron source casing is lacking, the modelling of the source was done with limited accuracy. This is also the main source of discrepancies.

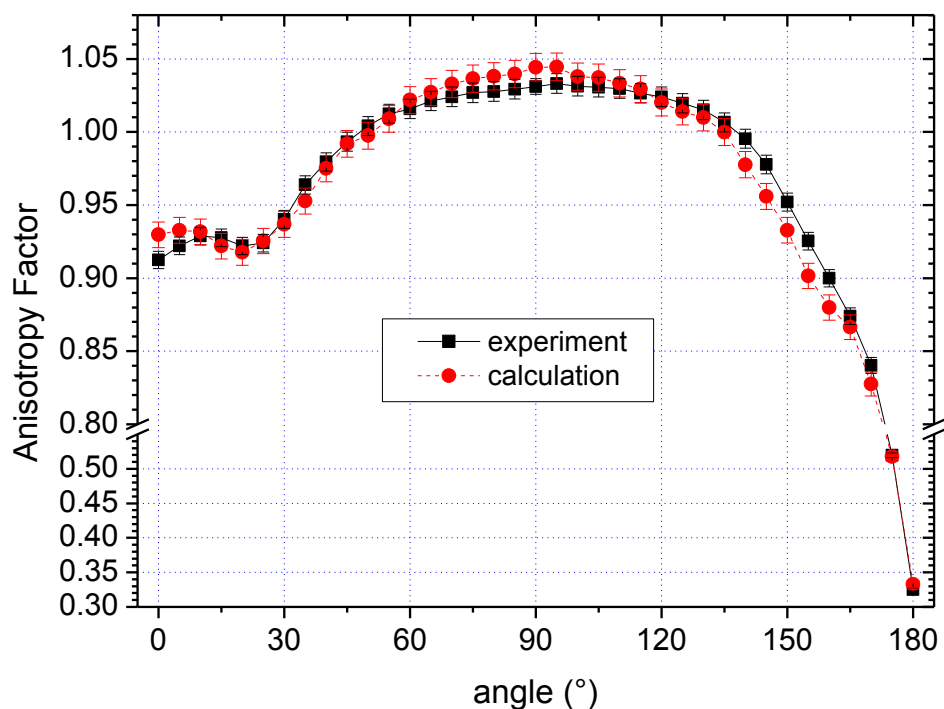


Figure 3: Plot of experimental and calculated anisotropy factor against angle. Error bars represent the combined uncertainty at the 95 % confidence level. The plotted line is an eye guide only.

Assessment of the use of neutron detector for plasma position monitoring system

We identified the reactions (detectors) to be monitored and we made changes to the JET model to be able to perform the assesment. Candiate materials and corresponding reactions for neutron detectors are (235U (n,f), 238U (n,f), 239Pu (n,f), 240Pu (n,f), diamond (n,p)) and reaction rates. We established a simplified MCNP model with top and bottom detectors.

For modelling the plasma source we used Mike Laughlin's script for plasma source in MCNP. With the following data: Major radius = 290 cm, Minor radius = 80 cm, Energy spectrum – DD and DT. Plasma vertical shift varied from -30 cm to + 30 cm from the tokamak mid-plane. For every plasma vertical position we calculated top detector response.

Main findings are the following:

- Ring source and plasma source results agree relatively well
- Highest sensitivity (rel. grad.) obtained with detectors sensitive to fast neutrons only (KN2, (n,f)U-238) → makes sense as they monitor mostly direct neutron from plasma
- U-235 not very good detector as it detects scattered neutrons → low sensitivity to plasma position

- Neutron based plasma position monitoring system should have detectors sensitive to fast neutrons only (If U-238 used, it should be as pure as possible to reduce the contribution of U-235)
- Disadvantage of fast neutron sensitive system is low sensitivity.

Average relative sensitivities of various detectors [%/cm] for different detectors and for two peaking factors (PF) are presented in Table 1. It can be seen that the highest sensitivity is obtained by threshold reactions. Sensitivity is almost independent on the peaking factor.

	DD, PF=1	DD, PF=5	DT, PF=1	DT, PF=5
Flux	0.18	0.18	0.23	0.22
¹¹⁵In (n,n')	0.49	0.47	0.45	0.41
²³⁵U (n,f)	0.061	0.062	0.073	0.077
²³⁸U (n,f)	0.51	0.48	0.58	0.54
²³⁹Pu (n,f)	0.059	0.058	0.081	0.083
²⁴⁰Pu (n,f)	0.35	0.33	0.44	0.42
²⁴¹Pu (n,f)	0.040	0.043	0.056	0.065
²⁴²Pu (n,f)	0.39	0.38	0.49	0.47
C (n, alpha)	/	/	0.61	0.57
C (n,n)	0.14	0.14	0.16	0.16

Table 1: Average relative sensitivities of various detectors [%/cm] for different detectors and for two peaking factors (PF).

3 CONCLUSIONS AND OUTLOOK FOR 2014

In 2014 we will continue with analysis of results of the KN1 calibration and will further expand activities related to assessment of the use of neutron detector for plasma position monitoring system by adding two detectors to the inner and outer side and additional detectors into the vacuum vessel, where neutron spectrum is different than behind the first wall. In addition we will investigate more materials and reactions, e.g. Th-232 and self-powered neutron detectors. We will also work on gathering all results and writing papers to be submitted to SCI journals. In 2014 we will start working on calculations to support JET DT calibration, where knowledge and experience gained in the past projects will be very valuable.

4 REFERENCES

- 1 Syme D.B. et al., Fusion Yield Measurements on JET and their Calibration, *Nuc. Eng. Des.*, vol. 246, p. 185-190, doi: 10.1016/j.nucengdes.2011.08.003,2011
- 2 Laundy B.J., Jarvis O. N., Numerical study of the calibration factors for the neutron counters in use at the Joint European Torus, , *Fusion technology*, vol.24, pages 150-160, September 1993.
- 3 Snoj L. et al., Calculations to support JET neutron yield calibration: contributions to the external neutron monitor responses, *Nuc. Eng. Des.*, vol. 246, p. 191-197, 2011
- 4 Snoj L. et al., Calculations to support JET neutron yield calibration: neutron scattering in source holder, *Fus. Eng. and Des.*, Vol. 87, Issue 11, November 2012, Pages 1846–1852.
- 5 X-5 Monte Carlo Team, MCNP - A general Monte Carlo N-particle Transport code, Version 5, LA-UR-03-1987, April 24, 2003 (revised June 30 2004).
- 6 Snoj L. et al., Calculations to support JET neutron yield calibration: modelling of the JET remote handling system, *Nuc. Eng. and Des.*, Vol. 261; str. 244-250, 2013
- 7 M. Gatu-Johnson et al. (2010). "Modelling and TOFOR measurements of scattered neutrons at JET." *Plasma Physics and Controlled Fusion* 52(8): 085002.

SHUTDOWN DOSE RATE AT JET WITH THE NEW ILW AND PREDICTION OF THE EXPECTED DOSE LEVEL AFTER FUTURE TRITIUM EXPERIMENT

I. Lengar, L. Snoj

Jožef Stefan Institute (IJS), Reactor Physics Department, Ljubljana, Slovenia
e-mail: igor.lengar@ijs.si

1 INTRODUCTION

The activity was a joint work of the associations ENEA, KIT, CCFE and MESCS-SFA. The shutdown dose rate in the JET torus was determined experimentally, in parallel calculations have been done. The activity was a follow-up of past activities, performed over several years. Basically two different methodological approaches have been developed in the frame of the Fusion Technology Program for the three-dimensional calculation of the shutdown dose rate: the so-called Rigorous two-step method (R2S) developed by KIT and the Direct one-step method (D1S) developed by the ITER team and ENEA. Both methods, even if with different approaches, use the MCNP Monte Carlo Code for transport calculation and the FISPACT inventory code.

The aim of the present task is the measurement and corresponding calculation of the shutdown dose rate at short cooling times, more accurate with respect to the previous ones. Additional information on the main contributors to the doses is also obtained through gamma spectrometry. The goals are the validation of the shutdown dose rate calculation with the new ILW through dose measurements during 2012 off-operational period and estimation of shutdown dose rate following hypothetical DT irradiations in preparation of the future tritium experiment.

The task of the MESCS-SFA was the preparation/upgrade of the MCNP model for the calculations. The last version of MCNP model of Octant 1, used to estimate the preliminary effect of ILW in the frame of a previous task has been modified in order to include the description of relevant components (geometry and material).

2 WORK PERFORMED IN 2013

The task of JSI was the preparation of the MCNP model to be used by other associations, also collaborating on the project, for their calculations. This has mainly been done during the year 2012. The resulting model is graphically presented in Figure 1.

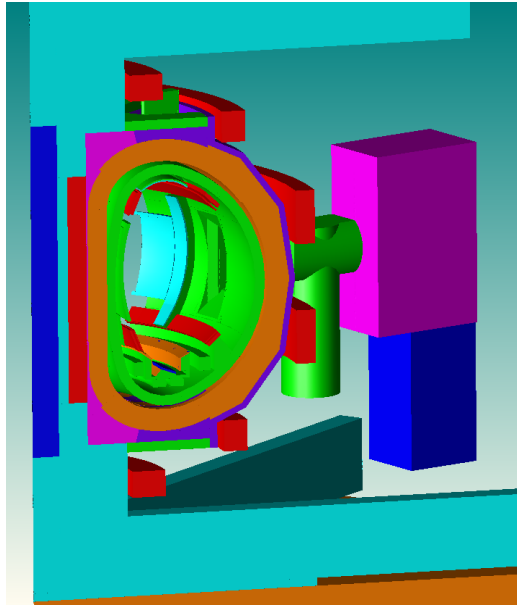


Figure 1: Graphical presentation of the final model (by MCAM graphical interface).

In 2013 the focus was on the improvement of the model, especially on the elimination of geometry errors, resulting in particles being lost during calculations. In long runs a few spots were identified in the model, where small geometrical errors were present and particles got lost. The spots were corrected and in this way the lost particles eliminated.

3 CONCLUSIONS AND OUTLOOK FOR 2014

The MCNP model of the Octant 1 of JET was further upgraded in order to be optimized for calculation of the shutdown doses, needed as support for the shut down dose measurements, carried out within the same project by ENEA and CCFE. The improvement was in a thorough examination of the model and elimination of geometry errors, resulting in lost particles during calculations.

The MCNP model will be, with regards to the experimental needs, further upgraded. The final calculations expected after the experimental data will be provided.

4 REFERENCES

- 1 Y. Wu, FDS Team, CAD-based interface programs for fusion neutron transport simulation, Fusion Engineering and Design 84 (2009) pp 1987 – 1992.

ESCAPING ALPHA PARTICLE MEASUREMENTS BY ACTIVATION FOILS IN JET - MCNP SIMULATION OF THE NEUTRON FLUX AT THE KA2 LOCATION

I. Lengar

Jožef Stefan Institute (IJS), Reactor Physics Department, Ljubljana, Slovenia
e-mail: igor.lengar@ijs.si

G. Bonheure

Forschungszentrum Juelich GmbH, 52425 Juelich, Germany

1 INTRODUCTION

The aim of the project is the test and development of escaping alpha particle measurements using the foil activation technique for real D-T fusion conditions and to provide for an absolute measurement of the fluence and the energy spectrum of escaping alpha particles at several poloidal positions and the collection of data for assessment of the activation induced at the reactor walls by MeV escaping ions. The activation measurements are expected to complement the results of other alpha particle diagnostics.

The KA2 faraday cup diagnostic array was chosen for the location for the activation foils to be used for alpha particle detection. This experimental part of the activity comprises:

- Irradiation of selected foils at a charged particle (alpha beam, IPNAS, Liege University)
- Characterization of foil materials in neutron field, to investigate experimentally the response to 14 MeV neutrons using a neutron generator (FNG, ENEA-Frascati)
- Analysis of activated foils (IPNAS-Liege, HADES-Mol, Gran Sasso-Italy,)

In addition simulations and calculational study of the response of the activation foils are required, what is partly done by the work, described in this document.

2 WORK PERFORMED IN 2013

The aim of the described sub-task was the improvement of the 2012 preliminary simulation results by taking a more realistic neutron spectrum into account. MCNP calculations of the neutron spectrum at the proposed location for the foils, i.e. the KA2-diagnostic, were calculated with the new JET ITER like wall configuration and materials.

The MCNP code (MCNP5, version 1.40) was used with a set of ENDFB/IIV cross-section data. The original MCNP model was developed in the frame of the previous tasks. The current MCNP model of JET covers the full 360° in-vessel and contains the ILW materials; Be and W. The level of detail is increased with respect to previous models in the regions, important for neutron diagnostics. A scheme of the in-vessel structures is presented in Figure 1.

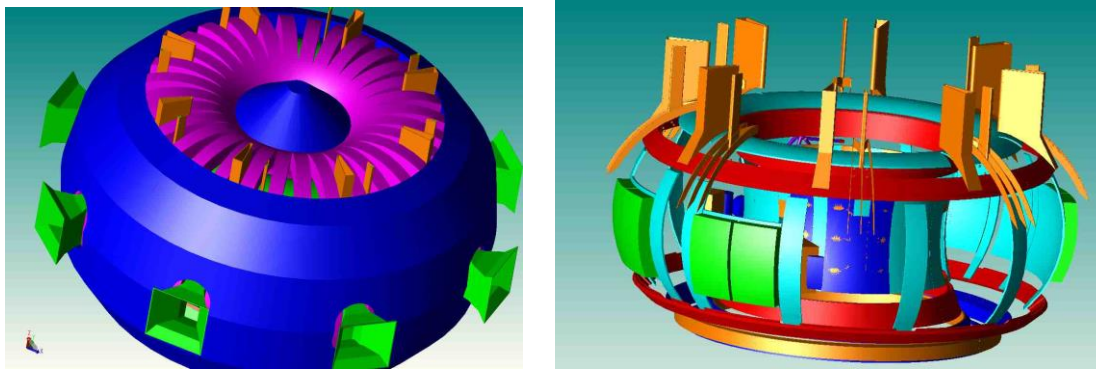


Figure 1: MCNP model of JET; presentation of the vessel (left) and some of the in-vessel structures (right); the level of detail of the model can be anticipated from the figures.

The neutron spectrum was required in the KA2 diagnostics, the Faraday cups, presented in detail in Figure 2.

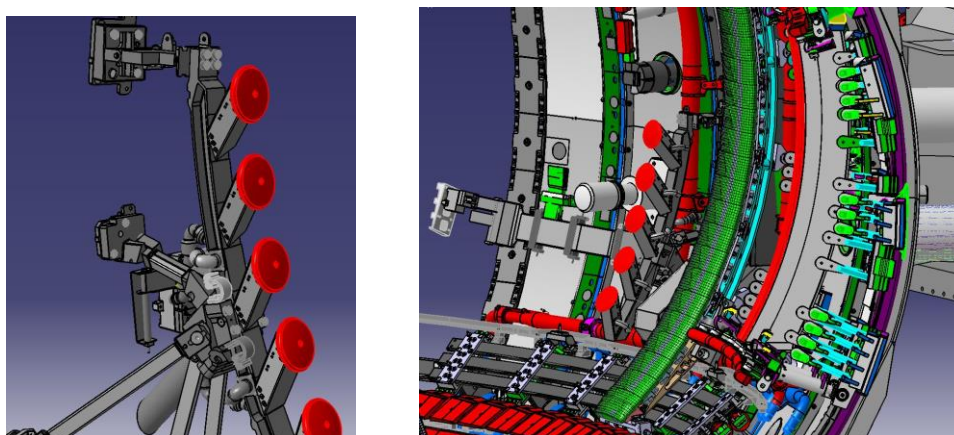


Figure 2: The KA2 diagnostics (left), and its position in the JET vessel, octant 7 (figures produced with CATIA).

The spectra have been calculated at the positions of the five cups of the KA2 diagnostics, visible in both pictures (colored in red). The modification of the spectrum due to the KA2 structures was not taken into account since the position of the foils was not known, i.e. the approximate spectrum, not perturbed by the structure itself, was determined. This should be, however, a good estimation of the true flux in the case of a DT plasma. The difference in the flux at the five different positions of the KA2 cups was studied. The exact locations, in absolute coordinates of the JET torus coordinate system, are presented in Table 1.

	position for spectrum calculation				
	M1	M2	M3	M4	M5
x (mm)	387.5	384.0	378.6	371.4	361.9
y (mm)	31.3	31.0	30.0	27.3	26.6
z (mm)	7.1	-13.1	-32.6	-51.3	-69.5

Table 1: Exact locations of the JET torus coordinate system.

The results of the spectra are presented in Figure 3 for a DT plasma. A typical DT JET plasma neutron source was used with the following characteristics – major radius 290 cm, minor radius 80 cm, elliptical elongation of 1.6, Gaussian neutron spectrum with a mean energy of 14.1 MeV. The graphs in Figure 3 present the neutron fluence (in cm^{-2}) per MeV, per 1 neutron, born in the plasma.

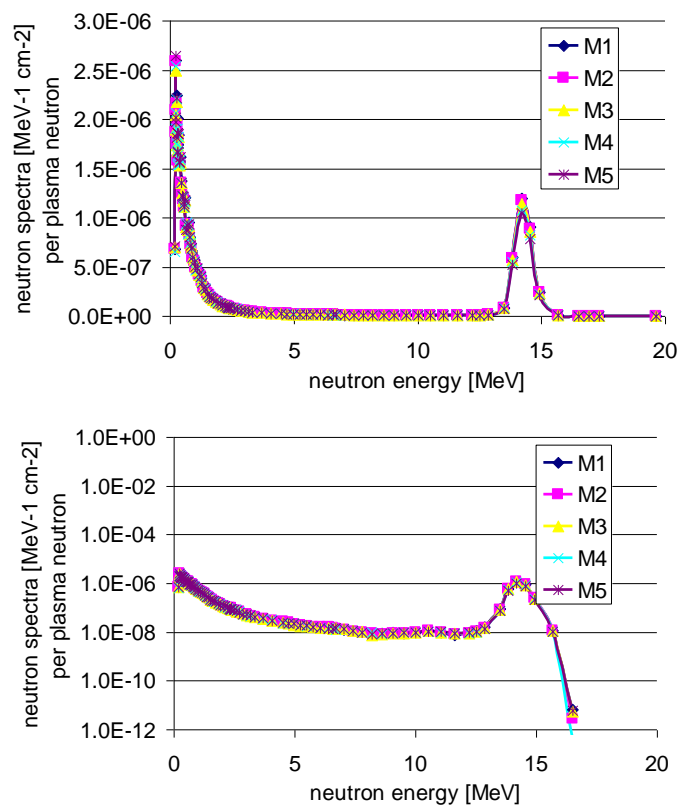


Figure 3: Spectra at the positions of the Faraday cups, DT plasma. Neutron fluence (in cm^{-2}) per MeV, per 1 neutron, born in the plasma. Linear scale (upper picture) and logarithmic scale (lower picture).

It can be observed from the figures that the change in the spectra with respect to the position of calculation (in the different Faraday cups, M1–M5) is minor.

3 CONCLUSIONS AND OUTLOOK FOR 2014

The spectra in the position of the Faraday cups – KA2 – have been calculated. In future, the calculations could be repeated after knowing the exact location of foils inside the Faraday cups, in order to examine the effect of the cup material on neutron spectra. The data are used for calculation of the reaction rates of charged particle detector material to neutrons.

ACTIVATION ANALYSIS OF JET IN-VESSEL COMPONENTS FOLLOWING DT IRRADIATION – NEUTRON FLUX CALCULATIONS

I. Lengar

Jožef Stefan Institute (IJS), Reactor Physics Department, Ljubljana, Slovenia
e-mail: igor.lengar@ijs.si

1 INTRODUCTION

The forthcoming Deuterium-Tritium (DT) campaign at the Joint European Torus (JET) will induce a significant activation of the system components. In the task the temporal evolution of the radioactive species in the main in-vessel components after the end of the future DT campaign, assuming different levels of neutron irradiation. The topic of the sub-task, described in this document is calculation of the neutron flux in the selected components, done by the MCNP5 code using the emission source by a typical DT plasma. Subsequently the resulting neutron spectra are input to the FISPACT code that computes the evolution of the radioactive species generated by the neutron activation process. For each irradiation scenario, the time behavior of the contact dose rate is determined.

2 WORK PERFORMED IN 2013

In order to be able to calculate the activation of components [1], the neutron flux was calculated using the Monte Carlo code MCNP5 with ENDF/B-VII nuclear data library. The neutron flux in the components of interest is calculated following the neutron emission in a typical DT plasma discharge using a three-dimensional model of the JET machine, upgraded with ITER-like wall on the basis of the original model for horizontal neutron camera calculations [2]. The Monte Carlo approach allows a detailed treatment of the geometrical configuration and the neutron flux is calculated in cells made of homogeneous materials. The flux has been calculated in four locations, marked in Figure 1.

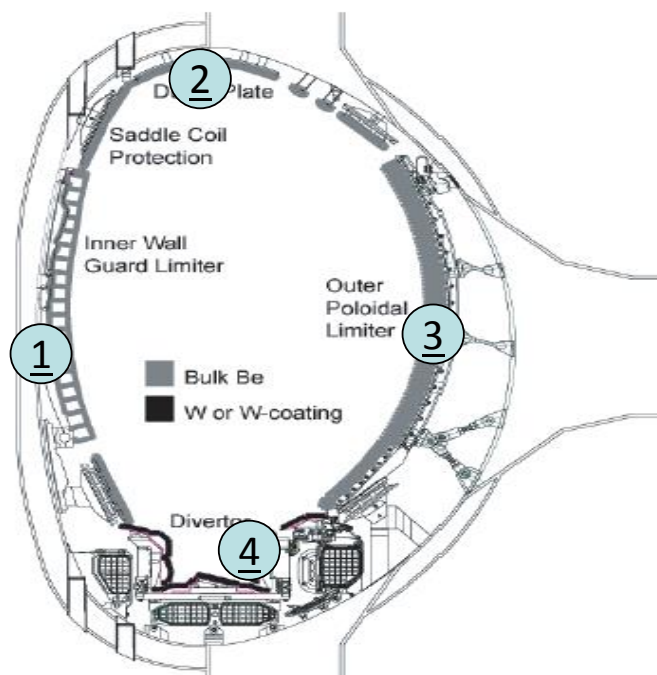


Figure 1: Sketch of the JET geometry and localization of the components considered in the present analysis.

The spectra have been calculated using the VITAMIN-J 175 energy group format for insertion into FISPACT and are presented in Figure 2.

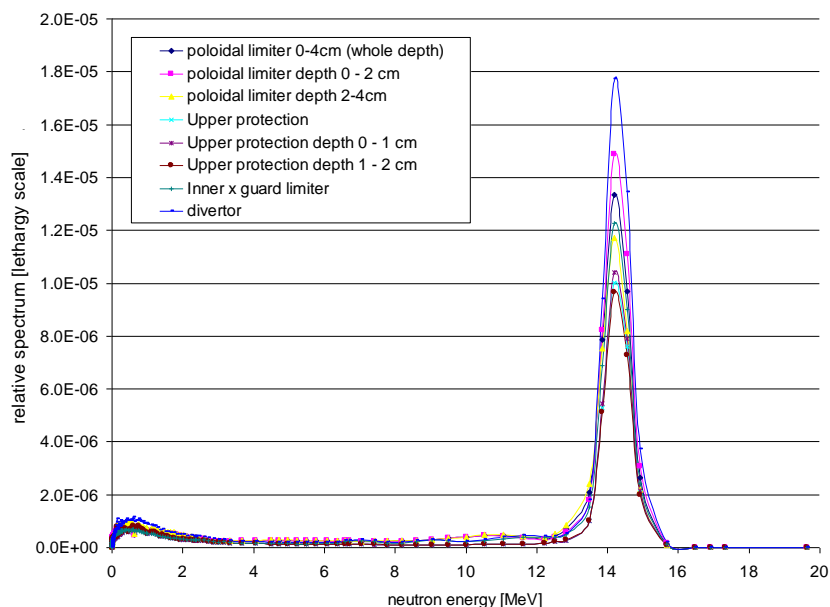


Figure 2: Spectra in four locations and two depths.

In order to determine the change of the spectra with the depth in material the spectrum has been determined in the poloidal limiter in the depth of 0-2 cm and 2-4 cm, what is graphically presented in Figure 3.

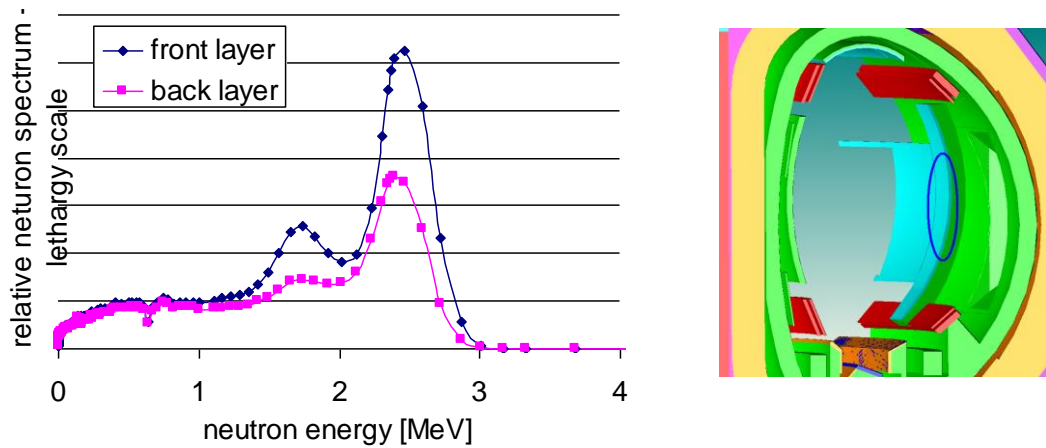


Figure 3: Spectra in the poloidal limiter in the depth of 0-2 cm and 2-4 cm and the approximate location of calculation in the poloidal limiter.

In order to examine the change of the spectra with the depth in material, the ratio of the flux in the surface layer of 2 cm with respect to the subsequent layer of equal thickness was plotted as function of energy (Figure 4)

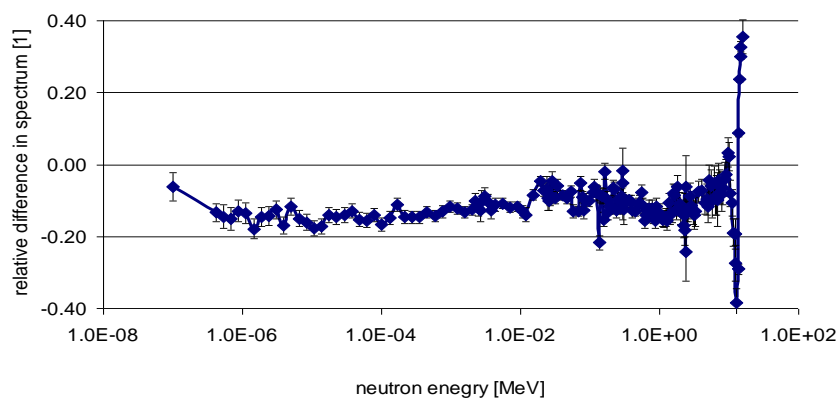


Figure 4: Ratio of the flux in the surface layer of 2 cm with respect to the subsequent layer of 2 cm as function of energy.

Subsequently the calculated neutron spectra have been used as input for the FISPACT 2010 activation code [3], what has been done in the frame of a different subproject.

The possible influence on results due to the usage of a specific library for fusion applications rather than the ENDF library was also investigated. The FENDL 2.1 library was used and the difference in the total neutron fluxes did not exceed 3% for any of the

components, this value being only slightly larger than the statistical accuracy. This has been assumed to be the uncertainty due to the influence of the data library on results.

3 CONCLUSIONS AND OUTLOOK FOR 2014

The spectra at specific locations in the JET torus has been predicted using the MCNP5 code for usage as input for the evolution of the dose rates of the main in-vessel components at the end of the forthcoming DT experimental campaign in JET. In perspective, further analyses will be performed with more accurate chemical materials compositions, including also trace impurities. This could necessitate also further more detailed calculations of neutron spectra. The final results could then be validated against experimental data, when they will be collected and made available.

4 REFERENCES

- 1 M.J. Loughlin, R.A. Forrest and J.E.G. Edwards, Neutron Activation Studies on JET, EFDA-JET-CP(00)01/12, Culham (2000).
- 2 I. Lengar, Verification of the JET MCNP Model and Transport Calculations, Estimation of Wall Activation, JW10-FT-5.34. Reports to EFDA-ITER Fusion Technology Programme (2010).
- 3 J.-C. C. Sublet, J.W. Eastwood and J.G. Morgan, The FISPACT user manual, CCFE-R(11) Issue 3, Culham Science Centre (2012).

FABRICATION AND CHARACTERISATION OF W-SiC COMPOSITES

Saša Novak, Aljaž Ivekovič

Jožef Stefan Institute, Jamova cesta 39, 1000 Ljubljana
e-mail: sasa.novak@ijs.si

1 INTRODUCTION

W considered as a plasma facing material and was also considered as a protective coating in the advanced concepts of fusion reactors envisioning the use of SiC fibre reinforced SiC composites (SiC_f/SiC) as structural material. Due to small thermal mismatch of W and SiC, such application is feasible; however the interfacial reactions at elevated temperatures require additional attention in order to prevent failure of the protective coating. The use of W in form of fibres or particles in SiC-based composites was also suggested as a possible path toward a material with improved thermal conductivity.

The use of liquid polymer precursor as a way to densify the material was investigated and also implemented in the SITE processing of SiC_f/SiC composites. One of the main drawbacks of the process is low volume yield of the polymer-to-ceramic transformation resulting in long processing times (several infiltration cycles are needed in order to achieve densification). One of the possible ways to enhance densification is the use of active-filler-controlled pyrolysis. Active filler material (typically metal or metallic silicide) expands during reaction with decomposition products of a polymer phase or the reactive atmosphere (N₂, NH₃ ...) and thus compensate for the shrinkage of the polymer during pyrolysis.

The work performed within EFDA coordinated project WP13-MAT-HHFM-03-01/MESCS proposes the application of SITE processing technology and active-filler controlled pyrolysis to the formation of W-SiC-based composites, suitable for armour applications in future fusion reactors or as stand-alone low-activation fusion material.

2 WORK PERFORMED IN 2013

In initial investigation, W-SiC composites were densified by polymer infiltration and pyrolysis at maximum heating temperature of 1600 °C, which revealed that samples with high tungsten content (>50 vol. %) in the initial powder mixture could be densified in a single densification step. The sample exhibited good mechanical properties: flexural strength of 250 MPa, hardness of ~ 500 HV and elastic modulus of up to 290 GPa. Room temperature thermal conductivity of such material was relatively low (~ 15

$\text{Wm}^{-1}\text{K}^{-1}$), however, unusual increase of conductivity with temperature was observed. The highest value measured at $1000\text{ }^\circ\text{C}$ was $\sim 25\text{ Wm}^{-1}\text{K}^{-1}$.

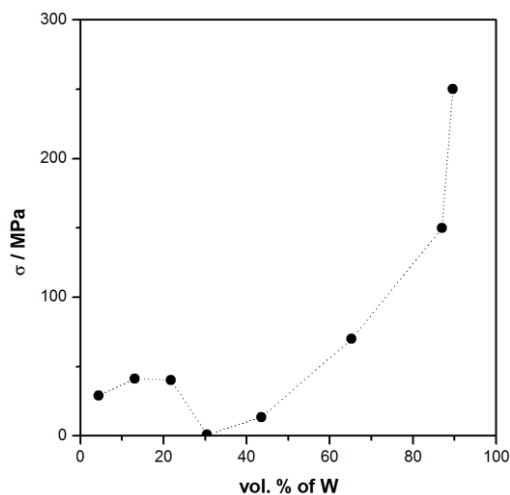


Figure 6: Flexural strength of W-SiC composite samples as a function of W content.

Based on preliminary results we planned further work in two directions, high tungsten content samples and low tungsten content samples.

The material fabricated from high tungsten content samples is an attractive material for low-activation armour applications as well as a coating and joining material in nuclear fusion environment. On the other hand low-tungsten content material might lead to SiC-based matrix with enhanced properties for the use in SiC-based fibre reinforced composite materials for structural application. First, the effect of fabrication temperature on mechanical and thermal properties of the material with high tungsten content was investigated.

Second, the effect of further densification of samples with low tungsten content (<35 vol % of W) was investigated.

High tungsten content

Next to samples containing 87 vol. % of W in the initial powder/polymer mixture (sample W7) fabricated by uniaxial pressing at 60 MPa, also samples containing 89.6 vol. % of W were fabricated by additional isostatical pressing of samples at 750 MPa (sample W8). Final densification of samples was performed at maximum temperatures of 1600, 1700, 1800 and 2000 $^\circ\text{C}$. As is evident from (Figure 7) the higher initial density of isostatically pressed samples (~ 60 vol.%) in contrast to uniaxially pressed samples (~ 50 vol.%) resulted in smaller shrinkage of densified material, which was especially evident at higher fabrication temperatures. Nevertheless, microstructural investigation of polished cross-sections with a field-emission scanning electron microscope (FEG-SEM) (JEOL JSM-7600F, Tokyo, Japan) revealed that the central part of W8 samples was not fully densified at all fabrication temperatures, exhibiting large areas of high porosity. The resulting microstructure is most likely the result of unsuccessful infiltration with pre-ceramic polymer due to increased green density and smaller pore size after isostatic pressing (Figure 8), preventing successful infiltration.

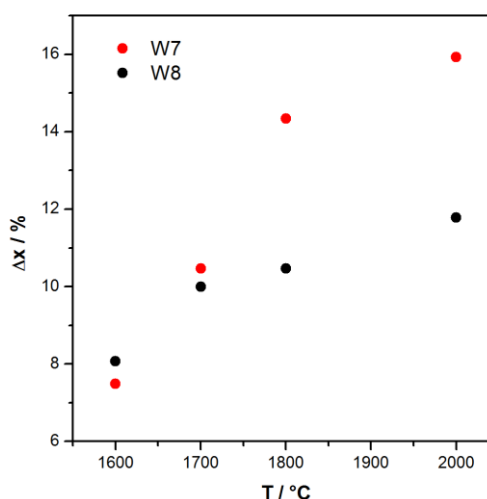


Figure 7: Shrinkage of W7 and W8 samples as a function of fabrication temperature.

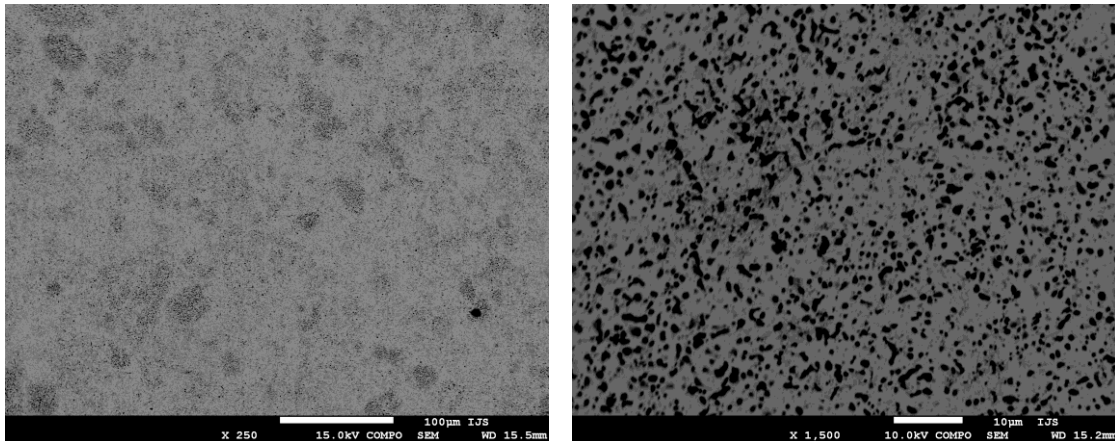


Figure 8: Polished cross-section of W8 sample densified at 1700 °C indicating poor densification in the centre of sample.

On the other hand W7 samples revealed a homogeneous microstructure through the entire thickness of the sample with high degree of densification. As is presented in (Figure 9) the microstructure is composed of three phases which were identified as W, W₂C and W₅Si₃ by X-ray diffraction (XRD) using a diffractometer (D4 Endeavor, Bruker AXS, Karlsruhe, Germany) with Bragg-Brentano geometry, a Cu K α radiation source and a Sol-X energy-dispersive detector.

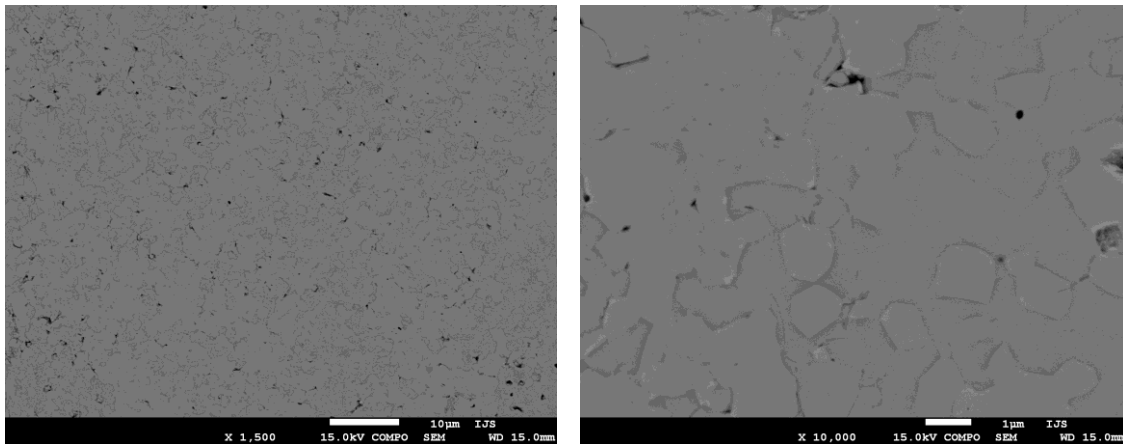


Figure 9: Polished cross-section of W7 sample densified at 1700 °C at different magnifications.

The strength was measured using piston-on-three ball biaxial strength testing (Galdabini Quasar 50, Italy). The strength of the material was increased for the samples heated at 1700 and 1800 °C, achieving 350 – 400 MPa. Samples fabricated at 2000 °C exhibited somewhat lower values of flexural strength, which can be attributed to grain growth during heat treatment. Grain size increased from initial <1 µm to ~ 3 µm.

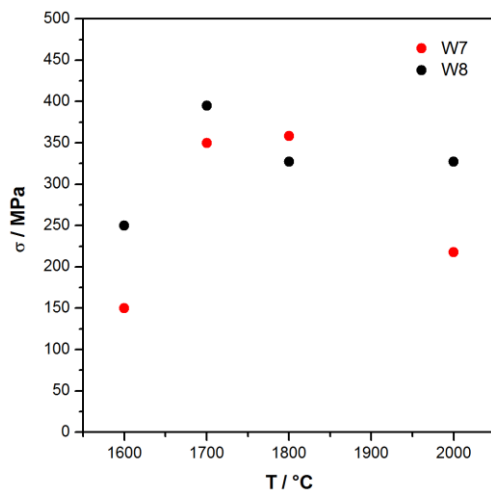


Figure 10 Flexural strength of W7 and W8 samples as a function of maximal fabrication temperature.

Hardness and indentation modulus were measured using Vickers nanoindentation (Fischeroscope H100C, Helmut Fischer, Sindelfingen-Maichingen, Germany). Hardness of the material increased with increasing fabrication temperature up to ~1100 HV for W7 as well as W8 samples (Figure 11a). Elastic modulus however exhibited a different behaviour. In the case of W8 samples the highest E_{IT} of 380 GPa was measured for samples fabricated at 2000 °C, whereas for W7 samples highest E_{IT} of 260 GPa was measured for samples fabricated at 1800 °C (Figure 11b).

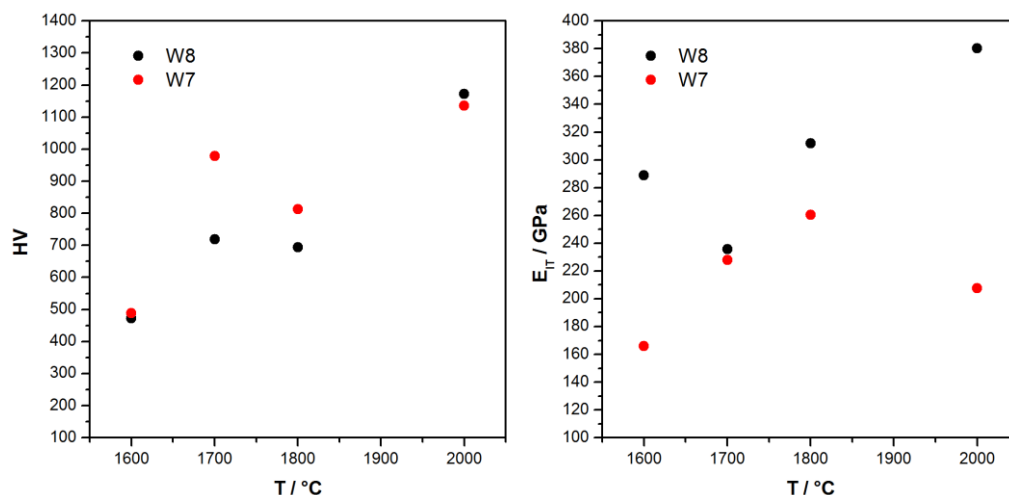


Figure 11: Hardness and indentation modulus of W7 and W8 samples as a function of fabrication temperature.

Low tungsten content

Sample with 21.75 vol % of W in the initial powder/polymer mixture (sample W3) was selected as a model sample for investigation of effect of densification of low tungsten content samples with additional PIP cycles. Since the main goal of this investigation was to apply such matrix material to the fabrication of SiC-based fibre reinforced composite materials only two maximum heating temperatures of 1700 and 1800 °C were selected.

The porosity and median pore size of the material decreased after each PIP cycle. After six cycles the porosity of samples was 15 % for samples fabricated at 1700 °C as well as 1800 °C. On the other hand pore size of samples fabricated at higher temperature (1800 °C) was higher than for those fabricated at lower temperature (1700 °C) which is in agreement with increase in pore size with temperature for sintered SiC.

After six densification cycles median pore size was 220 nm and 315 nm for samples fabricated at 1700 °C and 1800 °C, respectively.

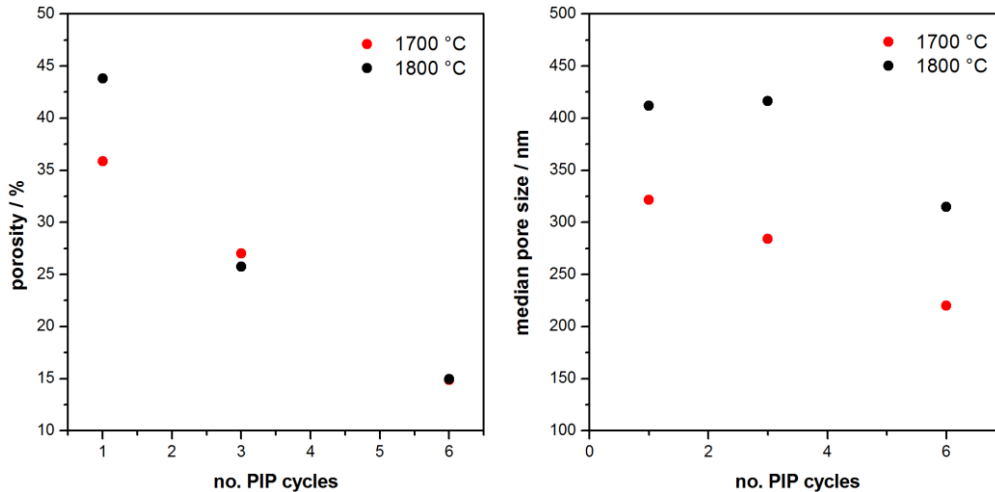


Figure 12: Evolution of porosity and median pore size with number of densification steps.

Decrease in porosity was also observed by investigation of microstructure on the polished cross-sections of samples after each densification step. As is evident from Figure 13, the density of the material after six PIP cycles (Figure 13b) was significantly increased in contrast to sample after only one densification step (Figure 13a).

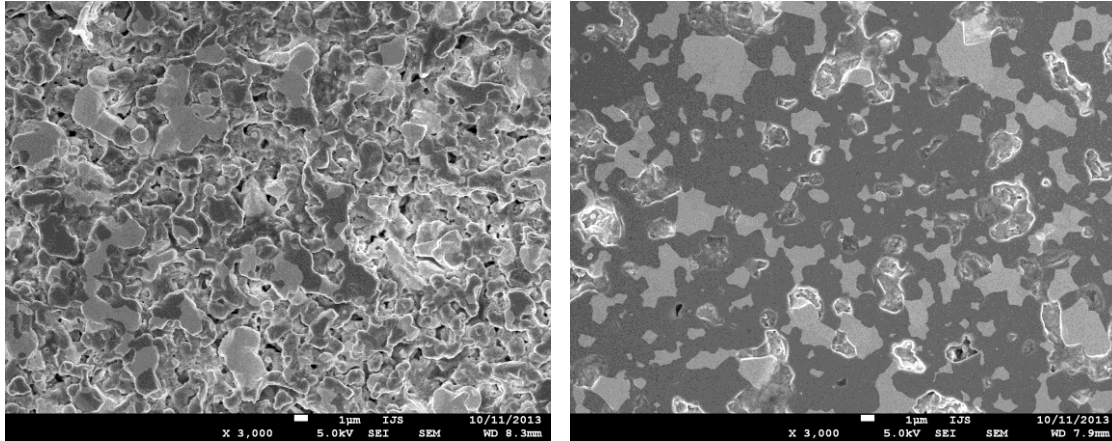


Figure 13: Polished cross-sections of W3 sample after densification with one a) and six b) PIP cycles.

Phase composition of W3 samples fabricated at 1700 °C and at 1800 °C was identical. The material was composed of SiC, WSi₂ and WC. The phase composition only changed if the samples were exposed to higher temperature (2000 °C) where WSi₂ and WC transformed to a more temperature stable W₅Si₃ and W₂C phases.

Flexural strength of the samples was increased with increase in density, achieving 300 MPa for samples densified at 1700 °C and above 400 MPa for samples fabricated at 1800 °C (Figure 14a). Increase in density also reflected in an increase in thermal conductivity. After six densification cycles, room temperature thermal conductivity was ~80 Wm⁻¹K⁻¹ for samples densified at 1700 °C and 100 Wm⁻¹K⁻¹ for

samples densified at 1800 °C. At 1000 °C values decreased to 26 and 32 Wm⁻¹K⁻¹ for samples fabricated at 1700 °C and 1800 °C respectively.

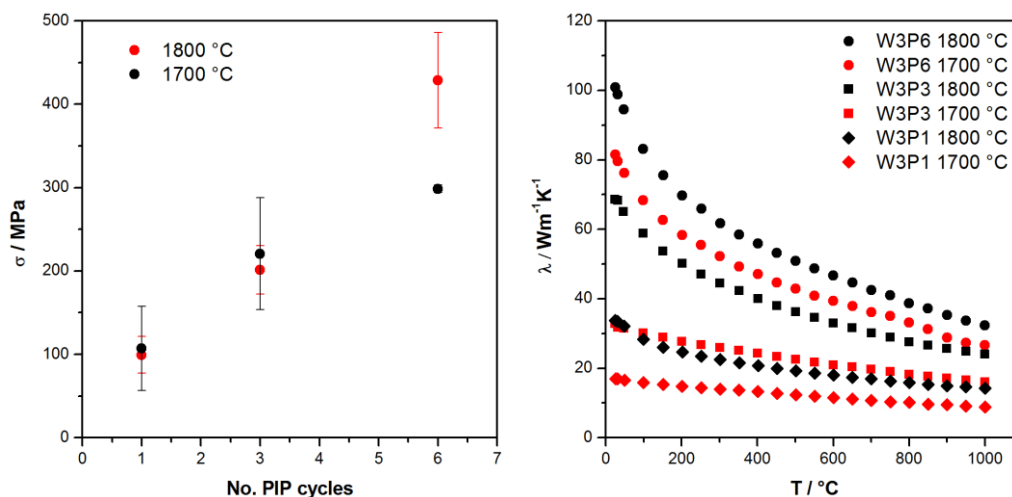


Figure 14: Increase in flexural strength a) and thermal conductivity b) as a function of density and fabrication temperature.

3 CONCLUSIONS AND OUTLOOK FOR 2014

Optimal fabrication temperature for high tungsten content samples was identified in the region between 1700 and 1800 °C, where samples achieved flexural strength above 350 MPa, hardness of 800 HV and indentation modulus of 250 GPa. Further increase in green density resulted in faster, however nonhomogeneous densification through the thickness of the samples.

Additional densification of low tungsten samples resulted in an increase in mechanical as well as thermal properties. After six PIP cycles the material exhibited flexural strength of ~300 MPa for samples fabricated at 1700 °C and >400 MPa for samples fabricated at 1800 °C. Room temperature thermal conductivity was ~80 Wm⁻¹K⁻¹ for samples densified at 1700 °C and 100 Wm⁻¹K⁻¹ for samples densified at 1800 °C. At 1000 °C values decreased to 26 and 32 Wm⁻¹K⁻¹ for samples fabricated at 1700 °C and 1800 °C respectively. Application of such matrix material to the fabrication of SiC-based fibre reinforced composite is foreseen.

A series of samples with high tungsten content (W7 and W8) densified at 1700 °C was also sent to Forschungszentrum Juelich - Institut fuer Energieforschung (IEK-2) for thermal shock tests at different base temperatures (RT, 400°C, 1000°C) with power density close to the damage threshold of pure tungsten (around 250 MW/m²) and exposure to 100 to 1000 ELM-like thermal shock events.

OPTIMIZATION OF SiC-BASED COMPOSITES

Saša Novak, Aljaž Ivekovič

Jožef Stefan Institute, Jamova cesta 39, 1000 Ljubljana
e-mail: sasa.novak@ijs.si

1 INTRODUCTION

SITE process, a combination of electrophoretic deposition and polymer infiltration and pyrolysis is an alternative technique for fabrication of SiC-based fibre reinforced composites. It was shown that SiC_f/SiC composites fabricated by SITE process exhibit high thermal conductivity in contrast to standard fabrication techniques, however the reaction of PyC interphase layer typically used in fabrication of such composites is unstable under fabrication conditions and therefore poor mechanical behaviour was observed. A multilayer (PyC-SiC)_n was already reported as being more stable under neutron irradiation in comparison to PyC and could also provide a more stable interphase under SITE processing conditions. Therefore a multilayer (PyC-SiC)_n was proposed or alternatively, since the fibres are already coated with PyC, a thin protective layer of SiC. The work performed within EFDA coordinated project WP13-MAT-HHFM-04-01/MESCS proposes the optimisation of existing SITE process by improvement of the interphase layer between the fibres and the matrix, investigation of fabrication temperature on thermal transport properties and by application of a closing coating to ensure He impermeability.

2 WORK PERFORMED IN 2013

In the previous investigations it was found that SiC_f/SiC composites prepared by SITE process exhibit favourable behaviour, however, they were characterised by the relatively low measured flexural strength. This was found to be the consequences of the too thin and discontinuous interphase layer on the fibre preform. During polymer pyrolysis and heat treatment > 1600 °C, the interphase layer reacted with polymer during polymer-to-ceramic transformation. Furthermore, during consecutive polymer infiltration and pyrolysis cycles partial sintering of the reinforcing fibres was observed. As a consequence, the fibres could no longer act as a reinforcing phase to deflect propagating crack and thus the material behaved as a porous bulk ceramic. Therefore, a more stable interphase layer is needed in order to protect the fibres and to obtain a material with desired mechanical properties. In collaboration with EU manufacturer of CVI-SiC_f/SiC composites MT Aerospace, a ~2 µm chemical vapour deposited SiC coating was applied over Tyranno SA Grade 3 fibres, previously coated by ~100 nm PyC interphase coating. Microstructure investigation of coated fibre bundle revealed that the coating was successfully applied over the fibres. The thickness of the coating

varied, depending on the position of deposition. In intrabundle areas the coating thickness is typically thinner ($\sim 1 \mu\text{m}$), due to the closing of the intrabundle porosity during CVI preventing further infiltration.

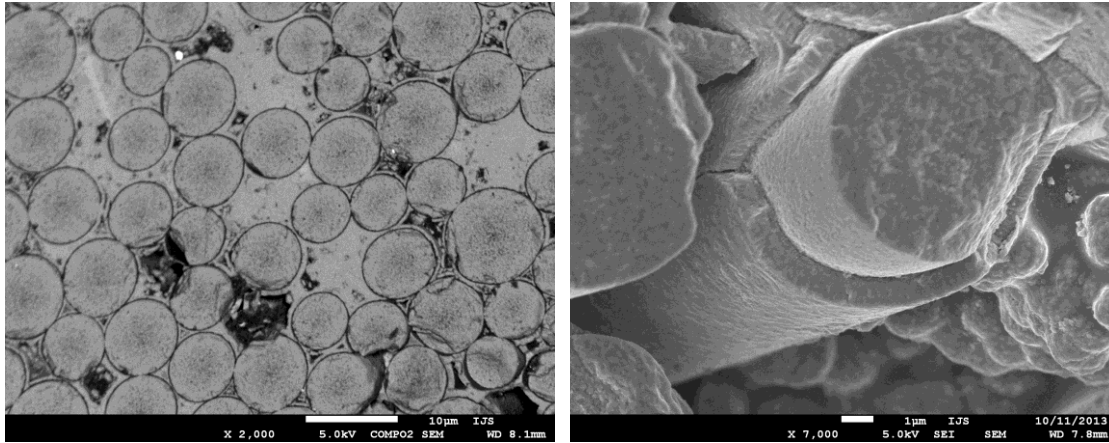


Figure 15: Polished cross-section a) and fracture surface b) of a Tyranno SA Grade 3 fibre bundle coated by $\sim 2 \mu\text{m}$ CVI-SiC coating.

In order to ensure the stability of SiC coating and especially the PyC coating already applied at the surface of the fibres, fibre bundle was heat treated up to $1800 \text{ }^\circ\text{C}$ in vacuum. As is evident from Figure 16 the 100 nm PyC coating is still observed indicating that there is no reaction of CVD-SiC coating with PyC at SITE fabrication conditions. Higher temperatures were not evaluated since the process itself is limited by the temperature stability of the reinforcing fibres ($\leq 1800 \text{ }^\circ\text{C}$).

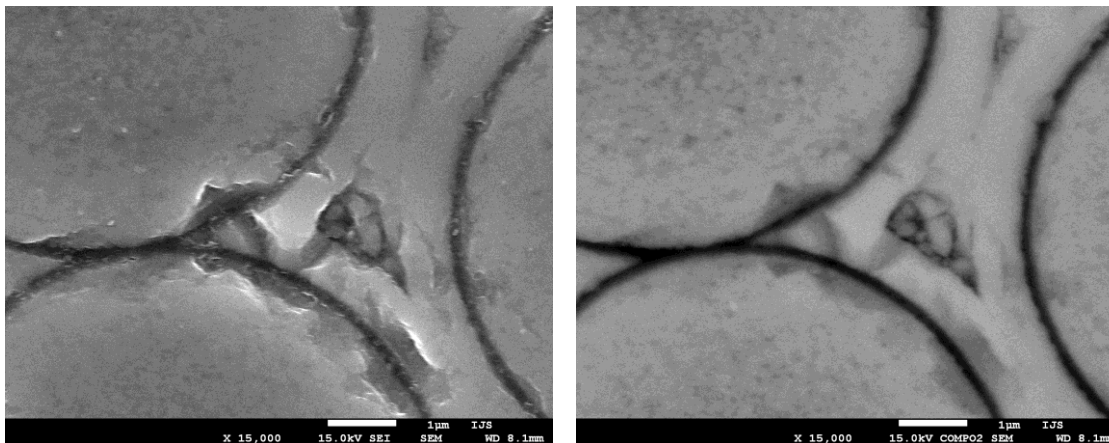


Figure 16: Secondary electron and backscattered electron image of SiC-coated SiC fibre bundle after annealing at $1800 \text{ }^\circ\text{C}$ for 2h in vacuum.

SiC coated fibre preform was infiltrated by electrophoretic (infiltration) deposition using standard SITE process parameters. The microstructural investigation indicates that the rate of infiltration was successful, however a full characterisation of mechanical and thermal transport properties is needed in order to fully characterise the material.

To study the effect of temperature on densification and thermal transport properties of the composite material, samples of european reference material (CVI-SiC_f/SiC) were heat treated at different temperatures (1700 °C, 1800 °C) and thermal diffusivity was measured in collaboration with NRG, Petten (Netherlands). Simultaneously the effect of annealing temperature on the microstructure (grain size, interphase) was evaluated. Thermal diffusivity of 2D reinforced reference material was increased by annealing at 1700 °C and even more for the material annealed at 1800 °C. This result was in agreement with expectations that higher annealing temperature and consequential SiC grain growth would lead to higher thermal conductivity. On the other hand, annealing of 3D reinforced reference material resulted in a slight decrease in thermal diffusivity. Since thermal diffusivity of 3D reinforced material is mainly governed by the properties of the fibres the effect of matrix grain growth on thermal transport was negligible.

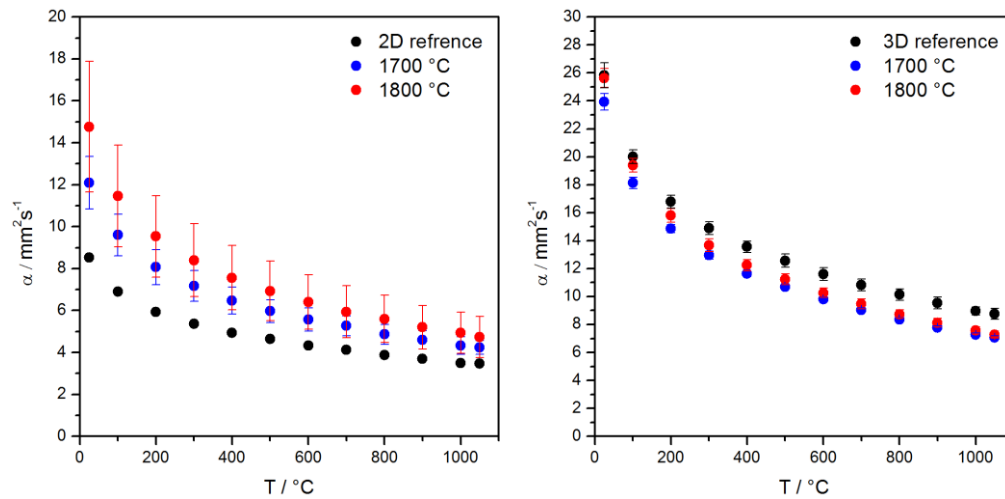


Figure 17: Thermal diffusivity of 2D and 3D EU reference material as a function of temperature and annealing conditions.

A part of the study was devoted also to He impermeability of the SITE SiC/SiC composite. Large effort was done to determine suitable experimental set up. As the current material is not fully dense, a certain degree of gas permeability was measured and therefore, to ensure impermeability, a closing layer should be applied on the composite surface. We proposed that a W-SiC composite based on the SITE technique could offer an appropriate solution for impermeable coating. In addition, this W-SiC composite was also examined as a joining material. The main problem is the formation of a good contact between the coating and the substrate. Therefore efforts were made in order to reduce the thickness of the coating to prevent possible cracking. In addition, another attempt is to improve infiltration of the W-SiC slurry into the outer layer of the porous substrate by reducing the viscosity of the coating slurry. With this purpose, mixtures of W powder, SMP-10 pre-ceramic polymer and n-Hexane were prepared at various ratios. Coatings fabricated with low-viscosity slurries formed a better adhered coating; however diluted coating suspensions led to a coating of low density which was not desired for this application.

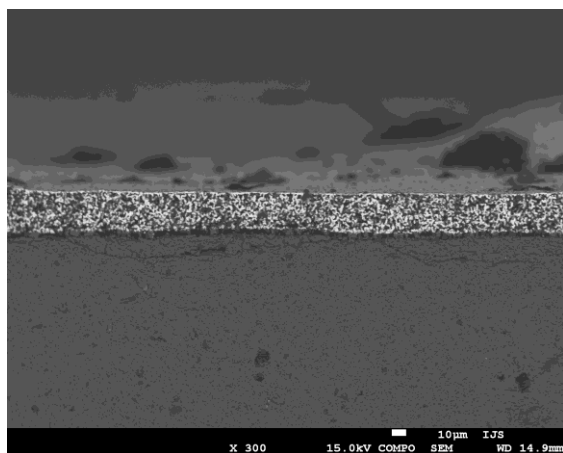


Figure 18: W-SiC EPD coating applied on the SiC surface from 50 wt. % EtOH suspension.

Alternatively, application of coatings was performed by electrophoretic deposition process. High solids fraction suspensions (50 wt. %) in ethanol have proven to provide the best rate of deposition with controllable thickness. The deposition cell geometry was modified in order to prevent the effect of gravity so deposition was performed in a cell with horizontal electrodes and the deposition was conducted upward. Eventhough the deposition itself was successful the densification with pre-ceramic polymer did not yield expected results, and the final coating remained porous. The reason for poor densification was identified in the formation of a thin closing layer during pre-sintering of the coating, a necessary step in order to obtain a well adherent coating.

3 CONCLUSIONS AND OUTLOOK FOR 2014

Protective 2 µm SiC coating was successfully applied on 3D woven SiC fabric coated by a thin (100 nm) PyC coating. PyC and SiC coating are thermally stable and do not react upon heating to 1800 °C and therefore such fabric preform is suitable for fabrication of SiC_f/SiC composites by SITE process. Successful infiltration of 3D woven preform indicates that application of a protective SiC coating might lead to a SITE-SiC_f/SiC with enhanced properties; however a full materials characterisation is still needed.

Additional thermal treatment of EU reference CVI-SiC_f/SiC composites revealed that for 2D reinforced CVI-SiC_f/SiC heat treatment resulted in an increased through thickness thermal diffusivity due to increase in grain size of SiC matrix which is favourable for heat transport properties. On the other hand for 3D reinforced CVI-SiC_f/SiC where through thickness oriented fibres are the main contributors to transport of heat, thermal diffusivity was even slightly decreased. High temperature heat treatment for increase of thermal conductivity is only useful, when the matrix phase plays an important role in heat transport.

The use of electrophoretic deposition for application of W coating layer on conductive substrate has proven to be a good option; however densification by polymer infiltration and pyrolysis was unsuccessful, due to formation of a closing W layer during pre-sintering, which prevented infiltration of pre-ceramic polymer.

THERMAL-HYDRAULIC ANALYSES OF SQUARE HELIUM-COOLED MULTI-JET FINGER USING T111 AS THIMBLE MATERIAL

Boštjan Končar, Samo Košmrlj

Jožef Stefan Institute, Jamova cesta 39, 1000 Ljubljana, Slovenia
e-mail: bostjan.koncar@ijs.si

1 INTRODUCTION

The reference design of modular He-cooled divertor for DEMO has been developed at Karlsruhe Institute of Technology (KIT) with the goal of removing 10 MW/m² of surface heat flux [1]. The concept is based on small cooling fingers composed of a hexagonal tungsten tile brazed on the thimble, made of tungsten lanthanum oxide (WL10). The inner side of the thimble is cooled by high pressure helium jets issued through the nozzles at the top of the steel cartridge.

At assembling of the helium-cooled divertor target plates the reference hexagonal tiles would form an undesirable jagged target edges. In the task WP12-DAS02-T05 [2] the integration of hexagonal finger concept into the outer target plate was investigated as well as the possibilities for alternative finger concepts focusing on forming a straight target plate edge. In WP12-DAS02-T06 [3], a thermal-hydraulic performance of pentagon-shaped and square-shaped finger design (both forming a straight edge of the target plate) were compared with the reference hexagonal design. While the asymmetric pentagonal finger with a 17.8 mm span showed about 100 °C higher thimble temperature maximum, the smaller square-shaped finger with a 16.5 mm edge had a very similar performance as the hexagonal one. Square-shaped fingers were therefore envisaged as the preferred solution for integration into the outer target plate. Another issue that was investigated in WP12-DAS02-T06, was the brittleness of the tungsten alloy at temperatures below 650 °C [4]. The use of Ta-based alloy (T111: Ta-8%W-2%Hf) for the thimble material was found to be an appropriate selection to reduce the operational temperature down to a similar range as for the helium-cooled blanket (and hence avoiding the need for ODS steel).

The aim of this task is to develop a design of a square-shaped finger and to assess its thermo-hydraulic performance for the Ta-based material for the thimble.

2 WORK PERFORMED IN 2013

The research activities in 2013 were carried out in the framework of the PPP&T program, workpackage Design Assessment Studies (DAS), Task DAS02-T12. The main objective of the task was to carry out thermal-hydraulic analyses of fabricated square

shape cooling finger with thimble made of Ta-alloy (T111). Its thermal-hydraulic performance and temperature loading on the structure materials are evaluated using the code ANSYS-CFX. The simulations were performed for the full finger geometry based on three-dimensional CAD model. The sensitivity analyses were performed for two different surface heat fluxes (10 MW/m^2 and 8.7 MW/m^2), two mass flow rates (6.8 and 9 g/s) and two helium inlet temperatures (350 and 450 °C). The results were also compared with the previous simulations of the 16.5 mm square finger (task WP12-DAS-02-T06).

3 DESIGN AND CFX INPUT MODEL OF THE SQUARE-SHAPED FINGER

Based on our recent investigations [2],[3], the prerequisites for the new finger design are the square shape of the tile (with the plasma facing surface similar to the hexagonal tile) and the selection of Ta-alloy for the thimble material in order to allow low temperature cooling.

In the present study the square tile with 17.1 mm of edge width was considered, which has been fabricated in Karlsruhe Institute of Technology (KIT) - Institute for Applied Materials-Materials Processing Technology. For fabrication purposes, the commercially available Ta-alloy T-222 was used for thimble material in order to enable low temperature cooling below 450 °C. The CAD model of the square-shaped finger assembly is shown in Figure 1. It should be noted here that, the cartridge design is also slightly changed; the upper part of the cartridge with a larger diameter is shorter than for the reference hexagonal finger.

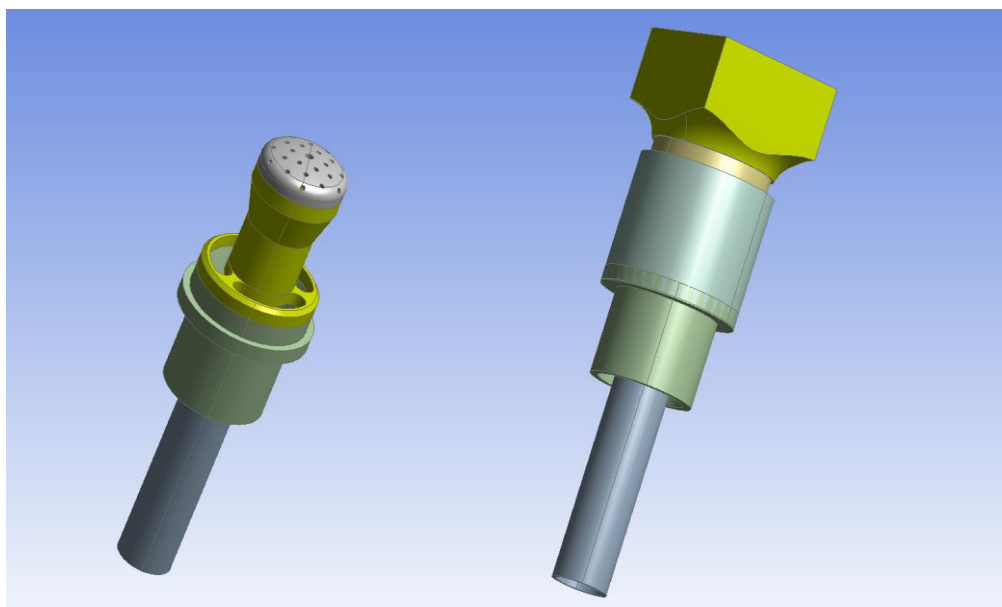


Figure 1: CAD model of the square finger design (courtesy of KIT): cartridge (left); finger assembly (right).

The thermal-hydraulic performance of the investigated square-shaped design was assessed by the means of CFD analyses using the ANSYS-CFX 13.0 code [5].

Flow fields in the helium coolant and temperature distributions in finger solid structures were calculated. Numerical domain consisted of 3 solid domains (tile, thimble and cartridge) and of one fluid domain. Heat transfer equations in fluid and solid domains were solved simultaneously using the conjugate heat transfer approach. In the fluid domain, the helium is modelled as an ideal gas. Shear stress transport (SST) two-equation turbulence model [6] was used to resolve the turbulence helium flow. In the solid domain the heat conduction equation is solved. Details of the modelling approach are described in [7].

The materials used in the CFX input model were tungsten for the tile, T-111 for the thimble and ODS Eurofer for the cartridge. Indeed, the thimble material in the CFX input model has slightly different characteristics than the one used for fabrication of the finger mock-up [8]. Namely, for fabrication purposes the commercially available material T-222 was used, which has somewhat different doping (10% of tungsten, 2.5 % of Hf) than T-111 (8% of tungsten, 2.% of Hf). But the database on T-222 material properties does not contain enough information to build the input model. The selection of a similar material T-111, though it has not been produced anymore, is therefore a reasonable choice as it possesses an extensive collection of material properties data originating from the past studies for space power applications [9].

For creating the computational mesh, hexahedral meshing was used. Full finger body based on CAD geometry in Figure 1 was constructed and simulated. The mesh was created with a minimum quality 0.35 for a single mesh element, which is a weighted average of determinant, angle and warpage of the cell. For the solver used, values above 0.1 are considered to be acceptable. The mesh was oriented in such way, that it followed the fluid flow direction and the mesh in the near-wall boundary layer was refined, so that the first node in the fluid domain was placed at the non-dimensional distance from the wall y^+ approximately 1. The mesh is divided into fluid and 3 solid domains (tile, thimble and cartridge) and consisted of 13.6 million hexa elements (Figure2).

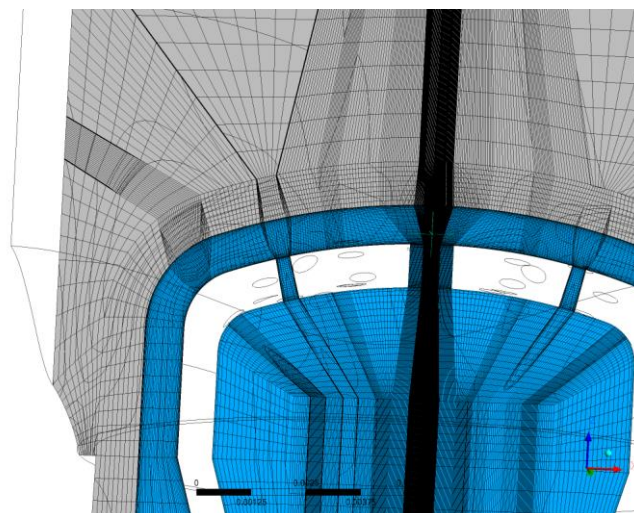


Figure 2: Computational mesh: mesh in the fluid domain (blue); mesh in thimble and tile regions (grey).

Uniform heat flux is applied at the upper surface of the tile and adiabatic boundary conditions are assumed at the outer walls. Helium flow enters the cartridge at the constant mass flow rate and exits the domain at the constant pressure of 10 MPa. For the purpose of this study the tile surface heat flux, mass flow rate and inlet temperature were varied as presented in Table 2 in the next section. A simplified homogeneous internal heat generation in solid structures due to neutron irradiation was assumed. The boundary condition values are collected in Table 1.

<i>B.C. parameter</i>	<i>B.C. values range</i>
Mass flow rate per finger	6.8 - 9 g/s
Heat flux	8.7 – 10 MW/m ²
Internal heat generation	17 MW/m ³
Helium outlet pressure	10 MPa
He inlet temperature	350 - 450 °C

Table 1: Boundary conditions

4 RESULTS

The ANSYS-CFX simulations were performed in the steady-state mode using at least 500 iterations to reach the converged solution. The most critical parameter to evaluate convergence criteria were mass and energy balance of the helium flow. The mass and energy errors arising from numerical solution were the highest in the case of higher mass flow rate (9 g/s) reaching about 0.1% for the mass balance and 0.2% for the energy balance, which fully acceptable numerical accuracy.

Main results consist of temperature distributions across the structures of the finger. Figure 3 shows the temperatures across the tile and thimble for the base calculation with the heat flux of 10 MW/m², mass flow rate of 6.8 g/s and He inlet temperature of 450 °C.

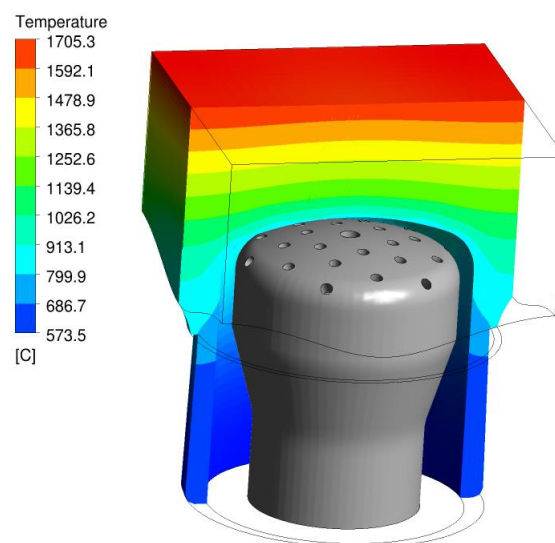


Figure 3: Temperature distribution across the finger structures for the case $q_w = 210 \text{ MW/m}^2$, $mfr = 6.8 \text{ g/s}$, $T_{He, inlet} = 450 \text{ °C}$

Varied operating conditions

To analyse the wider range of new square-shaped finger thermal performance, the temperature loading for the finger structures was investigated for two different surface heat fluxes (10 MW/m² and 8.7 MW/m²), two mass flow rates (6.8 and 9 g/s) and two helium inlet temperatures (350 and 450 °C). Here the lower heat flux represents the so-called relaxed DEMO-1 condition [10].

The results are summarized in Table 2 and graphically presented in Figures 4 to 6. As shown, maximum tile and thimble temperatures increase with the increased inlet helium temperature and decrease with increased mass flow rate. In all calculated cases the maximum thimble temperature stays well below the allowable temperature limit for the thimble (1200 °C). The pressure drop is significantly affected only by the mass flow rate and by the inlet temperature of the helium (Figure 6). Both inlet conditions (mass flow rate and inlet temperature) affect the pressure drop by the changed velocities. The influence of mass flow rate is straightforward, while the inlet temperature affects the density of the helium, a consequently the velocity.

Input BCs			Results			
q_w [MW/m ²]	mfr [g/s]	$T_{He,inlet}$ [°C]	T_{max} tile [°C]	T_{max} thimble [°C]	$T_{He,outlet}$ [°C]	Pressure loss [kPa]
10	6.8	450	1725	1126	534	115.2
10	6.8	350	1632	1042	434.5	99.8
10	9	450	1635	1044	514.5	198.7
10	9	350	1534.5	957	413	172.2
8.7	6.8	450	1548	1036	523	115.1
8.7	6.8	350	1450.5	950.5	423	99.4
8.7	9	450	1470	966	505.5	200.2
8.7	9	350	1368	875	405.2	171.7

Table 2: Calculated cases for the new square finger design

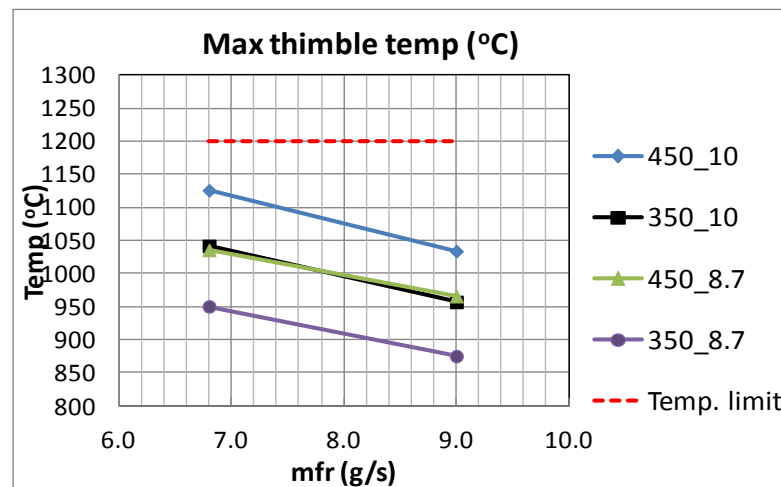


Figure 4: Maximum thimble temperatures for different boundary conditions.

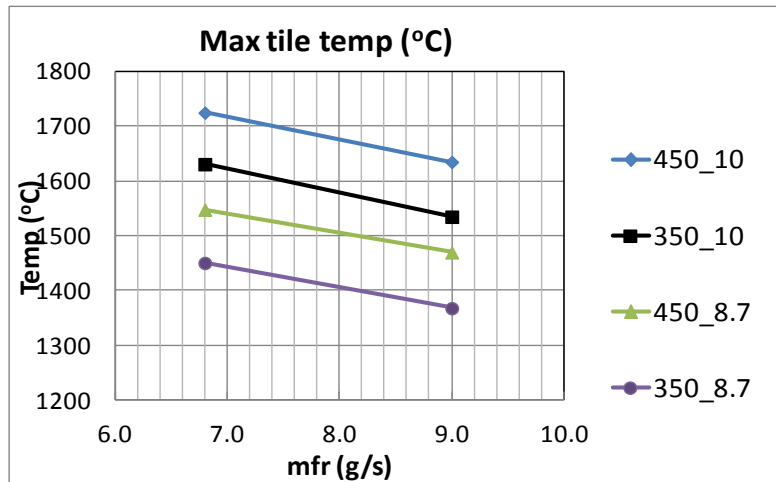


Figure 5: Maximum tile temperatures for different boundary conditions.

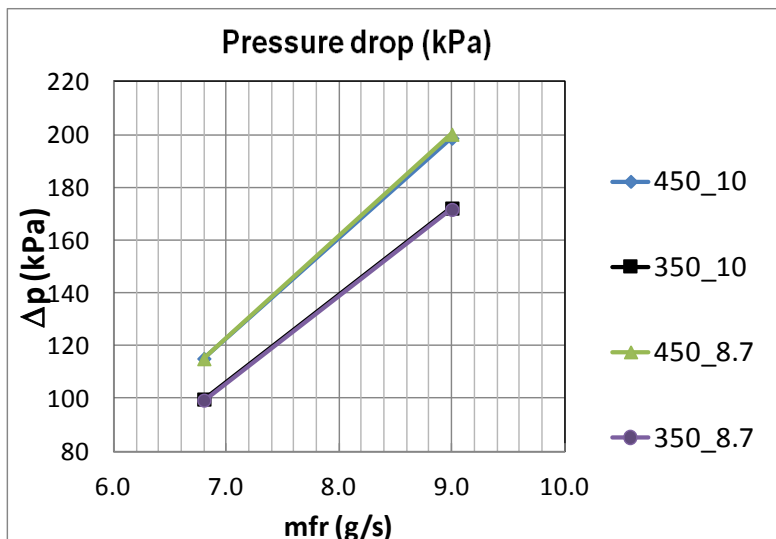


Figure 6: Pressure drop for different boundary conditions.

Comparison with 16.5 mm square finger

The effect of using different material for the thimble (WL10 vs. T-111) has been already discussed within the task WP12-DAS-02-T06 [3],[4], highlighting the low DBTT as the main advantage of T-111 material.

In this section we have rather focused on the comparison of two square-shaped finger designs with the same boundary conditions but with slightly different geometries. The results for the 16.5 mm square finger were calculated in the task WP12-DAS-02-T06 and are confronted with the results of the square-shaped finger of the present work WP13-DAS-02-T12. As presented in Table 3, the new finger has a slightly larger tile edge (17.1 mm vs. 16.5 mm), which as expected results in higher tile temperature. Somewhat surprising is perhaps the lower thimble temperature of the new finger design (1126 °C vs. 1138 °C). The main reason is however different shape of the cartridge. Though the upper part of the cartridge (jet region) is the same, the wider part of the cartridge is much shorter for the new finger design (see Figure 7). The cartridge of the

16.5 mm finger also has a narrower inlet part, but it hasn't been included in the simulation domain. Therefore the inlet cross-section of the helium is smaller for the new finger, resulting in higher inlet velocities at the same mass flow rate. The jet velocities and associated pressure drop for the new finger are higher (similar effect as in the case of convergent-divergent nozzle), resulting in more efficient cooling (lower thimble temperatures). To make a true comparison of both cartridges, the simulation of lower, narrower part of the cartridge would be necessary.

	T111 16_5 (WP12-DAS-02-T06)	Fabricated square finger (WP13-DAS-02-T12)
Tile size	16.5 mm	17.1 mm
Boundary conditions*	same	same
Max Tile temp	1701 °C	1725 °C
Max Thimble temp	1138 °C	1126 °C
He outlet temp	529 °C	534 °C
Pressure loss	97.1 kPa	115 kPa
Max He central jet velocity	182 m/s	211 m/s

* In both simulation the same BCs were applied ($q_w=10 \text{ MW/m}^2$; $T_{in}=450 \text{ °C}$; $mfr=6.8 \text{ g/s}$)

Table 3: Comparison between two square fingers

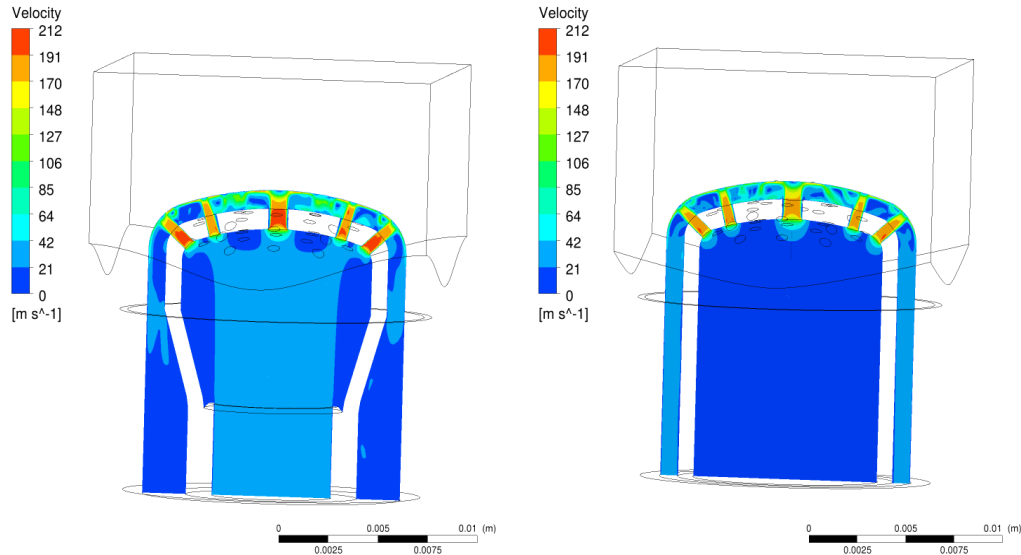


Figure 7: Comparison of nozzle velocities for the fabricated finger (left) and 16.5 mm finger (right).

5 CONCLUSIONS AND OUTLOOK FOR 2014

A new design of a square-shaped finger is based on 17.1 mm tile size and Ta-alloy material for the thimble. Its thermal-hydraulic performance and temperature loading on the structure materials is evaluated using the code ANSYS-CFX. The

sensitivity analyses were performed for two different surface heat fluxes (10 MW/m² and 8.7 MW/m²), two mass flow rates (6.8 and 9 g/s) and two helium inlet temperatures (350 and 450 °C). The results were compared with previous simulations of 16.5 mm square finger (task WP12-DAS-02-T06). The tile temperature was higher for the new finger as a consequence of larger tile edge (17.1 mm). On the contrary, the maximum thimble temperature was slightly lower for the new finger design, originating from different shape of the cartridge upper part.

In 2014 all work related to the technology of DEMO divertor will be covered in the Divertor workpackage of the PPP&T projects within the EUROFUSION program. As no further research in He-cooled divertor is planned in this workpackage, also no further activities related to design and TH assessment of He-cooled divertor fingers is envisaged in 2014.

6 REFERENCES

- 1 P. Norajitra, R. Giniyatulin, T. Ihli, G. Janeschitz, W. Krauss, R. Kruessmann, et al., He-cooled divertor development for DEMO, *Fusion Eng. Des.* 82, 2740–2744 (2007).
- 2 P. Norajitra, L. Spatafora, Design description report of a divertor outer target integrating the hexagonal finger concept, Report for TA WP12–DAS02–T05-D1, EFDA_D_2LDRJW, v.1.2, 2012.
- 3 B. Končar, Thermal-hydraulic analyses report of alternative He-cooled divertor concepts, Report for TA WP12-DAS02-T06, EFDA_D_2M7TFC, 2012.
- 4 P. Norajitra, W. Basuki, L. Spatafora, Design description report of alternative He-cooled divertor concepts, Report for TA WP12-DAS02-T06, EFDA_D_2M7TFC, 2012.
- 5 ANSYS CFX, Release13.0, ANSYS CFX-Solver Theory Guide, ANSYS, 2010.
- 6 F.R Menter., Multiscale model for turbulent flows, 24th Fluid Dynamics Conference, 1986, American institute of aeronautics and astronautics.
- 7 B. Končar, I. Simonovski, M. Draksler, Influence of multiple jet cooling on the heat transfer and thermal stresses in DEMO divertor cooling finger. *Fusion Eng. Des.*, 86, 167-173 (2011).
- 8 P. Norajitra, W. Basuki, L. Spatafora, Design description report of design and fabrication of helium cooled divertor fingers, Report for TA WP13-DAS02-T12-D1, EFDA_D_2M7APC, v1.0, 2013.
- 9 Moorhead P.E., Stone P. L., Survey of properties of T-111 (Tantalum-8 Tungsten-2 Hafnium), NASA Technical note D-5873, June 1970.
- 10 C. Bachmann, DEMOparametersMarch2012.pdf, personal email communication, 2012.

DIVERTOR HIGH FLUX HELIUM COOLING: LARGE EDDY SIMULATION (LES) OF MULTIPLE JET IMPINGEMENT CASE

Boštjan Končar, Martin Draksler

Jožef Stefan Institute, Jamova cesta 39, 1000 Ljubljana, Slovenia
e-mail: bostjan.koncar@ijs.si

1 INTRODUCTION

Jet impingement cooling is based on heat removal by fluid jets, usually gaseous and highly turbulent, which impinge on the target surface exposed to the high heat load. Configurations with multiple jets are usually employed to ensure the uniform heat transfer over wider area. The concept with multiple impinging jets has been proposed also for the cooling of the divertor, a plasma-facing component of the future fusion reactor DEMO [1]. A conceptual design of the divertor is the subject of different optimization studies [2,3], which require fast and efficient analyzing technique, and therefore a steady-state Reynolds-Averaged-Navier-Stokes (RANS) approach together with the two equation turbulence model is a preferable choice. The performance of the proposed cooling finger at the operating conditions has been predicted only by the means of numerical simulations, and therefore the estimation of the potential errors is very important.

The vast majority of physical phenomena and mechanisms of turbulent impinging jets can be sufficiently captured by Large Eddy Simulation (LES), where all larger spatial scales can be solved directly without any additional modelling. Additional models are required only on smaller, subgrid scales to capture the simpler, isotropic turbulence. Combined with subgrid-scale models LES can be used for the simulation of impinging jets at high Reynolds numbers [4]. In order to improve the understanding of the physical phenomena of impinging jets, the LES simulation of the multiple impinging jets in hexagonal configuration has been performed. The experimental test case of Geers [5] has been selected to resemble as far as possible the divertor working conditions. The simulations have been carried out with a three dimensional numerical solver PSIBoil (Parallel-Simulator) [6]. Subgrid-scale turbulence is modelled by an explicit Wall-Adaptive Local Eddy-viscosity (WALE) subgrid-scale model [7].

2 WORK PERFORMED IN 2013

The considered LES simulations present the continuation of the work that has been carried out in 2012 in cooperation with the Paul Sherrer Institute (PSI), Laboratory for Thermal-Hydraulics, Switzerland. The work in 2013 is being focused on validation

of the results against the experimental data, interpretation of results and carrying out the LES simulations of the heat transfer. One of the important objectives was also to evaluate the accuracy of inlet boundary conditions at the exit of the nozzles. Often, in the experiment only the mass flow rate is known, whereas detailed inlet profiles of the flow and turbulence fluctuations are not measured. Therefore three different flow profiles at the nozzles outlet were tested; the flat velocity profile (case 1), the profile obtained from precursor RANS simulation (case 2), and the flat profile with additional pseudo-random fluctuations (case 3). The time-averaged values of numerical simulations and experimental data were compared.

3 LARGE EDDY SIMULATION OF MULTIPLE JETS IN THE HEXAGONAL ARRANGEMENTS OF JETS

Our interest in cooling by impinging jets originates from optimisation studies of the helium-cooled divertor, therefore the geometry and boundary conditions of the selected experimental cases should resemble as far as possible the DEMO divertor conditions. Among all the available experiments in the literature, the experiment by Geers [5] turned out to be the most appropriate. In both geometries, in divertor cooling finger (Figure 1a) and in experimental case (Figure 1b) the nozzles are arranged in hexagonal configuration around the central ones, i.e. the central nozzle is surrounded by additional six at constant distance. The only difference between geometries is in number of additional rows – overall number of nozzles. The fluid exit condition is similar in both cases - Reynolds number at the nozzle exit is around 20000.

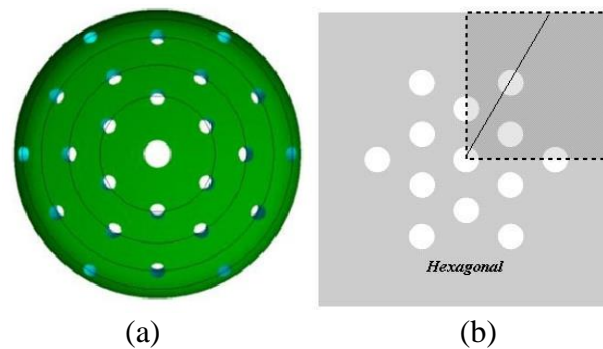


Figure 1: Nozzle arrangement of in the divertor cooling finger with 25 nozzles (a). Nozzle configurations used in the experiments by Geers [5].

Computational domain has to be sufficiently large, i.e. boundaries have to be far enough from the region of interest, in order to exclude any additional numerical effects on simulation results. A large number of mesh elements is required to have a proper mesh resolution. The smallest numerical mesh which has been used in our study consists of 9 million elements (384x384x64), whereas our most detailed simulation was carried out on the mesh consisting of 144 million elements (768x768x256). The LES simulations have been performed with the PSI-Boil code which is efficiently

parallelized to carry out fast transient simulations on high performance computer cluster.

Figure 2 shows the contours of instantaneous velocity field for the dense mesh at two different vertical planes for two different instants of time. It may be observed that spent-flow of inner jets creates strong up-wash flow where the fluid flows back to the nozzle plate. Strong interactions between individual jets and spent-flow are causing strong decay of jets, i.e. the jets are not impinging the target wall all the time.

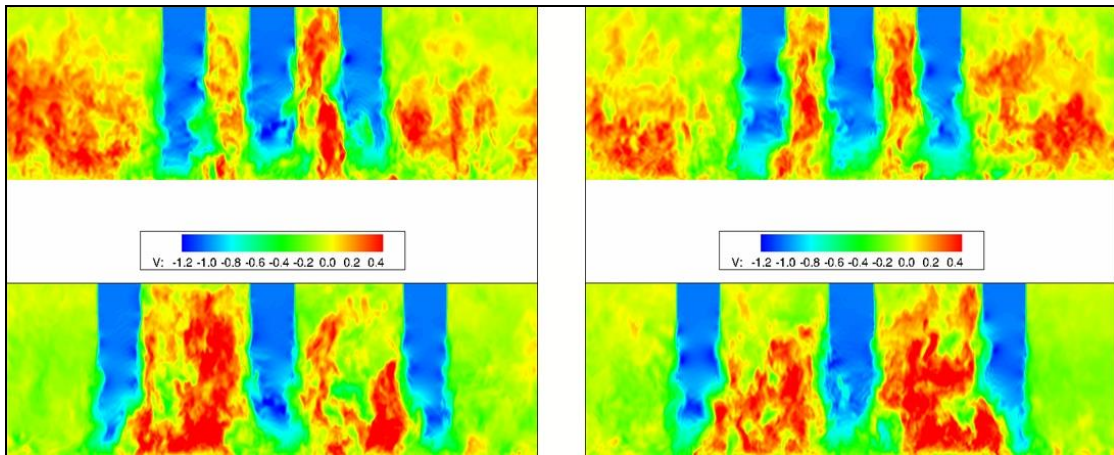


Figure 2: Instantaneous velocity field at two instants of time. $t = 4.5$ s (left) and $t = 6.0$ (right).

The comparison with experimental data [5] is shown in Figure 3, where the profiles of the statistically averaged mean axial velocity ratio and non-dimensional mean radial stresses are compared. As may be observed the simulation results very well reproduce the experimental data.

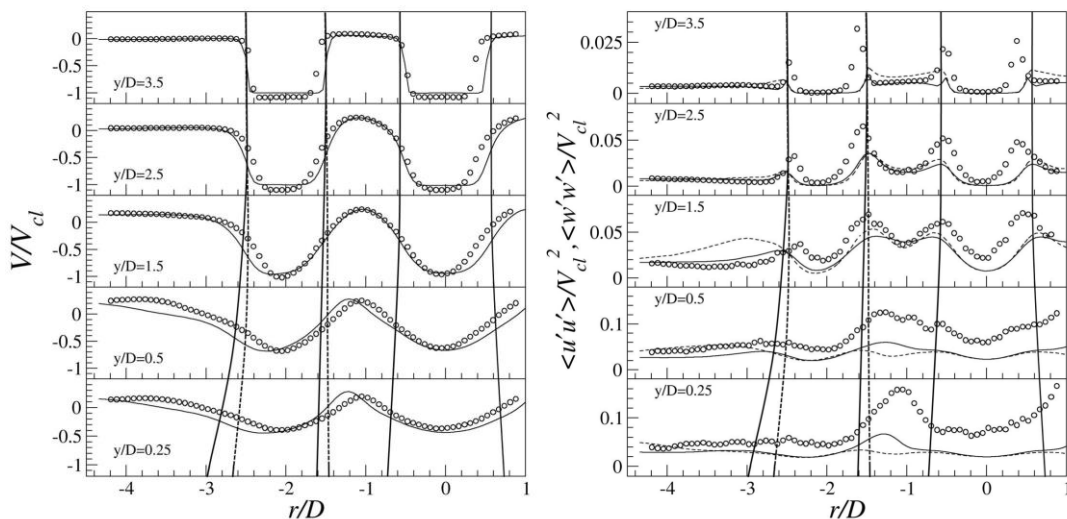


Figure 3: Profiles of the mean axial velocity (left) and mean radial stresses (right)

Inlet boundary conditions

Often, the exact flow conditions at the inlet are not known. Usually only the mass flow rate at the inlet is known as in the case of considered multiple jet experiment. The phenomena which occur prior to the nozzle exit must be described by the inlet boundary condition. For instance, it is known that low aspect-ratio orifices produce vena contracta phenomena where the jet becomes narrower and the fluid is additionally accelerated. Since the flow boundary conditions at the nozzle exit are not known, a sensitivity study with three different inlet velocity profiles at the domain inlet (see Figure 4) is performed. In the first case (case 1) the inlet velocity profile is simulated with the uniform axial velocity V_{cl} equal to 24 m/s (based on the Reynolds number at the nozzle [5]). In the second case (case 2) the velocity profile is adopted from the precursor RANS simulation where the flow through the nozzle plate is simulated and vena contracta is observed. In the third case (case 3) the fluctuations with the prescribed length scale (10% of the nozzle diameter D) and time scale ($\tau = 7 \cdot 10^{-4}$ s) are superimposed in axial direction on the uniform profile of the case 1. The fluctuations are obtained with the pseudo-random generator by Kraichnan [8].

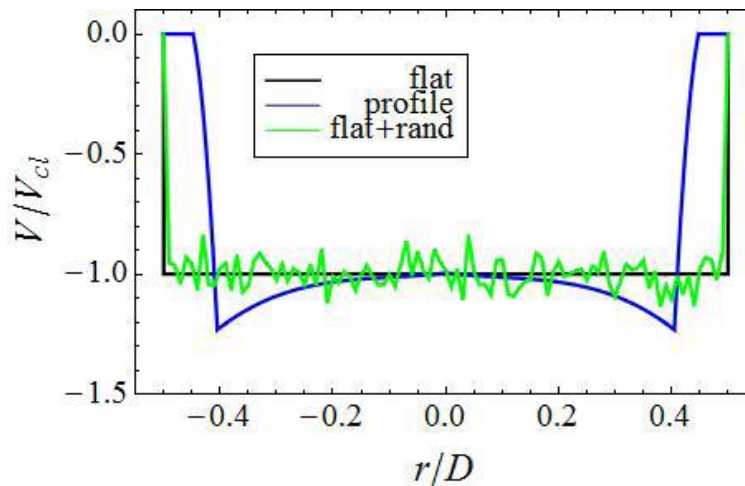


Figure 4: Simulated inlet velocity profiles

It is obvious that the inlet velocity profile affects the flow behaviour in the vicinity of the nozzle exit, but more important is to estimate how far downstream (towards the target plate) its influence extends. The answer can be obtained by applying the cross-correlation function between the pairs of points along the jet's axis, i.e. between the inlet and the local point at the centerline of the jet.

The results of two simulation cases (case 1 and 3) are shown in Figure 5. In both cases the cross-correlation function more or less rapidly decreases with the increasing distance from the nozzle. The correlation is completely lost before the jet reaches the half-height of the channel ($l/D = 2$). Higher values of cross-correlation function are obtained when additional fluctuations are imposed at the inlet (case 3) than in the simulation case with only flat velocity profile (case 1).

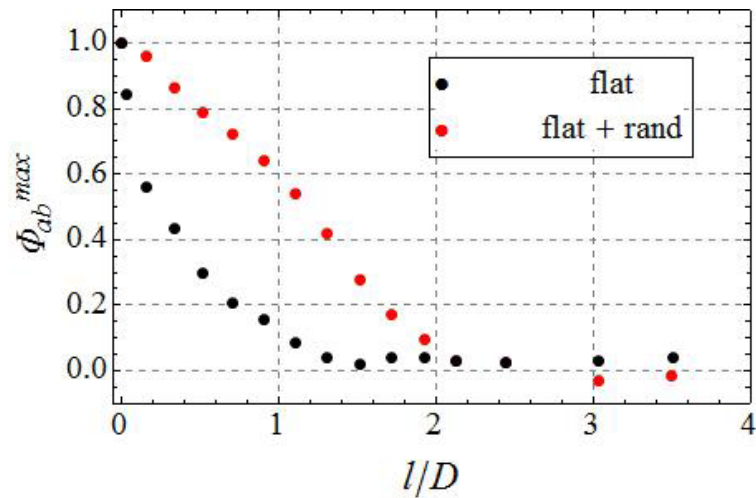


Figure 5: Cross-correlation function between the inlet and considered local points along the centerline of the central jet.

Radial distribution of the mean Nusselt number is presented in Figure 6. As shown, the highest heat transfer rates occur at the locations where the jets impinge on the target wall. Comparing to the experiment, the simulation cases 1 and 3 predict about 20% higher Nusselt number in the stagnation region of each jet. On the other hand, a much higher overprediction of the Nusselt number (for about 50 %) is obtained by the simulation case 2 (RANS profile) due to the higher local velocity and higher stresses in the vicinity of the target wall. Away from the stagnation region, discrepancy between the simulation results and experimental data is smaller.

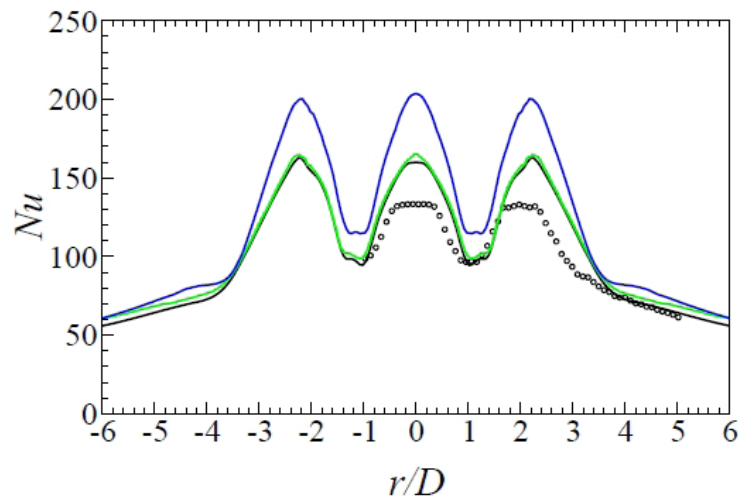


Figure 6: Radial distribution of the Nusselt number in plane P-1. Symbol: Experiment, Black: Flat profile, Blue: Profile from precursor RANS simulation, Green: Flat profile + random generator.

4 CONCLUSIONS AND OUTLOOK FOR 2014

Large Eddy Simulation was carried out in order to study the flow characteristics and heat transfer of multiple circular impinging jets at configurations and Reynolds numbers comparable to those in divertor cooling finger. The mean flow field is obtained by time-averaging of instantaneous results.

To gain confidence in simulation results, a validation study against available experimental data is performed. The results show that the LES simulation accurately predicts the key flow phenomena of multiple highly turbulent impinging jets. Minor discrepancies between experiment and simulation were still observed that may originate from inaccurate modelling of experimental inlet boundary conditions. Therefore three different flow profiles at the exit of the nozzles were tested; uniform velocity profile, the profile obtained from precursor RANS simulation and uniform profile with additional pseudo-random fluctuations. Results show that additionally imposed turbulence is rapidly dissipated from the flow, and that the levels of the stresses downstream the nozzles do not exceed the values that occur anyway (with the flat profile without additional fluctuations).

In general, the presented LES simulation provides sufficiently accurate results that could serve either as a benchmark case for validation of RANS turbulence models or could help to in depth interpretation of the local flow and heat transfer phenomena in multiple impinging jets. Especially the second topic is considered very important and will be part of the work in 2014. Ultimately, these results can serve as a validation benchmark for CFD models used in pre-conceptual and optimisation studies of divertor cooling finger.

5 REFERENCES

- 1 P. Norajitra, R. Giniyatulin, T. Ihli, G. Janeschitz, W. Krauss, R. Kruessmann, V. Kuznetsov, I. Mazul, V. Widak, I. Ovchinnikov, R. Ruprecht, and B. Zeep. He-cooled divertor development for DEMO. *Fus. Eng. Des.*, 82:2740–2744, 2007.
- 2 B. Končar, P. Norajitra, and K. Oblak. Effect of nozzle sizes on jet impingement heat transfer in he-cooled divertor. *Appl. Therm. Eng.*, 30:697–705, 2010.
- 3 B. Končar, I. Simonovski, and M. Draksler. Influence of multiple jet cooling on the heat transfer and thermal stresses in DEMO divertor cooling finger. *Fus. Eng. Des.*, 86:167–173, 2011.
- 4 T. Hällqvist. Large Eddy Simulation of Impinging Jets with Heat Transfer. PhD thesis, Royal Institute of Technology, Sweden, 2006.
- 5 L. F. G. Geers, K. Hanjalić, and M. J. Tummers. Wall imprint of turbulent structures and heat transfer in multiple impinging jet arrays. *J. Fluid Mech.*, 546:255, 2006.
- 6 B. Ničeno. PSI-Boil Tutorial. Paul Scherrer Institute, Switzerland, 2011.
- 7 Nicoud and F. Ducros. Subgrid-scale stress modelling based on the square of the velocity gradient tensor. *Flow Turbul. Combust.*, 62:183–200, 1999.
- 8 R.H. Kraichnan. Diffusion by a random velocity field. *Physics of Fluids*, 13, 1970.

TRITIUM BREEDING RATIO STUDY OF THE WCLL AND THE DCLL

Igor Lengar, Luka Snoj, Aljaž Čufar

Jožef Stefan Institute (IJS), Reactor Physics Department, Ljubljana, Slovenia
e-mail: igor.lengar@ijs.si

1 INTRODUCTION

A comparative study on the neutron shielding and tritium breeding ratio (TBR) of the WCLL and the DCLL blanket concepts was performed. A model of DEMO with empty blanket boxes was used as the basis for calculations. The model and results of calculations are presented in the report.

2 WORK PERFORMED IN 2013

2.1 DEMO MCNP model

A model of DEMO, prepared originally for activation calculations [1] was used for calculations rather than the generic model, originally planned to be used for the task. The model with is described in the continuation of the section.

Geometry

In October 2013 a model, developed for activation calculations was released [1]. In the described model the blanket modules are described with increased level of detail; the geometrical shape of the modules resembles the reality closer than in the generic model. The geometry is visible in Figure 2.

Materials

The (volumetric) fractions that were used for the homogeneous material mixes representing WCLL and DCLL breeding blanket concepts are described in Table 1:

	WCLL	DCLL
LiPb	85 %	85 %
Eurofer	10 %	8 %
SiC	/	4 %
Water	5 %	/
Void	/	3 %
Average density	8.9 g/cm ³	8.8 g/cm ³

Table 1: Volumetric fractions that of the homogeneous material mixes for WCLL and DCLL breeding blanket concepts.

Calculations were performed with MCNP5.14 neutron transport code. Mostly cross-section data from the FENDL 2.1 data library were used – as provided in the model. In some calculations ENDF libraries were used for the Li, Pb and water data because we experienced some difficulties.

As the neutron source the plasma source, provided together with the model, was used. Plasma parameters were: DT plasma, 15.4 keV, major radius 900 cm, minor radius 225 cm, elongation 1.66, triangularity 0.33, radial shift 0.0 cm, peaking factor 1.7 and vertical shift 0 cm. The source had the extent of 0° to 11.25° in the toroidal direction (1/32 of the whole reactor) and using reflecting planes on the vertical edges of the model.

Results

The neutron flux behind the blanket module at the equatorial plane was examined. For this purpose the flux in the void cell, positioned directly behind the breeding blanket, was calculated. Table 2 contains the neutron fluxes for the WCLL and DCLL concepts.

	Neutron flux*
WCLL	1.3 E+13 n/cm ² s
DCLL	4.2 E+13 n/cm ² s

*Neutron Flux is normalized on the 6.106E+20 n/s neutron emission.

Table 2: Total neutron fluxes behind the breeding blanket at the equatorial plane for the WCLL and DCLL concepts.

The neutron flux as a function of neutron energy in the equatorial plane behind the breeding blanket for the DCLL and WCLL is presented in Figure 1. From the figure also the fraction of the neutrons above particular energies (fast flux) with respect to the thermal flux can be observed.

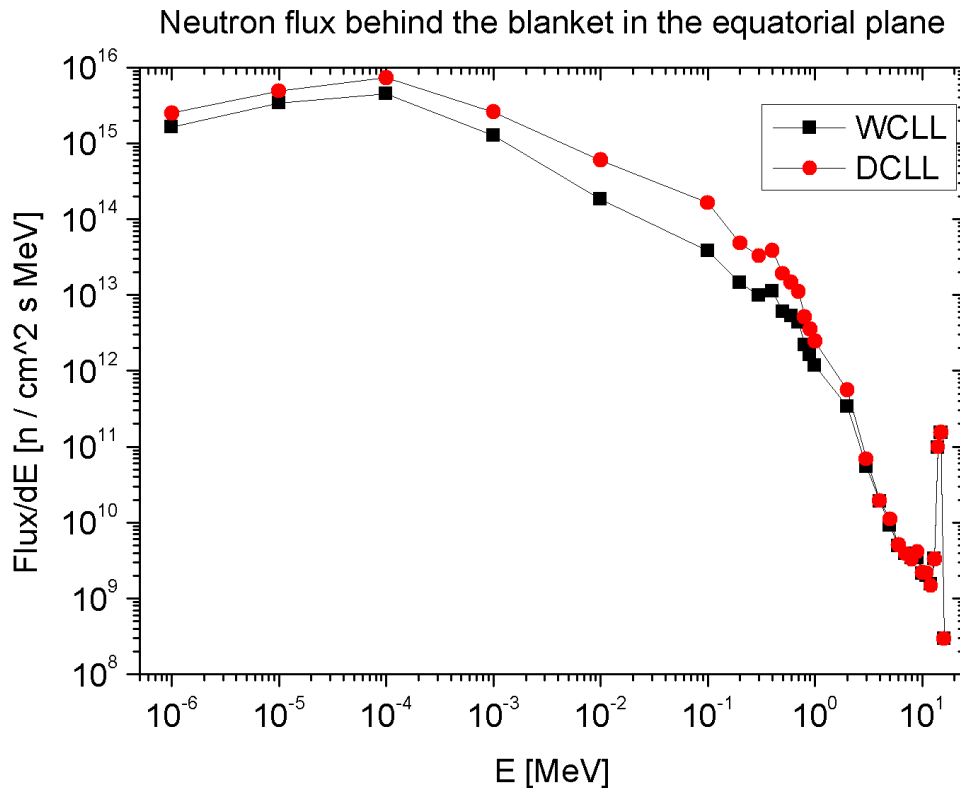


Figure 1: Neutron spectrum in equatorial plane behind the breeding blanket for the DCLL and WCLL concepts

The tritium breeding ratio for the whole reactor was calculated for both concepts and is presented in Table 3; it was calculated by using the FENDL 2.1 and ENDF/B VII.0 libraries for the estimation of the nuclear data influence on results.

	TBR
WCLL	1.159 (FENDL), 1.169 (ENDF)
DCLL	1.078 (FENDL), 1.089 (ENDF)

Table 3: The tritium breeding ratio for the whole reactor for the WCLL and CDLL concepts. FENDL of ENDF libraries were used.

It should be noted that the provided TBRs correspond to homogeneous material mixtures, as provided in Table 1, filling the blanket modules. In the real case the geometry between both concepts will vary and thus the above numbers are not necessary representative for the final TBR of both concepts; they are presented as an addition to describe the present calculations.

For the estimation of the importance of individual blanket modules on the TBR, it was calculated for all of the poloidal blanket modules. The numbering of the blanket modules is presented in Figure 2.

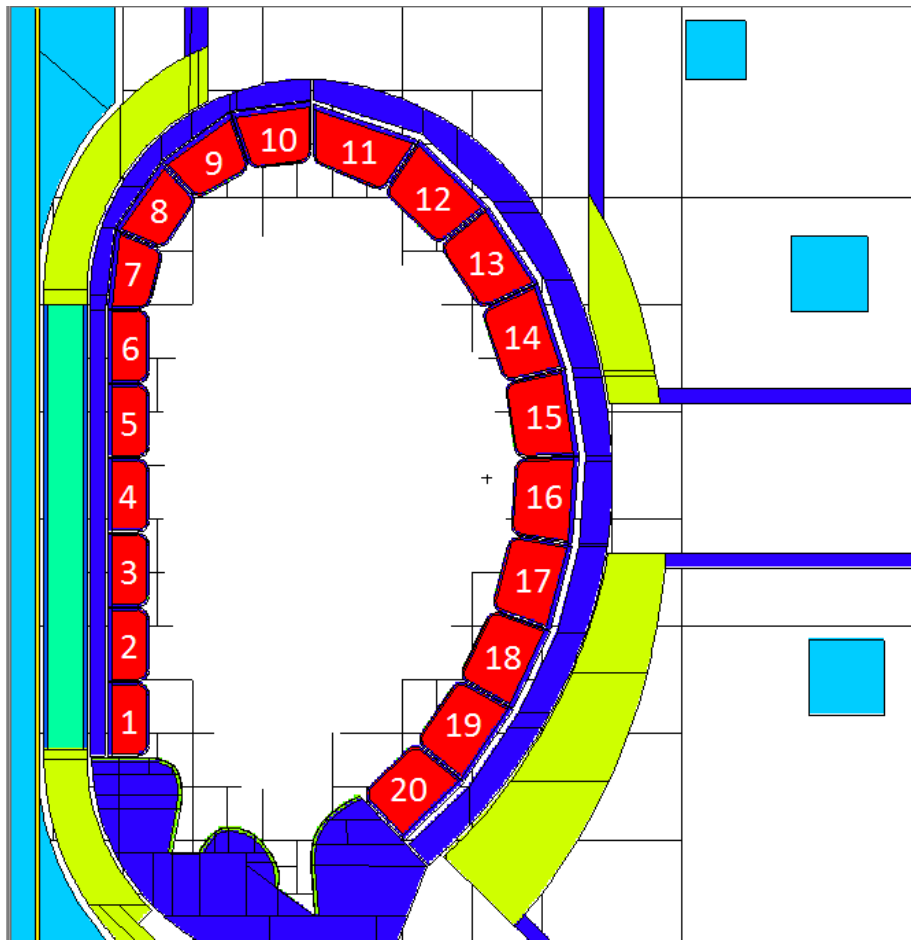


Figure 2: Poloidal numbering of the breeding blanket modules.

The volumes of the breeding sections of the blanket modules and their labels are presented in Table 4. The calculations for the outboard modules (numbers 11 to 20) were carried out for one and a half blanket module in the toroidal direction (in the whole reactor contains 48 modules with the same poloidal position number) while the inboard modules consist of only one module (32 modules in the whole reactor with the same poloidal position number).

Poloidal module position number	Cell number in 2LMNBT model [1]	Volume [10^5 cm^3]	Module name
1	705	4.75	1 inboard
2	706	4.75	2 inboard
3	707	4.75	3 inboard
4	708	4.75	4 inboard
5	709	4.75	5 inboard
6	710	4.74	6 inboard
7	711	4.99	7 inboard
8	712	6.05	8 inboard
9	713	7.43	9 inboard
10	714	9.02	10 inboard
11	715+716	13.63	10 top outboard (full + ½)
12	717+718	14.79	9 outboard (full + ½)
13	719+720	15.58	8 outboard (full + ½)
14	721+722	16.10	7 outboard (full + ½)
15	723+724	16.31	6 outboard (full + ½)
16	725+726	16.44	5 midplane down (full + ½)
17	727+728	16.08	4 outboard (full + ½)
18	729+730	15.44	3 outboard (full + ½)
19	731+732	14.72	2 outboard (full + ½)
20	733+734	13.15	1 bottom outboard (full + ½)

Table 4: Volumes of the breeding sections of the blanket modules and their labels.

The TBR values for individual modules as a function of the poloidal module position number are presented in Figure 3 (the sum of the presented values for the WCLL or DCLL model respectively is equal to the number, found in Table 3).

The radial profiles of the tritium production rates were calculated for the poloidal blanket modules. Two examples of the radial profiles for each of the two breeding blanket concepts for the tritium production rate are presented in Figure 4. The values in the figure are normalized to production of one tritium atom per 1 cm^3 of breeding blanket per one source neutron produced in the plasma.

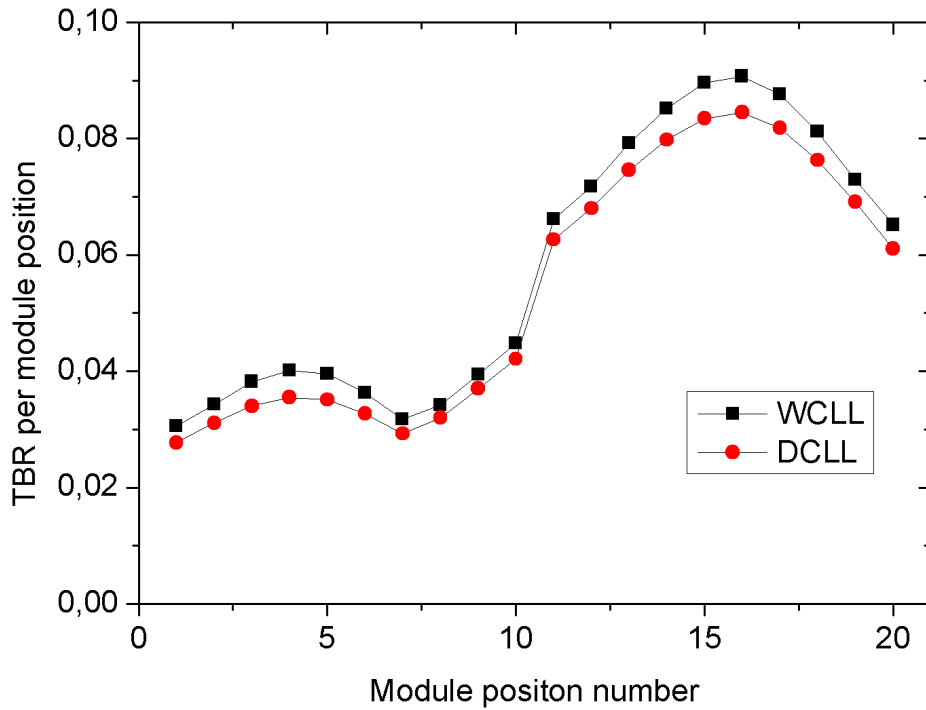


Figure 3: TBR values for individual modules as function of poloidal module position number. for the WCLL and DCLL models.

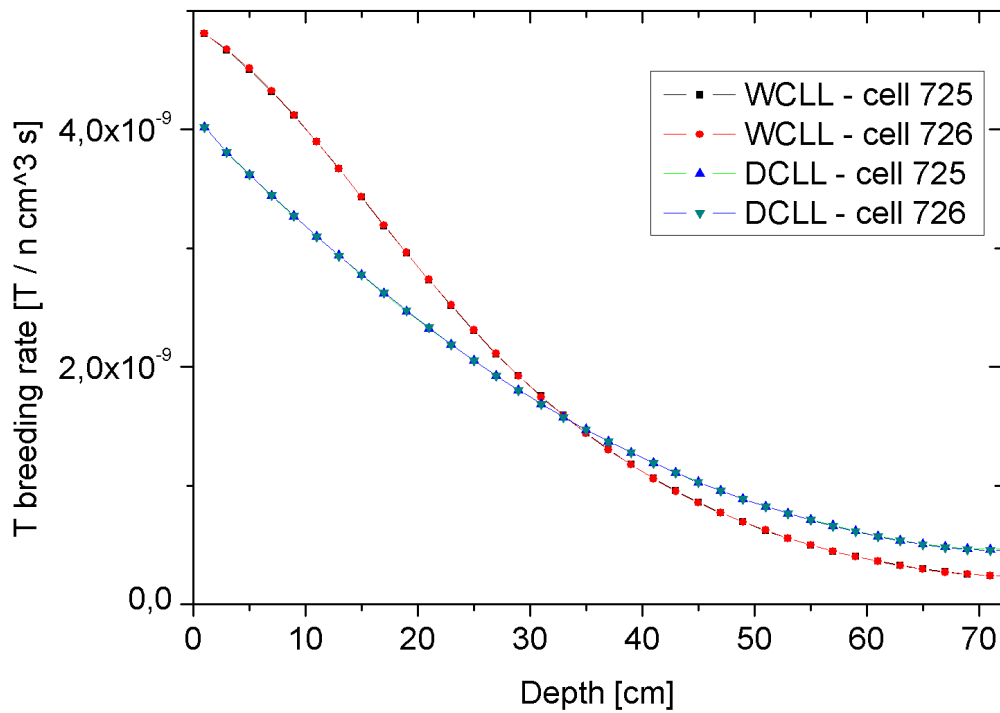


Figure 4: Radial profiles of the tritium production rate in the poloidal blanket modules.

Cells 725 and 726 are in the equatorial plane on the same poloidal position. The difference is in the geometry behind the cells; cell 726 is in front of the horizontal port while cell 725 is in front of the vacuum vessel.

Additionally the average neutron flux and the average tritium production as a function of the energy were calculated in the cells filled with breeder material. The results are presented in Figures 5 and 6.

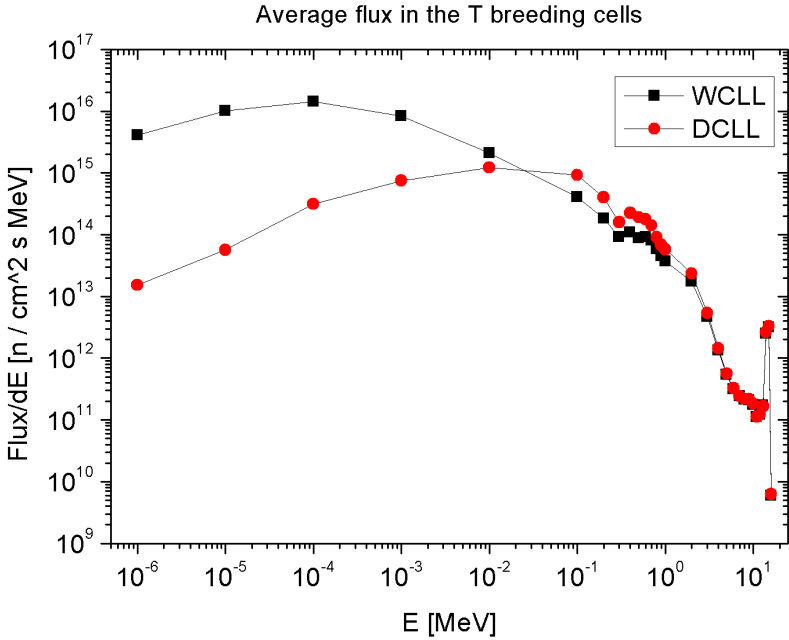


Figure 5: Average neutron spectrum – averaged over all cells filled with breeder material in the whole reactor.

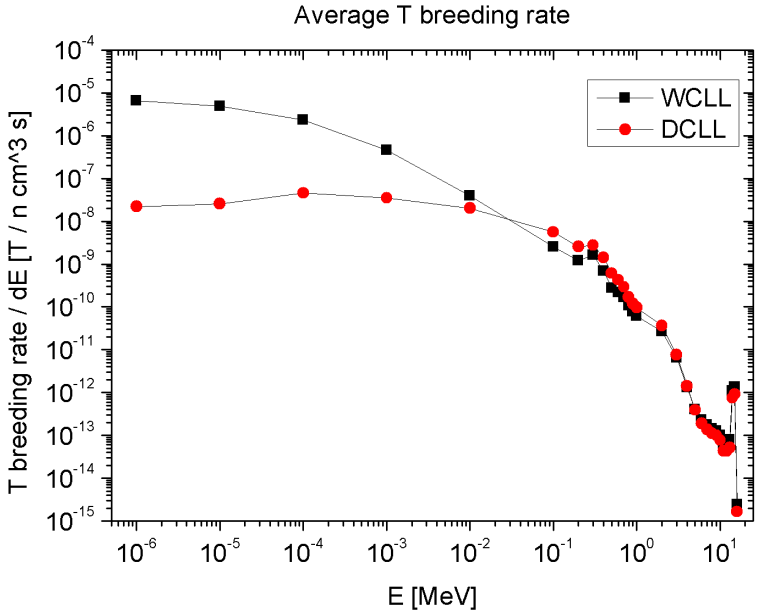


Figure 6: Average tritium production as a function of the neutron energy – averaged over all cells filled with breeder material in the whole reactor.

Neutron multiplication

Neutron multiplication in DEMO is essential since the necessary amount of tritium can not be bred otherwise. The amount and location of the (n,2n) and (n,3n) reactions was investigated; these reactions are not limited only to the breeding blanket since, due to the high – 14 MeV – source neutron energy, a lot of nuclei present in the torus exhibit noticeable cross-sections for the above reactions.

MCNP gives the total net neutron multiplication in a run as the total number of neutron present in the whole geometry per source neutron, i.e. a net multiplication of 1.53 means that per one source neutron 0.53 neutrons originated from nuclear reactions in addition to the source neutron. In Table 5 these numbers of additional neutrons per plasma source neutron are presented. The study of the origin of (n,xn) reactions was also made.

WCLL DEMO model

total additional neutrons per source neturon			0.535
breeding blanket	Pb	(n,2n)	0.328
		(n,3n)	4.14E-06
	Eurofer	(n,2n)	1.00E-02
		(n,3n)	1.60E-06
breeding blanket total			0.338
multiplication outside the BB			0.197

DCLL DEMO model

total additional neutrons per source neturon			0.550
breeding blanket	Pb	(n,2n)	0.345
		(n,3n)	4.37E-06
	Eurofer	(n,2n)	7.55E-03
		(n,3n)	1.21E-06
breeding blanket total			0.353
multiplication outside the BB			0.197

Table 5: Number of additional neutrons per one DT plasma source neutron with respect to their origin for a DEMO torus with the WCLL or DCLL blanket concepts.

It can be observed that roughly two thirds of all multiplication takes place inside the breeding blankets. In both cases the (n,2n) reaction in Pb is dominant. The (n,3n) reaction contributes negligible to neutron multiplication.

In order to observe the location of multiplication inside the torus the above listed reactions were visualized, what is presented in Figure 7.

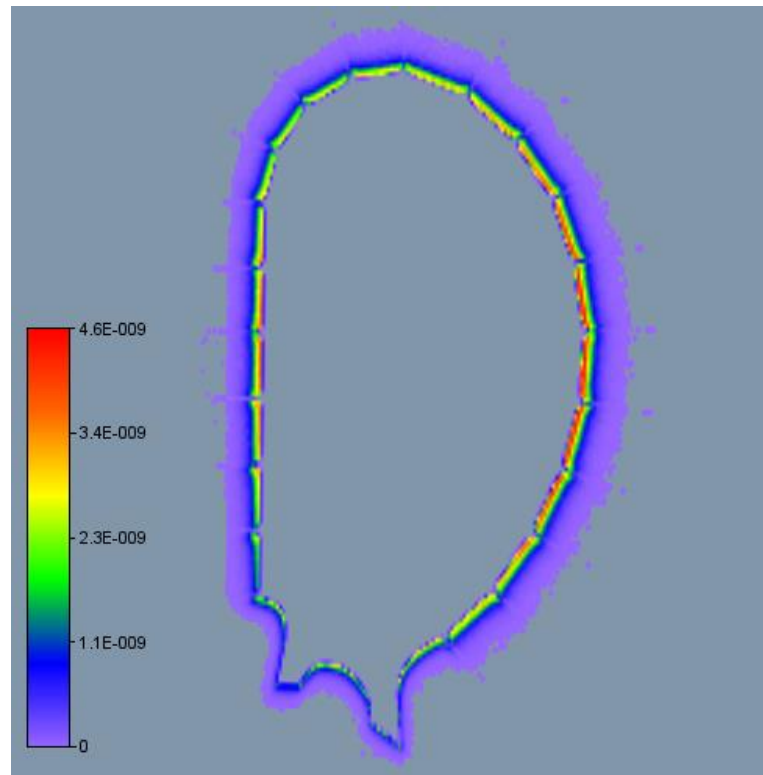


Figure 7: Visualization of the intensity of the $(n,2n)$ and $(n,3n)$ reactions in DEMO, the case for the DCLL breeding blanket; the situation is similar for the WCLL case. The geometry can be anticipated from the figure. Scale: 1 additional neutron / cm^3 / source neutron .

3 CONCLUSIONS AND OUTLOOK FOR 2014

The tritium breeding ratio (TBR) was calculated and the effects of the first wall (FW) on TBR investigated in a MCNP model of the DEMO reactor using empty blanket boxes for the WCLL and DCLL type of the breeding blankets. Simplified models using homogeneous breeding blanket mixtures were used. The results show the highest intensity of tritium breeding in the modules around the mid-plane.

The neutron multiplication was studied. It was found, that the dominant reaction is the $(n,2n)$ in lead of the breeding blankets, accounting roughly to two thirds of all multiplication in the torus. The rest of reactions take place outside the breeding blankets. The $(n,3n)$ reaction was found to negligibly contribute to neutron multiplication.

The corresponding values of the TBR were also calculated for both concepts, they are however, due to the simplification of using homogeneous BB material mixtures, of limited practical significance.

4 REFERENCES

- 1 EFDA IDM: 2LMNBT – WP13-SYS02 - MCNP DEMO model with empty HCPB blanket modules

PUBLIC INFORMATION ACTIVITIES

Tomaž Skobe, Saša Novak, Luka Snoj

Jožef Stefan Institute, Jamova cesta 39, SI-1000 Ljubljana
e-mail: tomaz.skobe@ijs.si

1 INTRODUCTION

The report summarizes various public information activities in 2013. It involves basic information on the permanent exposition run by the Nuclear Training Centre and on other regular activities.

2 WORK PERFORMED IN 2013

Permanent fusion exhibition at the Nuclear training centre (<http://www.icjt.org/an/index.htm>) of the Jožef Stefan Institute was visited in 2013 by 162 organized groups of 7100 visitors altogether, mainly youngsters from primary, secondary and high schools. We were often visited also by graduate and postgraduate students and organized groups of adults.

We gave 20 lectures on Fusion technology and ITER project and 23 on Radioactivity and radioactive waste. We also gave 117 lectures on electricity from nuclear energy, where we talk also about fusion as safe, sustainable and environmentally responsible source of energy in the future. We performed experiments on radioactivity and ionizing radiation and provided guided tours of the permanent exhibition on fusion.

In March, within the annual Jožef Stefan week and the open day at the Jožef Stefan Institute, Slovenian Fusion Association (SFA) contributed to the event with a lecture on fusion (it was presented by Dr. Luka Snoj) and an exhibition of the activities performed within the project Fusion Expo. We used this opportunity to increase the awareness of the fusion research. During the lecture a live coverage from JET an ITER was restored.

In May Dr. Luka Snoj gave an interview about fusion for the Slovenian National Radio. In the same month an article about fusion, ITER and Slovenian contribution (Activities of SFA) to fusion project was published in daily newspaper DELO.



Figure 1: Lecture on fusion, presented by dr. Luka Snoj.

In spring a new action for promotion of science has been established by Dr. Saša Novak and run under umbrella of the Slovenian Academic Society for Science and Engineering (SATENA). Within the action “Science on the street, knowledge and ideas on the go” lectures for general public take place in the City centre. The first one was devoted to fusion (Making stars on earth), presented by Dr. Luka Snoj and moderated by journalist Uroš Škerl Kramberger. The event was also reported as a part of daily news on Slovenian national television - an interview with Dr. Luka Snoj and Dr. Saša Novak.

Journalist Uroš Škerl Kramberger published an interview with Dr. Luka Snoj in daily newspaper DNEVNIK. Interview was about fusion basics, fusion research, ITER and future fusion power plant.

On Slovenian National Television there is a talk show about science each Thursday in the afternoon (An hour with Boštjan, A Bite of Science). In december it was about research reactor TRIGA at Jozef Stefan Institute and about fusion (Dobra ura z Boštjanom).



Figure 2: News on the Slovenian National television about the action “Science on the street, knowledge and ideas to go”.

3 CONCLUSIONS AND OUTLOOK FOR 2014

The tasks proposed for the 2013 have been done. In 2014 attention will be paid to spread information about new fusion achievements, especially on current activities of Slovenian Fusion Association in the fusion projects under Horizon 2020. One of the important goals are going to be different presentations of Slovenian fusion research for general public (like lectures and workshops for schools, articles for media, announcements on SFA web site).

4 REFERENCES

- 1 <http://www.delo.si/druzba/znanost/supervroca-pec-v-hladilniku.html>
- 2 <http://vimeo.com/67502564>
- 3 <http://ava.rtv slo.si/predvajaj/prvi-dnevnik/ava2.167891219/>
- 4 <http://www.dnevnik.si/ljudje/-dr-luka-snoj->
- 5 <http://www.rtv slo.si/dobraura/epizoda/238>
- 6 NOVAK, Saša (intervjuvanec), SNOJ, Luka (intervjuvanec), IVEKOVIĆ, Aljaž (intervjuvanec). Fuzija: RTV Slovenija 1, oddaja Dobra ura z Boštjanom: intervju. 5. dec. 2013. [COBISS.SI-ID 27416359]
- 7 SNOJ, Luka (intervjuvanec), NOVAK, Saša (intervjuvanec). Znanost na cesti, znanost in ideje na prepihu : Ni meja : prispevek v sklopu oddaje Prvi dnevnik RTV SLO 1, 30.5.2013. 2013. [COBISS.SI-ID 26822183]

FUSION EXPO SUPPORT ACTION WP10-PIN-FUSEX

Tomaž Skobe, Saša Bobič, Saša Novak, Mateja Južnik, Borut Mavec, Damjan Klep, Dušan Rudman, Jure Hribar, Luka Tavčar, Nina Udir and others

Jožef Stefan Institute, Jamova cesta 39, SI-1000 Ljubljana
tomaz.skobe@ijs.si

1 INTRODUCTION

Slovenian Fusion Association (SFA) EURATOM – MESCS has taken over responsibility to run the Fusion Expo from 6th October 2008. The first Fusion Expo Support Action (WP08-PIN-FUSEX) has finished on 31st July 2010. The new support action under WP10-PIN-FUSEX started on 1st August 2010 and was extended until the end of year 2013. With notification letter the support for the Fusion Expo Task Agreement was extended to the end of June 2014. The main goal and intention of this project remain the same since beginning of our task agreement: to run the Fusion Expo in the most efficient way possible and to follow our tasks, which needs to be fulfilled:

1. Scheduling the exhibition
2. Supervising the local organization
3. Graphical work and printing Fusion Expo panels
4. Moving the exhibits
5. Assembling/Disassembling Fusion Expo
6. Maintenance
7. Continuous report to EFDA
8. Organization of a supporting participation in international events for young generations
9. Providing the Fusion Expo with Fusion Show for larger events

2 WORK PERFORMED IN 2013

Fusion Expo is an itinerant exhibition presenting various aspects of fusion research such as: fusion as a natural phenomenon and energy source science, fusion as a European research project, history of fusion research, European research facilities, ITER, future plans toward a power plant, technological, environmental and sociological aspects of this energy source etc.

The main target group of Fusion Expo is general public. It is specifically designed to address young students and it is also appropriate to addressing other audiences, such as decision makers or journalists. Being modular, it can easily be adapted to different kind of events.

Activities described in this report were carried out in 2013. During this period six events were organized. For one event (Sziget festival) Fusion Expo contributed with a financial support (support action-participation in international events for young generations).

One planned event for September 2013 (Daugavpils Science festival in Latvia) was cancelled.

Host / Event	Type of participation	Place	Date
CCFE, The Big Bang Fair	Hands on experiments	London, England	14th – 17th March, 2013
Science Centre AHHA	Fusion Expo	Tartu, Estonia	17th May – 31st July, 2013
Business Bistro at ECSITE Annual Conference	Hands on experiments	Gothenburg, Sweden	6th June – 8th June, 2013
Sziget Festival	Support action	Sziget, Hungary	5th August – 12th August, 2013
Science Days 2013	Hands on experiments	Rust, Germany	10th October – 12th October, 2013
Scientific festival Week of Science and Technology 2013	Hands on experiments	Prague, Czech Republic	1st November – 15th November, 2013
Fusion show “Plasma’s. Fusie! Energie?”	Some parts of the Expo	Antwerp, Belgium	21st – 22nd and 26th – 27th November, 2013

Table 1: List of realized exhibitions in 2013.

London

The Big Bang is the largest celebration of science, technology, engineering and maths for young people in the UK. The event is aimed at showing young people (primarily aged 7-19) just how many exciting and rewarding opportunities there are out there for them with the right experience and qualifications. The main attraction at CCFE’s stall was the Remote Handling Demo provided by Fusion Expo.

It is an excellent demonstration at getting visitors' attention and as a tool to explain the complex remote handling work being done at JET. The demonstration worked very well at the stand and we are very happy to have been able to use it at the Big Bang Fair. From 14 – 17 March, the Big Bang Fair 2013 saw a record-breaking 65.000 visitors attend the event at ExCeL in London. According to CCFE's final report visitors really enjoyed the remote handling demonstration. It was also frequently mentioned how difficult it was to place all the pieces in its slots using just the camera view. There were around 1.000 visitors a day at the stall (approx. 4.000 overall).



Figure 1: Big Bang Fair in London.

Tartu

Second Fusion Expo exhibition in 2013 was presented in the AHHA Science Centre in Tartu in Estonia where since 1997 interactive science exhibitions let the visitors discover and experience science. It is likely that future generations face an insufficient energy supply, therefore, the AHHA science centre covers the topic energy with the display of renewables such as wind-energy and solar-power in Estonia. The venue hosting Fusion Expo the AHHA Science Centre is the largest in the Baltic States and it has been visited by 42.706 people in 2,5 months, of which 16.357 visitors were pre-booked groups of pupils and students.



Figure 2: Fusion Expo in AHHA centre in Tartu.

Gothenburg

ECSITE is the European network of science centres and museums, linking science communication professionals in more than 400 institutions in 50 countries. Founded 20 years ago, ECSITE connects member institutions through projects and activities and facilitates the exchange of ideas and best practice on current issues. Members include science centres and museums, science festivals, natural history museums, zoos, aquariums, universities, research organizations and companies

communicating and engaging the public in science through accessible, interactive exhibits and programmes.

As a member of Ecsite EFDA presented a newly developed (Beta version) fusion game at the Business Bistro in the booth no. 41. The Fusion Expo team received many suggestions how to improve the game and all remarks were sent to the game developer. Many visitors stopped at EFDA's booth asking questions about fusion, ITER and future research challenges. Very valuable was a visit to other booths in Business Bistro. There were developers and designers for science centers and museums. We collected many ideas and exchanged contacts for the new Fusion expo. The next ECSITE will be held in The Netherlands. According to the very positive feedback from this year it is planned to participate next year as well.



Figure 3: EFDA and Fusion Expo at the ECSITE Business Bistro in Gothenburg.

Sziget

Fusion Expo contributed with a financial support to the Hungarian fusion association at Sziget festival (August 2014). The visitors of the tent at the festival were guided through the most important aspects of energy production, introducing the advantages and disadvantages of different energy sources. A more detailed overview was given about basics of nuclear power, radioactivity, fission reactors, fusion research and experimental magnetic confinement devices. The composition of the visitors by nationality looked as follows: half of them were Hungarian, the other half were from (in descending order) the Netherlands, France, Germany, UK and Poland. There were a few people from Israel and Brazil and from many other European countries.

Rust

Fusion Expo exhibition was presented at Science Days in Rust organized by the Science und Technologie e.V. The aims of Science Days are to encourage the acceptance of science and technology among people in general, to focus more attention on science as a school subject, and to help teenagers orient themselves towards a future profession.

The activities supplemented regular school activities. Science Days showed new learning possibilities; informal and individual education turned into experience-oriented group learning. Science Days were based on a clear pedagogical concept that was implemented on every level in all festival activities.

The learning effects of interactive stands have been proven to be long-term and sustainable. The first two days were primarily for school classes that have booked in advance (pupils aged 7-15 years and their teachers) and some individual visitors and families. Day three, a Saturday, was open to the public and no application was required.

For the first time Fusion Expo was present with almost a full set of hands-on experiments: remote handling, turning table, roller coaster, smoke machine, human

powered power plant and fusion game on Ipad. All those experiments were very well accepted by visitors (they were especially very attractive for youngsters).

The exhibition was organized without any support from the local associations (IPP, KIT and FZJ) for translations of texts and providing guides for the exhibition. Therefore Fusion Expo team had to ask for a help EFDA personnel Dr. Christine Rueth for translations into German and Dr. Petra Niekchen for training of guides that were hired by the organizers of the event at the nearby University. However an option to hire excellent guides (students from universities) could be a solution also for future events. But engagement of national fusion association should still be the first and desirable option.

Prague

Fusion Expo exhibition was presented at Science and Technology Week of the Academy of Sciences which is the largest science festival in the Czech Republic organized by the Academy of Sciences of the Czech Republic along with partner organizations. This year's thirteenth annual festival took place from 1st to 15th November and its programme was spread all over the Czech Republic: Prague, Brno, Ostrava, České Budějovice, and many other places.



Figure 4: Science days 2013 in Rust.



Figure 5: Fusion Expo in Prague.

The festival was intended for the wider public, but primarily secondary-school students, whom it offered the possibility to look into scientific workplaces and find out more about the world of science. Scientific employees of the ASCR offered a broad range of excursions, lectures, science cafés, seminars and documentary films, in which they presented their work, research projects, the latest scientific instruments and introduced visitors to the latest trends in the area of science.

Antwerp

On 21, 22 and 26 November 2012 the University of Antwerp welcomed more than 3500 17- and 18-year-old pupils and teachers in an interactive show about nuclear fusion. This interactive show combines science and theatre techniques to illustrate the ongoing research about nuclear fusion. Nearby the aula where the show went on, the pupils could try some of the items of the Fusion Expo, which were manned by professors and PhD students from our departments of physics and chemistry. The repulsive target, the energy bicycle, and the roller coaster invited pupils to a hands-on experience of science. They were all much appreciated. The giant photograph of the fusion reactor was very popular for classes who wanted a souvenir of an interesting and stimulating day.



Figure 6: Event in Antwerp.

3 CONCLUSIONS AND OUTLOOK FOR 2014

Target venues for all events in 2013 were science festivals and different science centres. That was a huge success, because it was possible to attract a large number of visitors in just few days. Instead of static panels with texts and just few hands-on experiments Fusion Expo in 2013 showed a larger number of hand-on experiments (roller coaster, turning table, smoke machine, remote handling, Jacobs's ladder, Fusion game on Ipad). In first half of 2014 Fusion Expo team plans just few events and expects further steps after introduction of Eurofusion consortium.

PUBLICATIONS

1 JOURNAL ARTICLES

- [1] J. Grünwald, D. Tskhakaya, J. Kovačič, M. Čerček, T. Gyergyek, C. Ionita, R. Schrittwieser, Comparison of measured and simulated electron energy distribution functions in low-pressure helium plasmas, *Plasma Sources, Sci.& Tech.*, 22, 2013, pp. 1–7.
- [2] Tsv. K. Popov, M. Mitov, A. Bankova, P. Ivanonva, M. Dimitrova, S. Rupnik, J. Kovačič, T. Gyergyek, M. Čerček, F. M. Dias, Langmuir probe method for precise evaluation of the negative-ion density in electronegative gas discharge magnetized plasma, *Contrib. Plasma Phys.*, 53, 2013, pp. 51–56.
- [3] J. Adamek, M. Peterka, T. Gyergyek, P. Kudrna, M. Ramisch, U. Stroth, J. Cavalier, M. Tichy, Application of the ball-pen probe in two low-temperature magnetized plasma devices and in torsatron TJ-K, *Diagnostics of magnetized low temperature plasma by ball-pen probe*, *Contrib. Plasma Phys.*, 53, 2013, pp. 39–44.
- [4] T. Gyergyek, J. Kovačič, Potential formation in a bounded plasma system which is terminated by an electron emitting floating collector studied by a particle-in-cell computer simulation, *Contrib. Plasma Phys.*, 53, 2013, pp. 189–201.
- [5] S. Markelj, O. V. Ogorodnikova, T. Schwarz-Sellinger, P. Pelicon, K. Sugiyama and I. Čadež, Study of thermal hydrogen atom interaction with undamaged and self-damaged tungsten, *J. Nucl. Mater.*, 438, 2013, pp. 1027–1031.
- [6] S. Markelj, O. V. Ogorodnikova, P. Pelicon, Th. Schwarz-Selinger, I. Čadež, Temperature dependence of D atom adsorption on polycrystalline tungsten, *Appl. Surf. Sci.*, 282, 2013, pp. 478–486.
- [7] I. Čadež, S. Markelj, A. R. Milosavljević, Influence of hydrocarbons on vibrational excitation of H₂ molecules, *Nuclear Engineering and Design*, *Nucl. Eng. Des.*, 241, 2011, pp. 1267–1271.
- [8] R. Zaplotnik, A. Vesel, M. Mozetič, A powerful remote source of O atoms for the removal of hydrogenated carbon deposits, *J. Fusion Energy*, 32, no. 1, 2013, pp. 78–87.

- [9] A. Vesel, R. Zaplotnik, M. Mozetič, Inductively coupled oxygen plasma in H mode for removal of carbon from mixed a-C:H, W films, *Nucl. Eng. Des.*, **261**, 2013, pp. 275–278.
- [10] A. Drenik, P. Yuryev, A. Vesel, J. Margot, R. Clergereaux, Observation of plasma instabilities related to dust particle growth mechanisms in electron cyclotron resonance plasmas, *Phys. Plasmas*, **20**, no. 10, 2013, pp. 100701-1–100701-4.
- [11] A. Drenik, A. Vesel, M. Mozetič, P. Panjan, Recombination of atomic oxygen and hydrogen on amorphous carbon, *J. Nucl. Mater.*, **442**, 2013, pp. 751–754.
- [12] B. Zajec, V. Nemanič, M. Žumer, C. Porosnicu, C. Lungu, Hydrogen permeability through beryllium films and the impact of surface oxides, *J. Nucl. Mater.*, **443**, 2013, pp. 185–194.
- [13] A. Anders, M. Panjan, R. Franz, J. Andersson, P. A. Ni, Drifting potential humps in ionization zones : the propeller blades of high power impulse magnetron sputtering, *App. Phys. Lett.*, **103**, 2013, pp. 144103-1–144103-4.
- [14] N. Jelić, L. Kos, Ion-sound Velocity at the Plasma Edge in Fusion-Relevant Plasmas, *Nucl. Eng. Des.*, **261**, 2013, pp. 269–274.
- [15] L. Kos, D.D. Tskhakaya, Sr., S. Kuhn, N. Jelić, Debye-sheath properties in the Tonks–Langmuir discharge with warm neutrals, *J. Plas. Phys.*, **79**, 2014, pp. 1021–1024.
- [16] L. Snoj, I. Lengar, et al. Calculations to support JET neutron yield calibration: Modelling of the JET remote handling system, *Nucl. Eng. Des.*, **261**, 2013, pp. 244–250.
- [17] S. Novak, A. Iveković, Y. Hattori, Production of bulk SiC parts by electrophoretic deposition from concentrated aqueous suspension. *Adv. App. Ceram.*, **113**, 2013, pp. 14-21.
- [18] Iveković, S. Novak, G. Dražić, D. Blagoeva, S. Gonzalez De Vicente. Current status and prospects of SiC_f/SiC for fusion structural applications. *J. Europ. Cer. Soc.*, **33**, 2013, pp. 1577–1589.
- [19] B. Končar, M. Draksler, P. Norajitra, Design and cooling of the edge segments of the DEMO divertor target plates, *Nucl. Eng. Des.*, **88**, 2013, pp. 1831–1835.
- [20] S. Košmrlj, B. Končar, Simulating cyclic high heat flux loading of divertor cooling finger mock-up, *Nucl. Eng. Des.*, **261**, 2013, pp. 317–325.

2 CONFERENCE PAPERS

- [21] T. Gyergyek, J. Kovačič, N. Jelić, L. Kos, Sheath formation in front of a negative electrode close to plasma potential studied by PIC simulations, 49th International conference on microelectronics, devices and materials, Kranjska Gora, Slovenia, 25–27 September 2013, Proceedings. Ljubljana: MIDEM (2013) pp. 115–120.
- [22] J. Kovačič, Tsv. K. Popov, M. Dimitrova, T. Gyergyek, M. Čerček, R. Dejarnac, J. Stöckel, R. Panek. Kinetic simulations in support of probe measurements of COMPASS scrape-off-layer, In: Proceedings, 22nd International Conference Nuclear Energy for New Europe - NENE 2013, Bled, 9–12 September, Leon Cizelj, ed., Matjaž Leskovar, ed., Mitja Uršič, ed., Ljubljana, Nuclear Society of Slovenia, 2013, pp. 1–6.
- [23] A. Založnik, I. Čadež, S. Markelj and V. Žigman. Modelling hydrogen-metal surface interaction: the integral study, In: Proceedings, 22nd International Conference Nuclear Energy for New Europe - NENE 2013, Bled, 9–12 September, Leon Cizelj, ed., Matjaž Leskovar, ed., Mitja Uršič, ed., Ljubljana, Nuclear Society of Slovenia, 2013, pp. 1506.1–1406.7.
- [24] S. Markelj, I. Čadež, P. Pelicon, P. Vavpetič, C. Porosnicu, C. P. Lungu, Deuterium Thermal Desorption From Mixed Layers Relevant for ITER, 22nd In: Proceedings, 22nd International Conference Nuclear Energy for New Europe - NENE 2013, Bled, 9–12 September, Leon Cizelj, ed., Matjaž Leskovar, ed., Mitja Uršič, ed., Ljubljana, Nuclear Society of Slovenia, 2013, pp. 1405.1–1405.9.
- [25] S. Markelj, O.V. Ogorodnikova, P. Pelicon, T. Schwarz-Selinger, P. Vavpetič and I. Čadež, In-situ NRA analysis of D retention in undamaged and self-damaged tungsten under atomic D exposure, 14th PFMC conference, May 2013, Juelich, Germany ; accepted in *Physica Scripta*.
- [26] K. Kutasi, R. Zaplotnik, G. Primc, M. Mozetič, "Controlling the oxygen species density distribution in the flowing afterglow of an O₂ surface-wave microwave discharge", International Conference on Phenomena in Ionized Gases (IPCIG 2013, XXXI.), Granada, Spain, 2013, 4 pg.
- [27] A. Vesel, M. Mozetič, Marianne Balat-Pichelin, Reaction of oxygen plasma with hydrogenated W-C deposits, In: Proceedings, 22nd International Conference Nuclear Energy for New Europe - NENE 2013, Bled, 9–12 September, Leon Cizelj, ed., Matjaž Leskovar, ed., Mitja Uršič, ed., Ljubljana, Nuclear Society of Slovenia, 2013, pp. 1401-1–1401-9.
- [28] A. Drenik, L. Salamon, R. Zaplotnik, A. Vesel, M. Mozetič, Erosion of amorphous carbon layers in the afterglow of oxygen microwave plasma, In: Proceeding of the JVC-14, 14th Joint Vacuum Conference, EVC-12, 12th European Vacuum Conference, AMDVG-11, 11th Annual Meeting of the

- German Vacuum Society, CroSloVM-19, 19th Croatian-Slovenian Vacuum Meeting, 4–8 June 2012, Dubrovnik, Croatia, Nikola Radić, ed., Slobodan Milošević, ed., Zagreb, Croatian Vacuum Society, Vacuum, 98, 2013, pp. 45–48.
- [29] A. Drenik, A. Vesel, M. Mozetič, P. Panjan, "Recombination of atomic oxygen and hydrogen on amorphous carbon", In: Proceedings of the 15th International Conference on Fusion Reactor Materials, 16–21 October, 2011, Charleston, SC, J. Nucl. Mater., 442, 1/3, 2013, pp. S751-S754.
- [30] M. Panjan, A. Anders, Asymmetric distribution of ion and electron fluxes measured near the target plane in HiPIMS and DCMS discharges, In: 19th International Vacuum Congress, 9–13 September, 2013, Paris, France.
- [31] L. Kos, H.-J. Klingshirn, P.L. Garcia Muller, F. Imbeaux and EFDA ITM-TF contributors, Unified Approach to Visualizations within the European Integrated Tokamak Modelling Framework, In: Proceedings, 22nd International Conference Nuclear Energy for New Europe - NENE 2013, Bled, 9–12 September, Leon Cizelj, ed., Matjaž Leskovar, ed., Mitja Uršič, ed., Ljubljana, Nuclear Society of Slovenia, 2013, pp. 1402.1–1402.8.
- [32] N. Jelić, L. Kos, Towards Possible Control of Plasma Outflow in Fusion-Relevant Devices via Employing Virtual Terminating Surfaces, 22nd Int. Conf. Nuclear Energy for New Europe, Bled, Slovenia, 9–12 Sept 2013, pp. 1403.1–1403.8.
- [33] S. Kuhn, D. D. Tskhakaya, L. Kos, The non-marginal Bohm condition in the collisionless plasma diode, 40th European Physical Society Conference on Plasma Physics, Espoo, Finland, 1–5 July 2013, P1.410[1–4].
- [34] N. Jelić, L. Kos, J. Krek, J. Kovačič, T. Gyergyek, A. J. Christlieb, J. P. Verboncoeur, Ionization front in a gas-filled diode during electrical breakdown. 49th International Conference on Microelectronics, Devices and Materials & the Workshop on Digital Electronic Systems, 25–27 September, 2013, Kranjska Gora, Slovenia, pp. 109–114.
- [35] T. Gyergyek, J. Kovačič, N. Jelić, L. Kos. Sheath formation in front of a negative electrode close to plasma potential studied by PIC simulations. 49th International Conference on Microelectronics, Devices and Materials & the Workshop on Digital Electronic Systems, 25–27 September 27, 2013, Kranjska Gora, Slovenia, pp. 115–120.
- [36] N. Jelić, L. Kos, J. Krek, J. Duhovnik, Kinetic theory and simulations of moderately strong stationary double layers with warm ions, IEEE International Conference on Plasma Science (ICOPS), 16–21 June 2013, San Francisco, California, USA.

-
- [37] S. Novak, A. Iveković, D. Blagoeva, L. Evans, A. Galatanu, J.Y. Pastor, Fabrication and properties of the SITE-SiC/SiC composite, 16th International Conference on Fusion Reactor Materials, Beijing, China, 20-26 October, 2013.
- [38] M. Draksler, B. Končar, L. Cizelj, B. Ničeno, Flow and heat transfer characteristics of multiple impinging jets : Large Eddy Simulation. In: Proceedings, 22nd International Conference Nuclear Energy for New Europe - NENE 2013, Bled, 9–12 September, Leon Cizelj, ed., Matjaž Leskovar, ed., Mitja Uršič, ed., Ljubljana, Nuclear Society of Slovenia, 2013, pp. 1412-1-1412-9.
- [39] P. Norajitra, W. Basuki, B. Končar, L. Spatafora, He-cooled divertor : study on low-temperature design using Ta alloy as thimble material. In: 25th Symposium on Fusion Engineering (SOFE 25), June 10-14, 2013, San Francisco, California, Institute of Electrical and Electronics Engineers, 5 pg.

3 REPORTS AND PRESENTATIONS

- [40] S. Markelj In situ ERDA and NRA studies of Hydrogen Retention in Tungsten, Second SPIRIT Joint Research Activity Meeting, Bled, Slovenia, April 11-12, 2013.
- [41] S. Markelj, P. Pelicon, I. Čadež, P. Vavpetič, A. Založnik, D re-adsorption/re-saturation of W surfaces subjected to RF-discharge as a fuel removal technique, IPH-A02-P2 meeting, September, 2013, Garching, Germany
- [42] S. Markelj, P. Pelicon, I. Čadež, P. Vavpetič, A. Založnik, Hydrogen retention in self-damaged and He irradiated tungsten and alloys of PFC, 1st CRP meeting “PWI with irradiated tungsten.”, 26-28 November, 2013, Vienna, Austria.
- [43] A. Založnik, I Čadež, S. Markelj, P. Pelicon, Recombination of hydrogen and deuterium atoms on metal surfaces, IBA workshop, 2013 Trieste, Italy.
- [44] A. Založnik, I Čadež, S. Markelj, P. Pelicon, DEA application to vibrational spectroscopy of hydrogen molecules, The 1st meeting of the DEA club, 16-19 September, 2013, Trieste, Italy.
- [45] P. Pelicon, S. Markelj, I. Čadež, P. Vavpetič, A. Založnik, Analyzes of the deuterium trapping in mixed materials(WP13-IPH-A01-P3-01/MESCS), Midterm monitoring meeting WP13-IPH-A01-P1, P2 and P3, September 11, 2013, Garching, Germany.
- [46] M. Bizjak, J. Benda, F. Breclj, N. Jelić, L. Kos, V. Nemanič, J. Perme, A. Piriš, A. Pregelj, R. Rozman, A. Štagoj, A. Tavčar, B. Zajec, M. Žumer, Rezultati teoretičnih, numeričnih in eksperimentalnih raziskav prebojev v niskotlačnih laboratorijskih, tehnološko-industrijsko usmerjenih in fuzijsko

relevantnih razelektrivah, Technical report on project MINIGDT:L2-3652, Ljubljana, Fakulteta za strojništvo, 2013.

- [47] L. Snoj, Measuring power of fusion reactors, Monday colloquium at the faculty of mathematics and physics at the University of Ljubljana.
- [48] B. Končar, P. Norajitra, S. Košmrlj, Design description report of square helium-cooled multi-jet fingers using WL10 or T111 as thimble material : report for TA WP13DAS02T12-D2, (EFDA = European fusion development agreement), Ljubljana, Jožef Stefan, 2013, 11 pg.

4 THESES

- [49] J. Kovačič, Študij formiranja potenciala pred negativno elektrodo v fuzijsko relevantnih plazmah (=Studying potential formation in front of a negative electrode in fusion relevant plasmas), doctoral dissertation, University of Ljubljana, 2013, 141 pg.
- [50] A. Čufar, Analysis of neutron detector response in tokamak, diploma thesis University of Ljubljana, Ljubljana, 2013, 46 pg.
- [51] A. Iveković, Development of SiC-based composite material for fusion application (=Priprava kompozitnega materiala na osnovi SiC za uporabo v fuzijskem reaktorju), doctoral dissertation, Jožef Stefan Postgraduate School, Ljubljana, 2013, 108 pg.

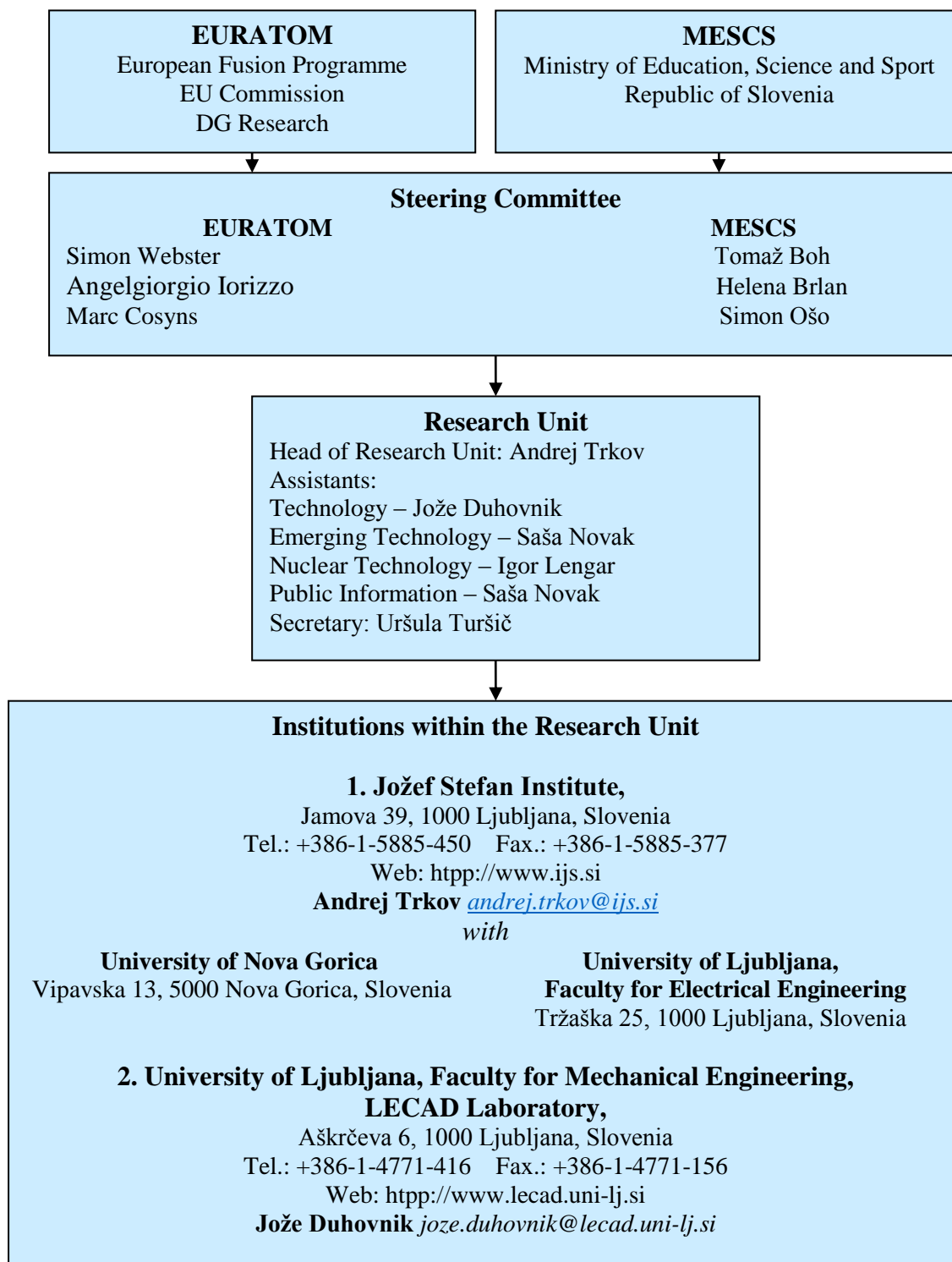
5 GENERAL PUBLICATIONS

- [52] I. Lengar, L. Snoj, B. Končar, Fuzija : energija prihodnosti, TV dnevnik, accessible at: <http://ava.rtv slo.si/predvajaj/prvi-dnevnik/ava2.174250307/>, RTV Slovenija 1, Dec 4th, 2013.
- [53] S. Novak (interviewee), L. Snoj (interviewee), oddaja Dobra ura z Boštjanom, accessible at: <http://4d.rtv slo.si/arhiv/ugriznimo-znanost/174250632>, RTV Slovenija 1, Dec 5th, 2013.
- [54] L. Snoj (interviewee), Dr. Luka Snoj, accessible at: <http://www.dnevnik.si/ljudje/-dr-luka-snoj-/>, Dnevnik, July 22nd, 2013.
- [55] L. Snoj (interviewee), Luka Snoj: Osebno doživljam fuzijo kot enega največjih izzivov človeštva, accessible at: <http://blogslo.videlectures.net/luka-snoj-osebno-doživljam-fuzijo-kot-enea-najvecjih-izzivov-clovestva/>, videlectures.net, 2013.
- [56] L. Snoj, Ali bomo pridobivali energijo iz vode?, Lecture, accessible at: http://videlectures.net/dnevi_snoj_voda/, March 2013, Jožef Stefan Institute, Ljubljana.

- [57] L. Snoj, Ustvarjanje zvezd na Zemlji, Lecture, Scienec on the street (= Znanost na cesti), accessible at: <http://www.znanostnacesti.si/predavanja/ustvarjanje-zvezd-na-zemlji.aspx>, Satena, May 22nd, 2013, Ljubljana.
- [58] L.Snoj (interviewee), oddaja Glasovi svetov, Jedrska fuzija, accessible at: <http://ava.rtvsllo.si/predvajaj/glasovi-svetov/ava2.165787638>, May 9th, 2013, Radio Slovenija 3, Ljubljana.
- [59] L. Snoj (interviewee), S. Novak (interviewee), Prvi dnevnik: Znanost na cesti, znanost in ideje na prepihu: Ni meja: prispevek v sklopu oddaje Prvi dnevnik RTV Slovenija 1, May 30th, 2013, Ljubljana.

Annex 1

Association EURATOM-MESCS management structure



Annex 2

Slovenian representatives in the European committees relevant to fusion research and development

Consultative Committee for the EURATOM Specific Programme on Nuclear Energy Research – Fusion (CCE-FU)

Ivan Skubic Ministry for Education, Science, Culture and Sport of
 Republic of Slovenia

Andrej Trkov Head of Research Unit, Jožef Stefan Institute, Ljubljana

EFDA Steering Committee

Andrej Trkov Head of Research Unit, Jožef Stefan Institute, Ljubljana

Public Information Group

Saša Novak Jožef Stefan Institute, Ljubljana

Tomaž Skobe Jožef Stefan Institute, Ljubljana

Annex 3

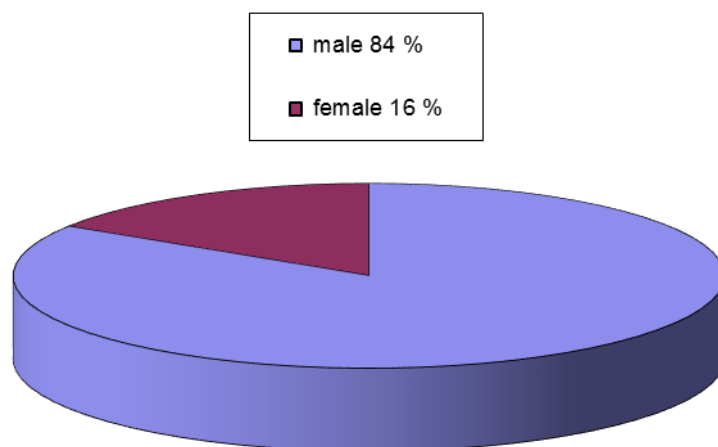
Statistics

R&D projects in the Association EURATOM-MESCS for 2013

	JSI	ULJ	
Physics	11	1	12
JET	5	-	5
Fusion Expo	1	-	1
TOTAL	17	1	18

Manpower (ppy) for 2013

	Professional	Non professional	TOTAL
JSI	15,2	3,5	18,7
ULJ	1,8	0,2	2,0
	17,0	3,7	20,7



Association EURATOM-MESCS staff in 2013 by gender

